Palestine Polytechnic University

Deanship of Graduate Studies and Scientific Research

Master of Civil Engineering

Strengthening and Retrofitting of RC Beams by Titanium Alloys Using NSM Technique

Done by:

Khaleel Fadel Khaleel Numan

Supervisor:

Ph.D. Abdulsamee Halahla

Thesis submitted in partial fulfillment of requirements of the degree

Master of Civil Engineering

August, 2023

The undersigned hereby certify that they have read, examined and recommended to the Deanship of Graduate Studies and Scientific Research at Palestine Polytechnic University:

Strengthening and Retrofitting of RC Beams by Titanium Alloys Using NSM Technique

Khaleel Fadel Khaleel Numan

in partial fulfillment of the requirements for the degree of Master in Civil Engineering.

Graduate Advisory Committee:

Prof./Dr. …… University: ……

Signature:———————————— Date:————————————

Prof./Dr. …… University: ……
Signature:———————————— Date:————————————

Prof./Dr. …… University: ……
Signature:———————————— Date:————————————

Prof./Dr. …… University: ……
Signature:———————————— Date:————————————

Thesis Approved by:

Name:

Dean of Graduate Studies & Scientific Research

Palestine Polytechnic University

Signature: …….

Date: …….

Strengthening and Retrofitting of RC Beams by Titanium Alloys Using NSM Technique

Khaleel Fadel Khaleel Numan

Abstract

Reinforced concrete (RC) beams are structural elements can have some deformation due to applied loads on. The amount of deformation depends on many factors like the compressive strength of the concrete (f_c`), the reinforcement percentage, the reinforcement design, etc. Deformation can be minimized using some strengthening and retrofitting techniques like wrapping structures with fibers to act as additional reinforcement, replacing some steel reinforcement with alternatives, or any other strengthening technique. This study will discuss the Near-Surface Mounted (NSM) reinforcement technique that can be used by making grooves in the concrete cover and apply the desired material in (Titanium Alloys will be used here) to examine the effects of used material on the strength of beams. Titanium Alloys are made up of mixing Titanium with other chemical elements. This mixture has some special properties like obtaining high tensile strength, corrosion resistance, light weight, etc. which make it possible to be used in RC structures. A T-shaped 5490 mm long beam with a deck of size (165x914) mm and (229x749) mm stem was in one half of the specimen and enlarged to be (321 x 1048) mm stem with reinforcement and two (25×25) mm Titanium bars was modeled to verify results with the data given by (Higgins et al., 2017). A new control beam was modeled without using Titanium to examine the enhancement when changing parameters for other 11 beams. Parametric study was done to explore the best method, location, and the number of Titanium bars used to strengthen T-beam with having a transitional point in which the T-beam dimension changed. As a result for this study, to have the best enhancement in the maximum moment capacity for T-Beam with different dimension, two Titanium bars with dimension (25×25) mm on each side should be used.

تقوية وترميم الجسور الخرسانية المسلحة بسبائك التيتانيوم باستخدام تقنية التثبيت بالقرب من السطح.

خليل فضل خليل نعمان

المستخلص

الجسور الخرسانة المسلحة (RCB) هي عناصر هيكلية إنشائية يمكن أن يكون لها بعض التشوه بسبب الأحمال المطبقة عليها. يعتمد مقدار التشوه على العديد من العوامل مثل قوة الضغط للخرسانة (f_c`)، نسبة التسليح، وتصميم حديد التسليح بداخل العناصر، الخ.

يمكن تقليل التشوه باستخدام بعض تقنيات التقوية والترميم مثل تغليف الهياكل بالألياف لتكون بمثابة تعزيز إضافي لحديد التسليح، استبدال بعض حديد التسليح بالبدائل الأخرى، أو أي تقنية تقوية مستخدمة بمجال الهندسة المدنية وهندسة المباني والإنشاءات.

ستناقش هذه الدراسة إحدى الطرق التقنية للتقوية وهي التقوية المثبتة بالقرب من السطح (NSM) حيث يمكن تطبيقها عن طريق استحداث بعض الفتحات المحدودة الحجم بالغطاء الخرساني وإضافة المواد المرغوبة بداخلها (سبائك التيتانيوم مستخدمة في هذه الدراسة) لفحص تأثيرات هذه المواد على مقدار قوة العزم التي يمكن للعنصر الإنشائي تحملها بعد التقوية.

تتكون سبائك التيتانيوم من مزج التيتانيوم مع العناصر الكيميائية الأخرى حيث يحتوي هذا المزيج على بعض الخصائص المميزة له مثل الحصول على قوة شد عالية، ومقاومته للتآكل، وخفة الوزن، وما إلى ذلك مما يجعل من الممكن استخدامه في العناصر الإنشائية الخرسانية المسلحة.

جسر خرساني بطول 5490 مم على شكل حرف T مع سطح بحجم (165 × 914) مم وساق (229 × 749) مم لغاية نصف المسافة وتم تكبيره ليكون ساقه (321 × 1048) مم وتم مقارنة نتائج النموذج باستخدام الحاسوب مع التجربة الواقعية وتجربة نموذج آخر بدون استخدام قضبان التقوية لمقارنة نتائج 11 نموذج آخر بطرق تقوية مختلفة باستخدام قضبان التيتانيوم لمعرفة أفضل طريقة وموقع وعدد قضبان التيتانيوم المستخدمة لتقوية الجسر بنقطة انتقالية تغير فيها بُعد الجسر.

نتيجة لهذه الدراسة ، للحصول على أفضل تحسين في قوة العزم القصوى للتحمّل لجسر على شكل T بأبعاد مختلفة ، يجب استخدام قضيبين من التيتانيوم بأبعاد (25 × 25) مم على كل جانب.

Declaration

I declare that the Master Thesis entitled ”Strengthening and Retrofitting of RC Beams by Titanium Alloys Using NSM Technique” is my own original work, and herby certify that unless stated, all work contained within this thesis is my own independent research and has not been submitted for the award of any other degree at any institution, except where due acknowledgement is made in the text.

Student Name: Khaleel Fadel Khaleel Numan

Signature:———————————— Date:————————————

Dedication

Thanks be to God Who is always helping us to success

To my loving parents that are a great support in the life

To my brothers and sister

To all friends and colleagues

To my teachers

To my precious persons

To all of them

Acknowledgement

I would like to thank my supervisor Ph.D. Abdulsamee Halahla for his continuous support and motivation while preparing this work. Ph.D. Belal Almassri the head of the Civil Engineering Department who worked hard to establish the plan for the Master's Degree in Civil Engineering. Ph.D. Haitham Ayyad and Ph.D. Maher Amro who I learned so much from their knowledge. All persons who worked to make me able to be graduated from “Imam Abdulrahman Bin Faisal University” in Dammam-KSA with a strong engineering background. Everybody was having a job at “Al-Tahtheeb Private School”, and everyone I learned anything from.

Table of Contents

List of Figures

List of Tables

List of Equations

Chapter 1: Introduction

1.1 Background

Now adays, most buildings are made up of sand, water, aggregate and cement, which we call concrete, with steel embedded inside to make a very strong combination to resist loads with different shapes and directions. Concrete can resist high compression loads, but can not deal with tension as much as with compression. Steel is combined with concrete due to the ability of steel to be loaded with high tensile stress. These two components were mixed together to form a new design (Reinforced Concrete Structure) to be reliable when the structure is exposed to tension and compression loads. Concrete and steel have very close thermal expansion factors, this can help maintaining the cohesion between both of them when structures are in locations with high variation in the temperature. As the time goes by, structures are subjected to loads opposite in direction, long lasting and high in magnitude which affecting the elements and making some cracks. These points lead to weaken building and make the need maintenance and strengthening to keep working. This could be by different ways like jacketing with steel or reinforced concrete, FRP confining, of using Shape Memory Alloys (SMAs).

Shape memory alloys are metallic substances can return to the original shape after being stretched over than the elastic limit. SMAs are highly used recently due to their amazing properties. They are corrosion resistance, durable, have light weight (which promote them to be used in lightweight structures), and the shape can be modified easily like being bent, twisted, stretched, or deformed and return to the original shape. These properties are very important in all manufacturing and construction areas so SMAs can be used in a wide range of applications. SMAs can be used for manufacturing sensors, actuators, aircrafts, in some medical equipment, and for developing the way we build and make new structures with amazing properties.

SMAs can be found in several types and forms. Copper-Zinc-Aluminum alloys (AlCuZn) have the ability to resist the corrosion excellently and have high strength. Highly recommended in areas where durability is important. Iron-Manganese-Silicon alloys (FeMnSi) can resist fatigue and can be used when low transformation temperature needed. Nickel-Titanium alloys (NiTi) can highly remember the original shape and can be used when the application of load is done repeatedly.

According to (Tabrizikahou et al., 2021), shape memory alloys have different internal energy levels. The level of internal energy determines the composition of SMA. The crystal structure must allow for the minimal energy state at a specific temperature. The martensitic transition and its inverse transformation are two crystal phases that can change when subjected to external force. The difference between the Gibbs free energies of the two phases, which can be produced by a temperature gradient or mechanical loading, is what drives the phase transformation. Temperature and external stress play a comparable part in the transformation mechanism from a thermomechanical perspective (Saadat et al., 2002). There are thus two different forms of martensite transformations: the change brought on by temperature, which leads in SME, and the transition brought on by stress, which generates superelasticity. In (Figure 1) the phases transformations are shown.

According to a temperature excitation cycle, Fig. 1 depicts a typical stress-free temperature-induced martensitic transition and its inverse transformation. The martensite start temperature (M_s), the martensite finish temperature (M_f), the austenite start temperature (A_s), and the austenite finish temperature (A_f) are the four transition temperatures that define the transformation loop. The onset and termination of the forward (martensite) and inverse transformations are determined by these crucial temperatures. Due to internal phase friction, the temperature-deformation loop is clearly hysteretic.

An SMA specimen's typical stress-strain curve at constant low temperature ($T < M_f$) is shown in Fig. 2. When the martensite SMA is under tension, the elastic deformation is followed by a significant increase in strain that is approximately exactly proportional to the stress. The hysteresis mobility of the twined variation interfaces and faults inside the martensite phase are to blame for this yielding. Only elastic strain is recovered after unloading, while the residual strain brought on by martensite reorientation can only be recovered through the reverse phase change after heating (SME). Permanent plastic deformation happens if distortion is more than what martensite can withstand through its reorientation process. So, in order to avoid permanent plastic deformation, the applied stress should, for practical purposes, not be more than this maximum value. The stress-strain cycle of a superelastic SMA specimen going thru a stress-induced transformation of SMA at a fixed temperature is displayed in Figure 3 ($>A_f$).

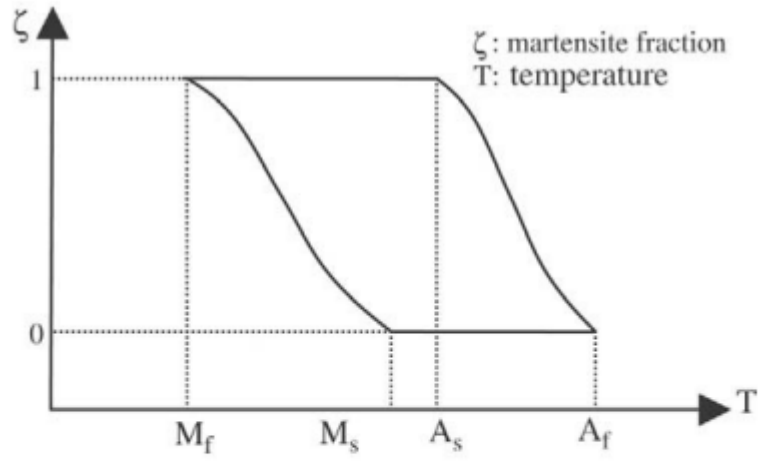

Fig. 1. Stress-free martensitic phase transformation.

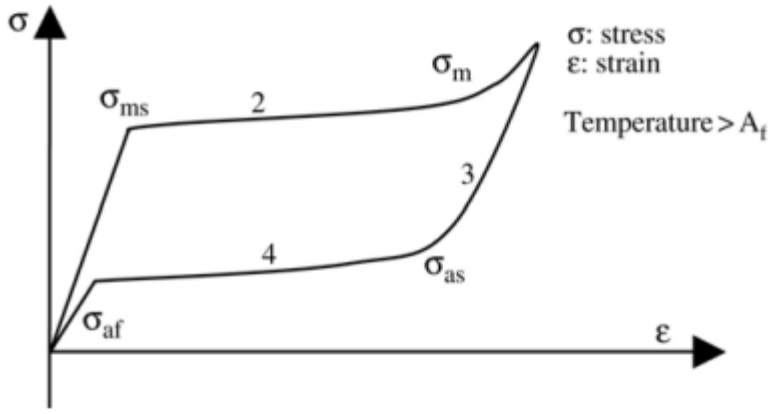

Fig. 2. Isothermal stress-induced martensitic phase transformation.

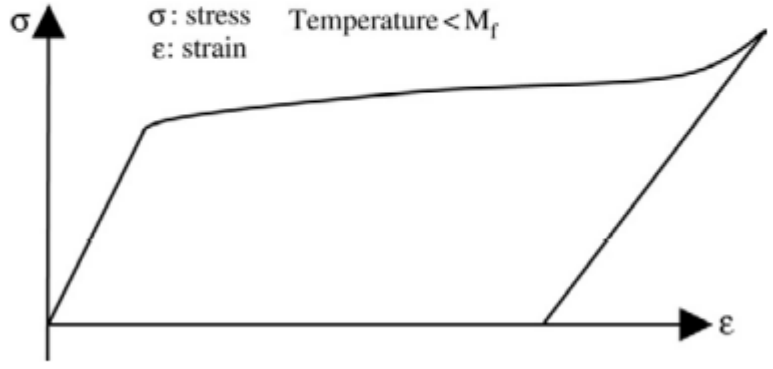

Fig. 3. Stress–strain relationship of the martensitic SMAs ($T < M_f$).

Figure 1: Shape Memory Alloys phase transformations and energy dissipated (Tabrizikahou et al., 2021)

The following table illustrates some kinds for the famous shape memory alloys and the corresponding properties according to (Motavalli et al., 2009):

Table 1: Properties of some Shape Memory Alloys (Motavalli et al., 2009)

Property	Unit	Ni-Ti	Cu-Zn-Al	Cu-Al-Ni
Young's modulus	GPa	70 – 98	70 – 100	80 – 100
Yielding Strength	MPa	100 – 800	150 – 350	150 – 300
Ultimate Tensile Strength	MPa	800 – 1500	400 – 900	500 – 1200
Elongation at Failure	%	15 – 20	10 – 15	8 – 10
Recovery Strain	%	8	3.5	2
Maximum Recovery Stress	MPa	600 – 900	400 – 700	300 – 600

1.2 Problem

Beams have many shapes of failure. The two types of failure are flexural and shear. Flexural failure can be identified when beam has approximately vertical main cracks, unlike the failure due to shear which makes diagonal cracks. This can be illustrated in the following figures:

(a) Beam 3

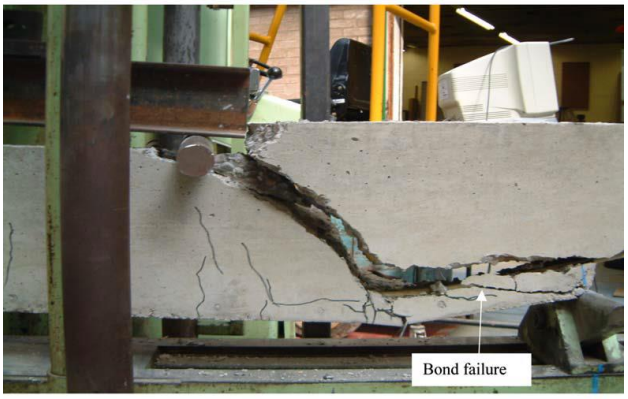

(b) Beam 11

Figure 2: Shear Failure (Ashour, 2006)

(a) Beam 8

(b) Beam 10

Figure 3: Flexural Failure (Ashour, 2006)

This study will be focusing on the flexural failure and trying to strengthen beams and increase the capacity to resist a such failure using a type of shape memory alloys.

1.3 Research Significance and objectives

The work done in the thesis is to investigate using Shape Memory Alloys (SMAs) for flexure strengthening of Reinforced Concrete (RC) beams using Titanium Alloy Bars (TiABs) and to study different installation methods and determine which one is structurally effective approach for flexural strengthening. The characteristics of this alloy make it suitable to use and stable at service temperatures of civil engineering. The main contribution of this research will be the development of a flexure strengthening technology with Titanium SMA.

1.4 Methodology

Numerical Analysis will be used for this study which offers a low-cost model development with less time required to obtain the results and provides the opportunity to study many variables easily. ABAQUS software will be hired to model a beam subjected to loads cause some deformation, this deformation will be treated and analyzed by Finite Element Method (FEM), compared and verified with laboratory work done by (Higgins et al., 2017) and then will be some upgrades and different parameters to be studied.

Chapter 2: Literature Review

This chapter will contain a summary of previous experiments and studies exploring the use of retrofitting strategies which shape memory alloys is one of, near-surface mounting (NSM), performance for anchorages and techniques in external unbonded reinforcement strengthening.

2.1 Different ways of strengthening

(Saadatmanesh et al., 1994) in a study on the effect of wrapping columns with high-strength fiber composite straps in a spiral or tie formation to improve the confinement of the column cores, presented an alternative to continuous FRP jackets that proposed increased ductility, strength, and restraint against buckling of the longitudinal bars. Carbon fiber straps and E-glass straps were put through their paces, and carbon fiber straps were chosen as the materials that would be best suited for retrofitting concrete columns. The E-glass strap increased ultimate axial load by 92% and maximum moment capacity by 48% in testing of circular columns, while the carbon fiber strap increased ultimate axial load by 162% and maximum moment capacity by 83%. The retrofitted columns' ductility factor increased linearly with the thickness of the strap. In contrast, the rate of increase decreased with strap spacing.

(Xiao and Wu, 2000) performed a compression test study on concrete cylinders wrapped in CFRP revealed a brittle failure mode upon CFRP rupture. A total of 36 cylinders tested, each with a diameter of 152 mm and a height of 305 mm. The concrete strength and number of layers of CFRP applied varied. Explosive rupture of the carbon fiber jackets represented the final failure mode of the cylinders, which means that CFRP is a brittle material and preferred not to be used if the ductility is needed in that structure.

Strengthening with CFRP can be used when finding corroded steel reinforcement using NSM technique like what has been done (Almassri and Halahla, 2020) using Abaqus to explore the mechanical properties of naturally corroded reinforced beams. In this study, they chose a sample of 72 beams were cast in 1984 and concluded by stating that using NSM have some limitations and can be solved by adding a steel plate externally. And noticing that the corroded reinforced concrete beam repaired using NSM CFRP rod with combination with external steel plate demonstrates an increase in moment and yielding capacities to be close to the data obtained from non-corroded “control” beam repaired only with NSM.

(Balendran et al., 2004) presented the results of an experimental study on the bending behavior of sand-coated GFRP bars in concrete. A total of 18 reinforced concrete beams were subjected to bending tests. Identical specimens reinforced with mild steel bars where appropriate were used for comparison. Tensile tests showed that the ultimate tensile strength and Young's modulus of the GFRP rod were about 2.5 times and 25% higher than that of the mild steel rod, respectively. Beam test results showed that the ultimate strength of the sand-coated GFRP reinforced samples was 1.4-2 times higher than that of the mild steel reinforced samples, but the deflection was higher.

(Mohammed et al., 2013) developed a Finite Element (FE) model and finalized with that it was clear that using FRP in strengthening reinforced concrete beams improved the shear behavior of the beams. While (El-Sokkary, 2023) supports that result by numerical study to investigate the effectiveness of FRP in upgrading the seismic performance for conventional RC shear walls in 10 and 15-story buildings.

(Saikia et al., 2005) concluded in their experimental work to examine the behavior of hybrid GFRP and steel bars used as longitudinal reinforcement on normal strength concrete beams that for the same load hybrid system showed a better ductility than using steel alone.

(Rojob and El-Hacha, 2017) studied the behavior of reinforced concrete beams that included iron-based shape memory alloy (Fe-SMA) bars near-surface mounted (NSM). At the tension side of the RC beam (2000x305x150) mm, the pre-strained Fe-SMA bar was fastened within a groove that had been previously carved. The bar was then activated by heating it to a temperature above 300ºC (572ºF), which resulted in a prestressing force. Then the beam was put through a four-point bending setup test until it failed. The yielding and ultimate load capabilities increased significantly, according to the findings. And the ductility of the beam was significantly improved due to the yielding nature of the Fe-SMA material as mentioned by the authors.

Shape Memory Alloys can be used in many shapes: spirals, wires, braces, bars and strips to enhance the strength of the reinforced concrete structure. Strengthening using SMA is not only for beams, it can be for columns, beam-column joints and walls in both flexure and shear: (Choi et al., 2012), (Shin and Andrawes, 2011a), (Shin and Andrawes, 2011b), (Mas et al., 2016), (Yurdakul et al., 2018), (Cladera et al., 2020), (Jung et al., 2018), (Montoya-Coronado et al., 2019), (Strieder et al., 2019), (Rezapour et al., 2021), (Elkafrawy et al., 2023), and (Effendy et al., 2006) tried to strengthen different RC structures.

2.2 Anchorage effects

37 pullout samples with #6 and #9 deformed reinforcing bars that had a yield strength of about 92,000 psi were tested according to (Untrauer and Henry, 1965). The embedment length for each specimen was 6 inches. The pullout specimens were subjected to standard pressures ranging from 0 to 2370 psi. When all other elements are held constant, bond strength was found to rise with normal pressure relative to the square root of the normal pressure as well as with concrete strength. The bond strength was higher for the #9 bar than for the #6 bar for loaded-end slips of 0.005 and 0.01 in. However, at ultimate, the bar size had no impact on the ultimate bond strength. Normal pressure increased the bond strength more for both bar sizes.

(Jirsa and Marques, 1972), looked at the impact of various confinement levels on the effectiveness of bent bar anchorage in a beam-column joint. Nineteen full-scale column specimens were constructed with bars sticking out from one face to approximate stress reinforcement for adjacent beams. Column axial load, longitudinal column reinforcement, side cover, and column ties at the joint all worked together to confine the space. With standard (ACI 318-71) hook details, which advise a tail length of 12db and a bend radius of 3db for 22M and 4db for 36M bars, the columns were either (305×305) mm or (305×381) mm in size. Measurements of stress-slip and slip-strain were utilized to compare specimens. Results indicated that anchorage performance was not significantly impacted by either concrete cover or column axial load. In addition, concrete cover was apparently immaterial as long as enough was there to avoid localized failure inside the hook bend. This was because spalling side cover (produced by significant slip and hook bearing stress) still governed the failure of most specimens (no matter the cover thickness). Only a little difference in capacity was discovered between 90° and 180° hooks where 180° hooks demonstrated more slip at a given force. The lead-in embedment length of the hooks was discovered to be a crucial element in the anchoring

capacity. Lastly, with increased loading it was discovered that the bar stress, which is zero at the end of the tail, increased most substantially along the curve and further increased along the straight embedded length.

(Minor and Jirsa, 1975) studied many factors affecting the performance of anchorage of hooked deformed reinforcement: the length of the bond, radius of bend, bend angle, and bar diameter. There is some slip between bars and concrete, this error was measured and used for the comparison. This research was done on 80 samples with 37 different rebar configurations. 414 MPa rebars used were having sizes of 16M, 22M, and 29M. Length and depth were variable from 305 to 406 mm with the variation of width from 203 to 305 mm for normal strength concrete. Bars were only bonded from the start of the bend to the end of the tail. Tail lengths ranged from 1.0 db to 5.8 db, while bending radii ranged from 1.6 db to 4 db for specimens with 90° hooked 16M bars. The key finding of relevance was that, given an identical bond length to bar diameter ratio, higher slip (more error) will occur at greater bend angles and smaller ratios of bend radii to bar diameter. It was advised that bars be secured with a 90° bend angle and the maximum feasible bend radius in order to reduce slide and optimize stiffness. Additionally, it was noted that with higher loading, concrete at the bend's inner radius starts to crush, which causes a loss of bond throughout the bend's outer radius which increases the demands on the parts that are still linked and puts stress inside the hook.

Similar lateral pressures were used in 1988 (Thrö et al.) pullout experiments, the bars were anchored over significantly reduced development lengths (3db). Throughout the test, they maintained a consistent ratio between the lateral pressure and the steel stress. They discovered that as lateral pressure increased, bond tension increased as well. He suggested a development length reduction factor with a cutoff of 1,160 psi that is linearly proportional to the active lateral pressure. At such number, the reduction factor cuts the development length in half. Though it should be emphasized that specimens used a short bar embedment length that may not be transferable to longer growth lengths, the results demonstrated a significantly stronger impact on bond from lateral compression when compared to prior tests.

In his research, (Mattock, 1994) investigated lateral applied pressure on U-bent bars. Mattock discovered that for bars with the smallest permitted bend diameter (6db), the anchoring capacity increased with lateral pressure. He suggested using the capacity formula $(f_n/f_{ct})^{0.7}$, where f_n is the applied lateral pressure and f_{ct} is the concrete's tensile strength.

(Ciancone, 2007) established an in-service loading condition at the hook with a C-C-T node for the strut and tie model to look into whether high-strength, corrosion-resistant steel bars may use typical hook design proportions. Results showed that bars in 93% unconfined specimens reached yield with standard hook details and development lengths prescribed by ACI 318-05.

In terms of the anchorage length for the formation and transfer of the prestress in using shape memory alloys (SMAs), (Hong et al., 2018) advised utilizing Fe-SMA strips with a minimum length of 600 mm for NSM applications, but (Fawaz and Murcia-Delso, 2020) suggested a minimum transfer length of 11db, where db is the rebar diameter, for well-confined conditions.

There are many researches and experiments done for showing the effects of bending bars to be anchored to reinforced concrete on the varying types of concrete (low, normal and high compressive concrete strength) and the bond characteristics such as in: (Hadi, 2008), (Bamonte and Gambarova, 2007), (Choi et al., 2015) and (Fareed, 2014).

Chapter 3: Modeling

3.1 General

A previous laboratory experiment was done by Higgins et al(Higgins et al., 2017). A new simulation will be developed for beams used in the mentioned paper using Abaqus "Finite Element" software and verify results obtained from the software model with laboratory data to have the ability to study new points and develop the model to examine different parameters.

3.2 Geometry of Beam

The beam used to verify the data got from Abaqus with the real data mentioned in the paper (Higgins et al., 2017) was a full-scaled T-shaped beam with a long of 5.49 m having a deck of size (165x914) mm. The stem was (229x749) mm in one half of the specimen and transitioned to be (321 x 1048) mm through horizontal and vertical tapering after the middle of the beam long with reinforcement and two (25×25) mm Titanium bars located as seen in the following figures:

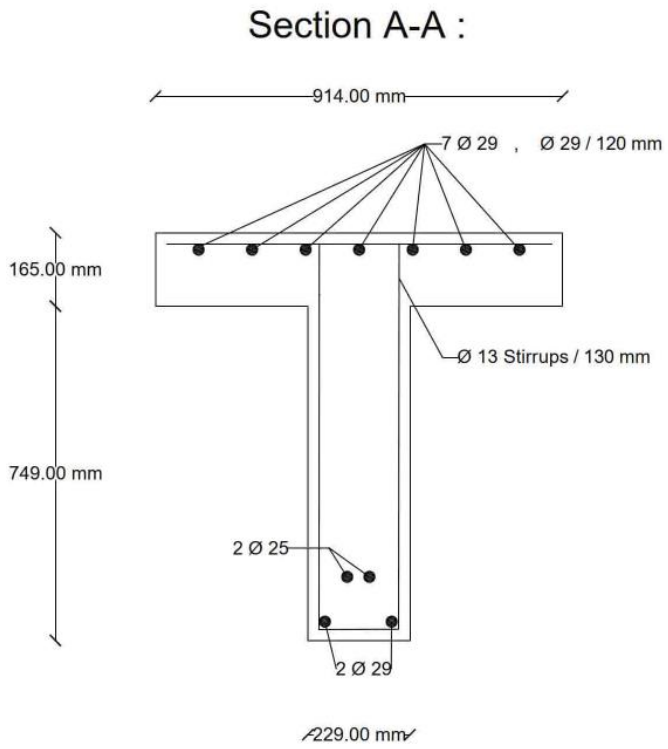

Figure 4: Section A-A in beam

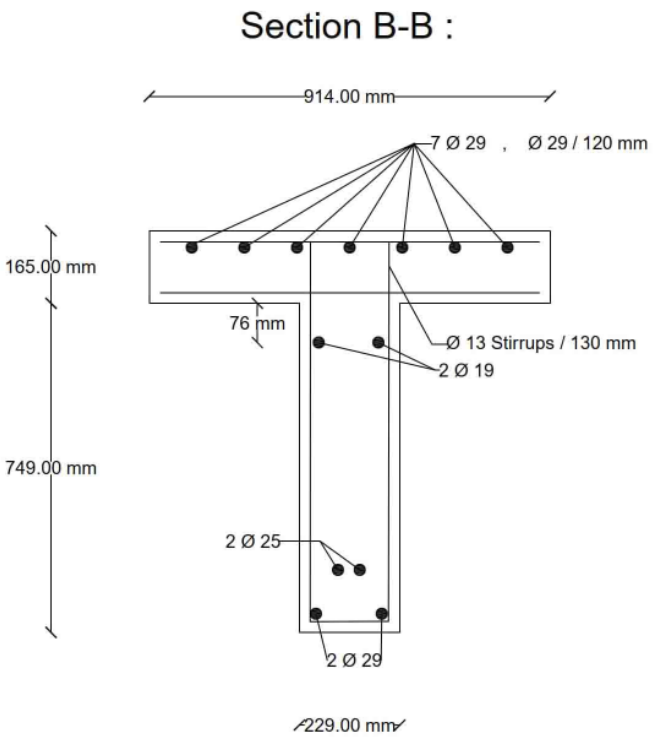

Figure 5: Section B-B in beam

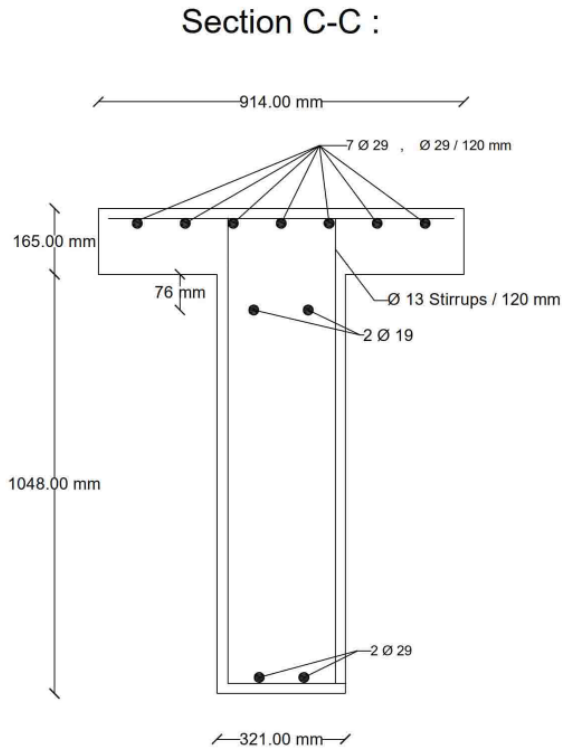

Figure 6: Section C-C in beam

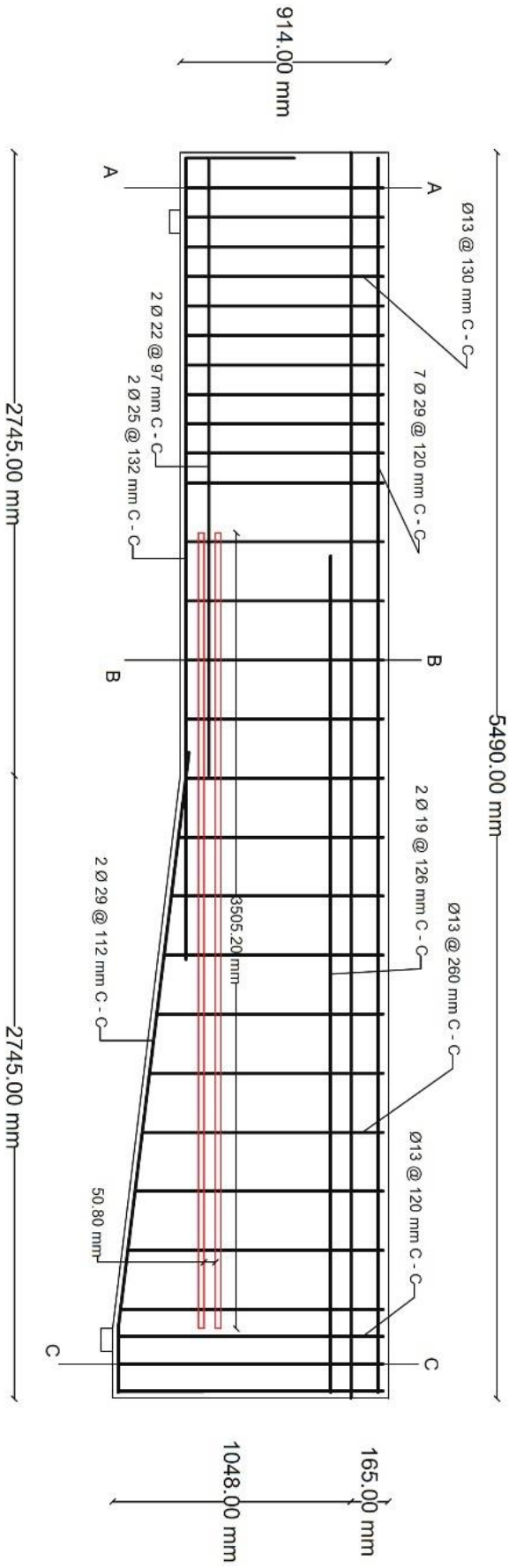

Figure 7: Elevation View

3.3 Specifications of materials used

The modulus of elasticity of steel bars is fixed to be 200,000 MPa with a Poisson's Ration of 0.3. For the Titanium alloy bars they were fixed to be 105,000 MPa and 0.27 for the modulus of elasticity and Poisson's Ratio respectively. The following table illustrates the other properties of the materials used (all are in MPa):

Table 2: Materials Properties

Concrete Compressive Strength	**Steel**										**SMA**	
	Phi 29		**Phi 25**		**Phi 22**		**Phi 19**		**Phi 13**		**Titanium**	
	fy	fu	fy	fu	fy	fu	fy	fu	fy	fu	fy	fu
23.1	432	703	438	773	450	721	434	733	346	549	1000	1090

TiABs are having a thermal expansion coefficient which is very close to coefficients of steel and concrete, these coefficients are illustrated below:

Table 3: Thermal expansion coefficients

Material	**Thermal expansion coefficient**
Steel	12×10^{-6} /ºC
Concrete	10×10^{-6} /ºC
TiABs – Ti6Al4V (0-100) ºC	9×10^{-6} /ºC

It is particularly challenging to model the constitutive behavior of concrete using elastic damage models or elastic plastic laws. The irreversible strains cannot be described by an elastic damage model. The following figure (a) illustrates how a zero stress and zero strain result in an inflated damage value. However, if the elastic plastic relation is used, the unloading curve will follow the elastic slope, which will cause the strain to be overestimated (b). The constitutive behavior of experimental unloading can be captured by the Concrete Damage Plasticity (CDP) model, which integrates these two techniques as showed in part (c) of the figure below as mentioned by (Jason et al., 2004). Two primary failure methods are assumed in this model: concrete crushing and tensile cracking. Plastic strains that are equivalent to those of tensile and compressive forces govern how the yield surface expands.

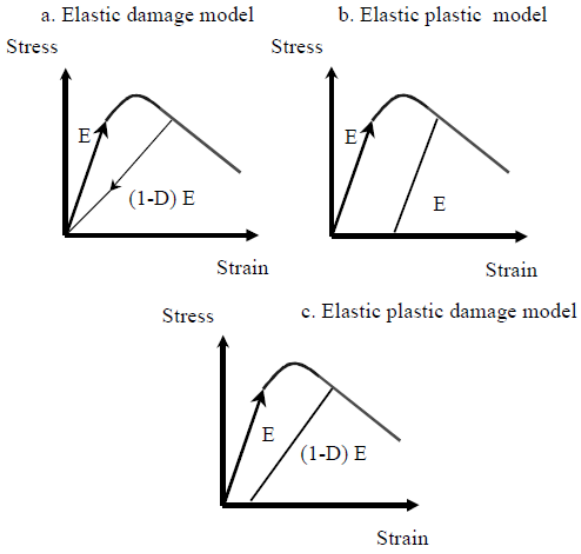

Figure 8: Unloading response of different models (Jason et al., 2004)

As seen in figure below, the elastic stiffness of the concrete model appears to be compromised or degraded, which tends to reduce its unloaded response. Two damage factors, d_t and d_c, which have values ranging from zero to one, describe how the elastic stiffness degrades on the strain softening branch of the stress-strain curve. One symbolizes complete loss of strength, while zero denotes completely intact material (ABAQUS_Manual, 2008). E0 is the initial (undamaged) elastic stiffness of the material and $\varepsilon_c^{\sim pl}$, $\varepsilon_t^{\sim pl}$, $\varepsilon_c^{\sim in}$, $\varepsilon_t^{\sim in}$ are compressive and tension plastic strain, compressive and tensile inelastic strain respectively. In Equations (1) and (2), the stress-strain relationships under uniaxial tension and compression are taken into consideration.

Equation 1

$$\sigma_t = (1-d_t) \cdot E_0 \cdot (\varepsilon_t - \varepsilon_t^{\sim pl})$$

Equation 2

$$\sigma_c = (1-d_c) \cdot E_0 \cdot (\varepsilon_c - \varepsilon_c^{\sim pl})$$

By using tension stiffening in the concrete modeling to simulate load transmission across the fractures through the rebar, interface behavior between rebar and concrete is modeled. Additionally, strain-softening behavior for cracked concrete can be modeled using tension stiffening. As a result, the CDP model needs to define tension stiffening. In accordance to the ABAQUS User Manual from 2008, we can use the post failure stress-strain relation or the fracture energy cracking criterion to describe tension stiffening.

(Hillerborg et al., 1976) stated that there is a mesh sensitivity problem when cracking failure in not distributed evenly. This phenomenon exists when there is no reinforcement in significant regions of the model. To overcome this unreasonable mesh sensitivity problem Hillerborg's (1976) fracture energy approach can be used instead of post failure stress-strain relation.
This method takes as a material property the amount of energy (G_F) needed to open a unit area of crack. As a result, the stress-displacement reaction rather than the stress-strain response best describes the brittle behavior of concrete. This method can be described by specifying the post failure stress versus the associated cracking displacement, as illustrated below.

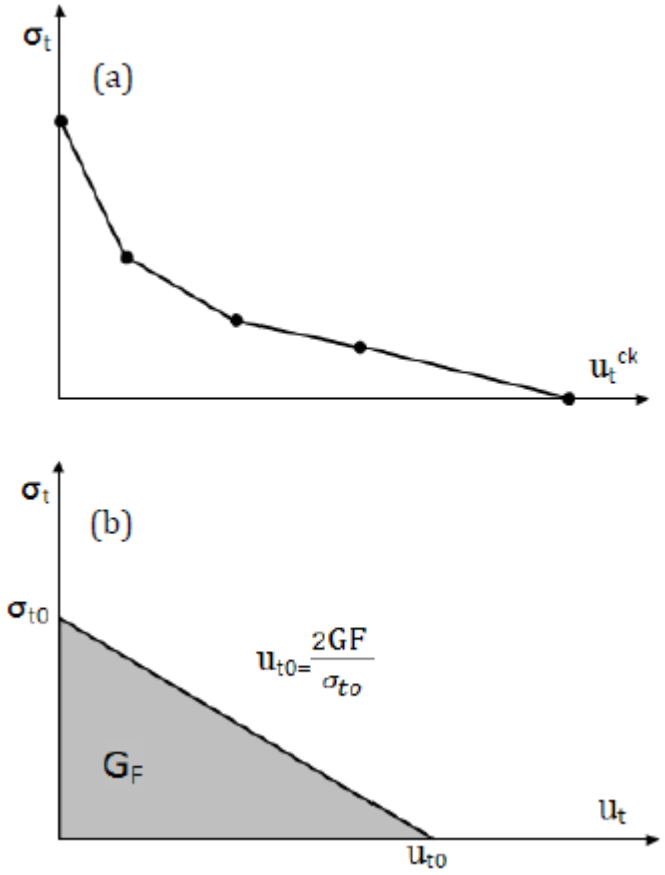

Figure 9: Fracture energy strategy using the post failure stress-strain relationship (Sümer and Aktaş, 2015)

GF can also be applied directly as a material property. But in this instance, it is assumed that strength declines linearly after fracture. Using Equations (3) and (4), ABAQUS automatically determines both plastic displacement values from the CDP perspective.

Equation 3

$$u_t^{pl} = u_t^{ck} - [dt\ (\sigma_t I_0)]/[(1-dt)\ .\ E_0]$$

Equation 4

$$\varepsilon_c^{\sim pl} = \varepsilon_c^{\sim in} - (d_c \,.\, \sigma_c)/[(1-d_c) \,.\, E_0]$$

These equations lead to the following "effective" definitions of tensile and compressive cohesion stresses ($\bar{\sigma_t}$,$\bar{\sigma_c}$):

Equation 5

$$\bar{\sigma_t} = \sigma_t\,(1-d_t) = E_0(u_t - u_t^{pl})$$

Equation 6

$$\bar{\sigma_c} = \sigma_c\,(1-d_c) = E_0(\varepsilon_c - \varepsilon_c^{\sim pl})$$

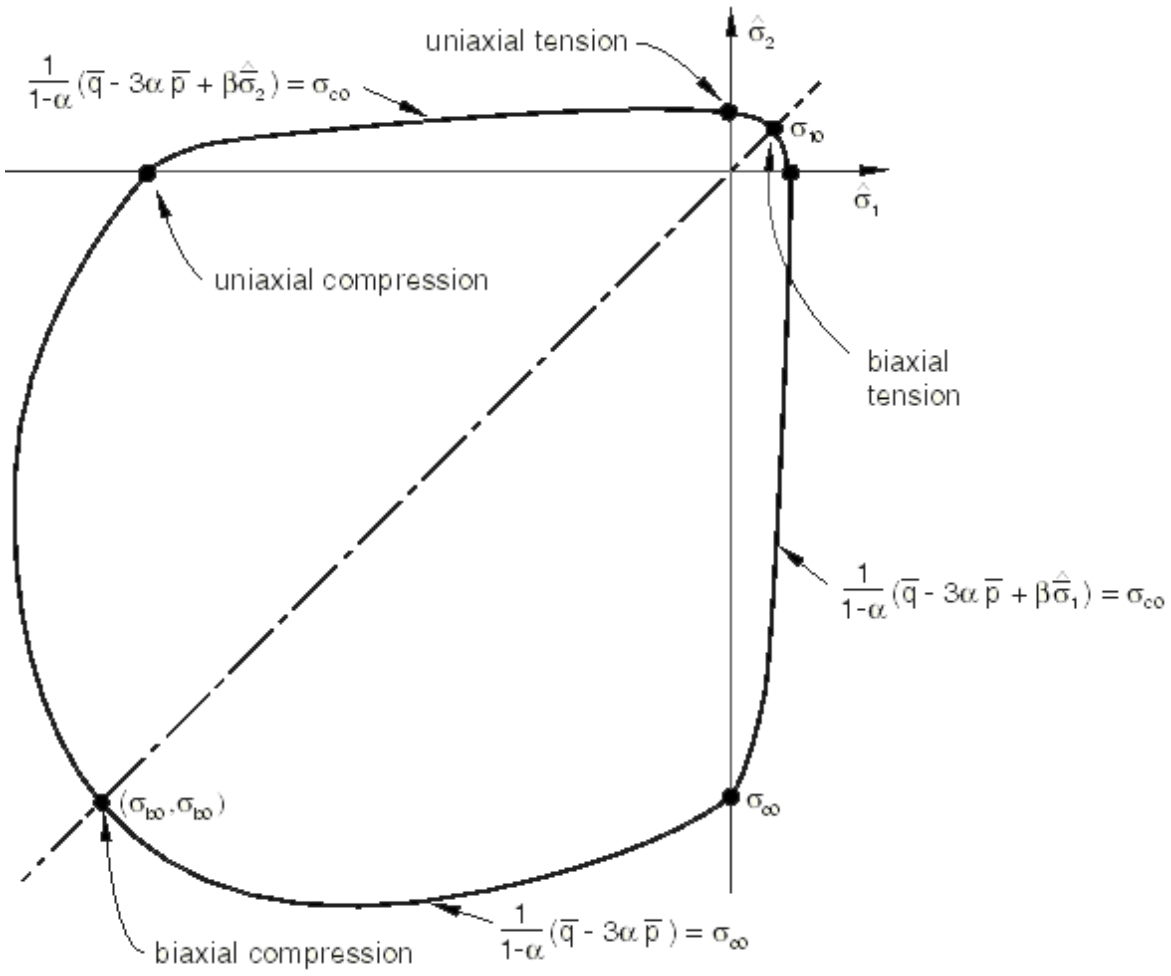

Figure 10: Biaxial yield surface, CDP Model (ABAQUS_Manual, 2008)

The Titanium Alloy bars were considered to be fully bonded with concrete without using epoxy due to the very small impact of the epoxy and modelling become easier and saving for the time.

The concrete compressive strength was obtained from the compressive test while the procedure of the experiment. The concrete curves were not given and our research is not about calculating and generating CDP model in Abaqus, so we shall use Elkady's tool(Elkady, 2023) to obtained data from depending on the Chinese Code (GB 50010-2010) as follows:

Table 4: Elkady's Tool Data for 23.1MPa Concrete

f_{cu} (MPa)	**E** (MPa)	ε_c	f_{tu} (MPa)
23.1	22094	0.00152	0.95

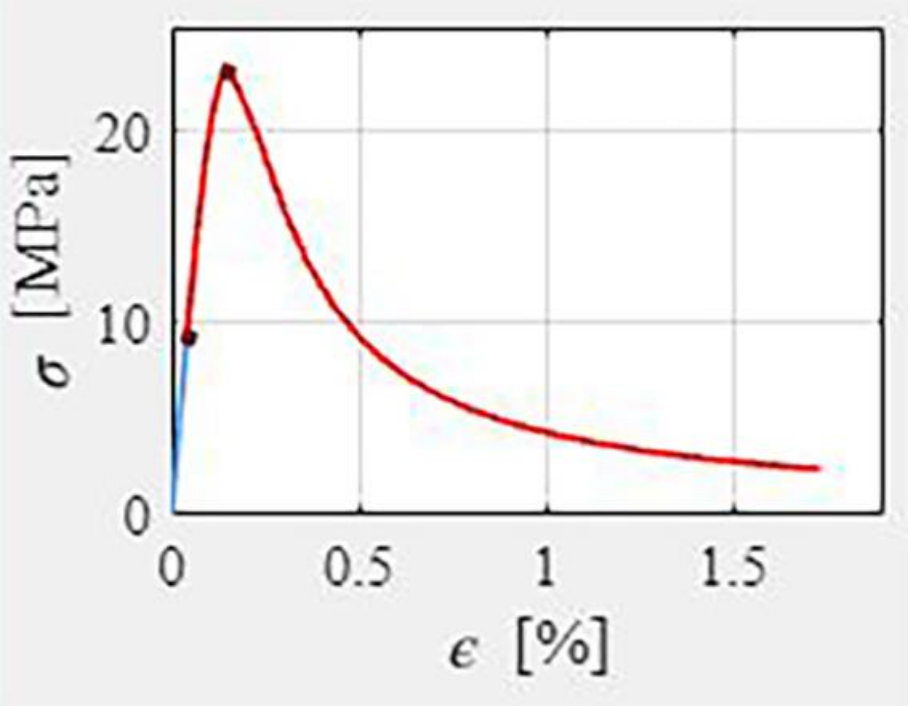

Figure 11: Compression Stress-Strain Curve for CDP (Elkady, 2023)

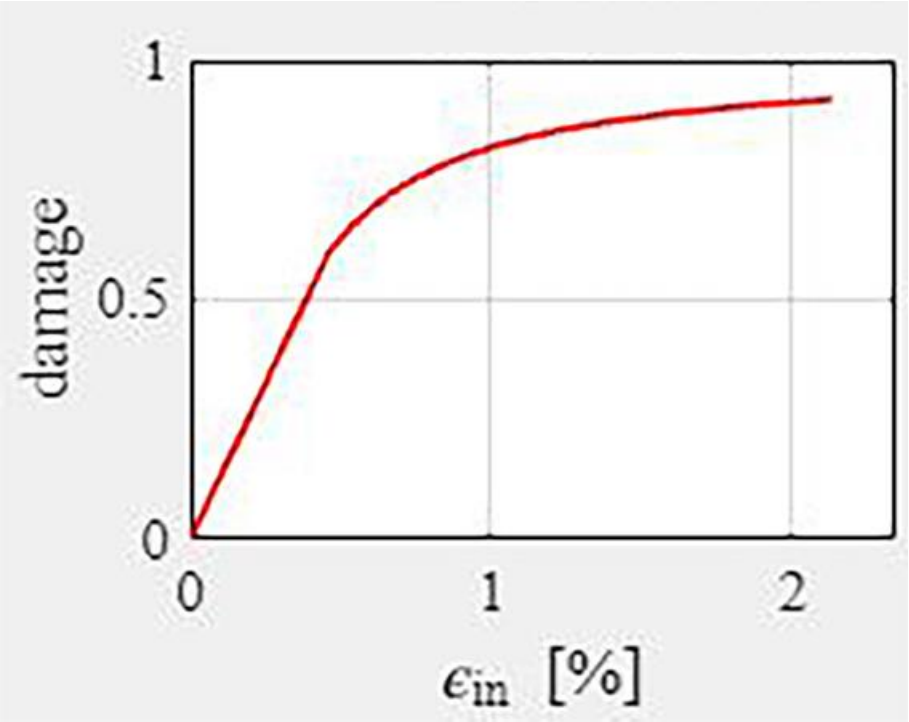

Figure 12: Compression Damage Curve for CDP (Elkady, 2023)

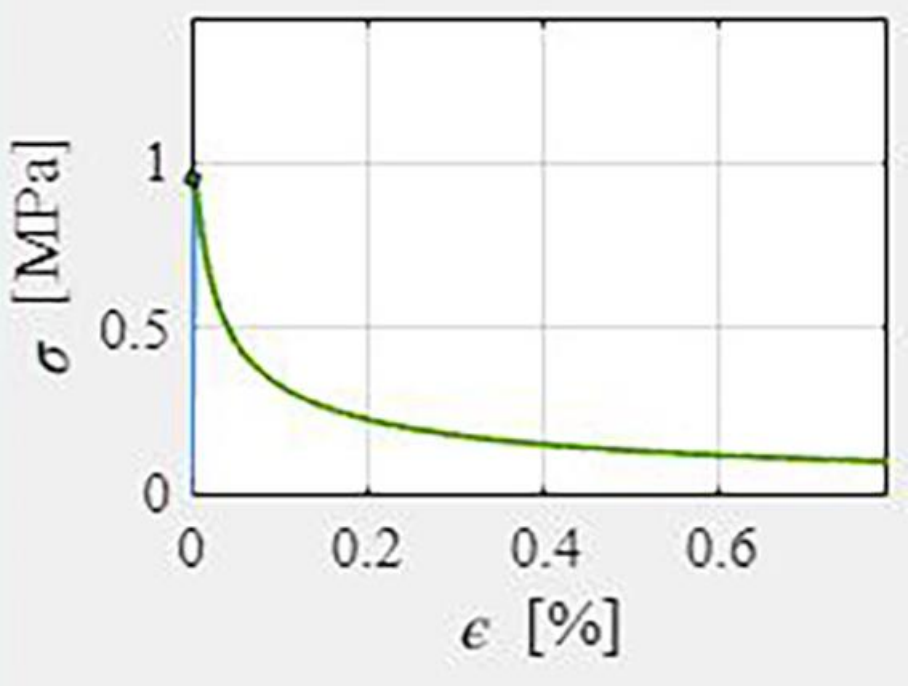

Figure 13: Tension Stress-Strain Curve for CDP (Elkady, 2023)

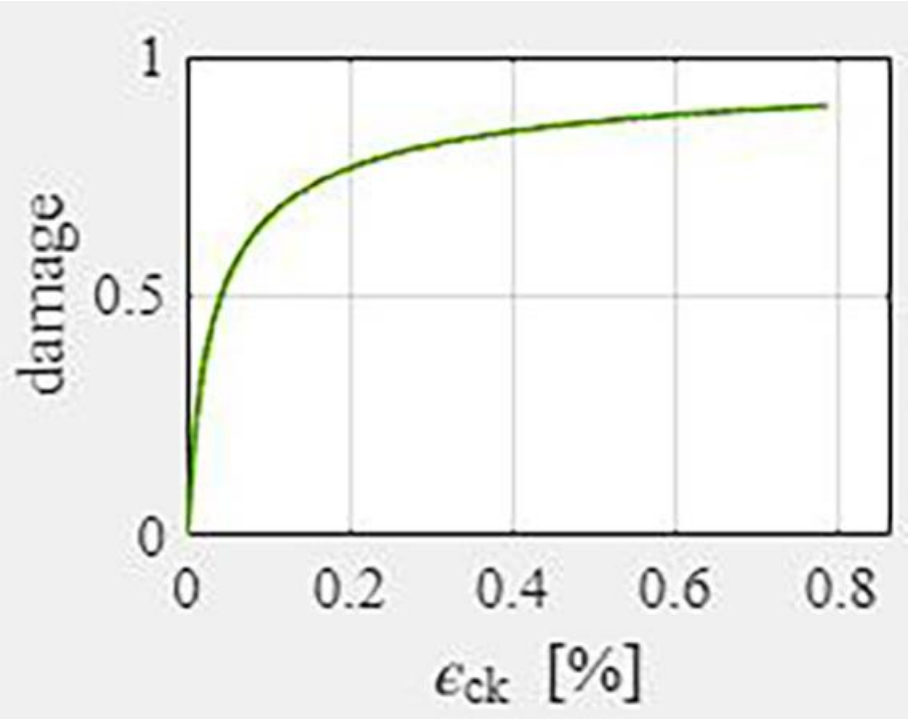

Figure 14: Tension Damage Curve for CDP (Elkady, 2023)

Table 5: Plasticity parameters used for Concrete Damage Plasticity

Dilation Angle	Eccentricity	fb0/fc0	K	Viscosity Parameter
36	0.1	1.16	0.677	0.002

The TiABs' stress-strain curve was given in the paper (Higgins et al., 2017) as in the figure below:

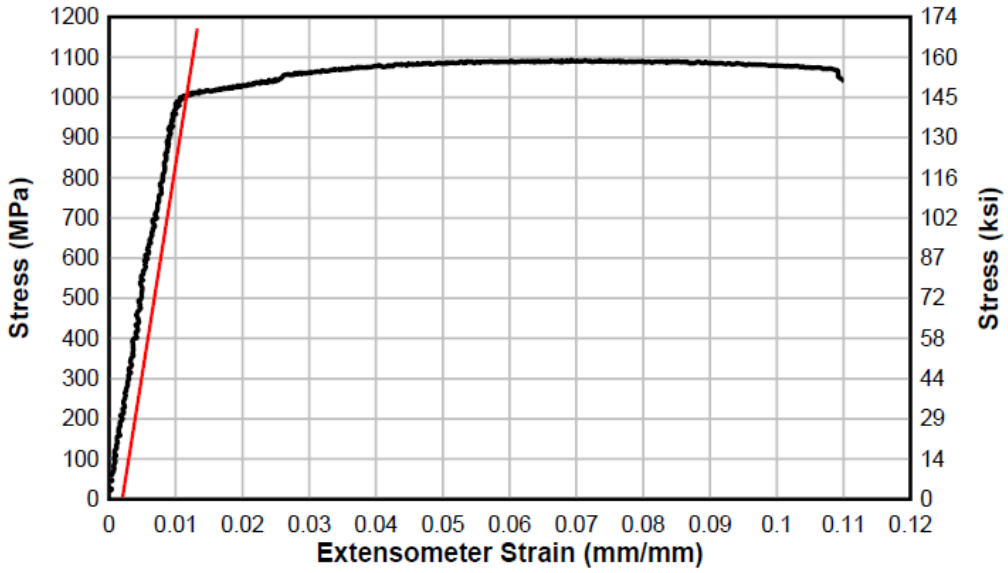

Figure 15: Uniaxial tension stress-strain curve for Titanium alloy bar with special surface treatment. (Higgins et al., 2017)

Figure 16: View of flexural specimen in Experimental test setup (Higgins et al., 2017)

3.4 Research hypothesis

This research was done while considering the following points which are based on the previous data taken from literature review and believed that will not affect the results given:

- The beam was supported by two steel plates on the bottom of the beam, one was acting as roller and the other one was acting as a pin support. And two upper steel plates were fixed to transfer the load to the beam. This method is known as four-point load test.
- All the four steel plates are completely fastened to beams to ensure that loads are transferred completely.
- Load applied on beams was increasing statically.
- Static loads were used to investigate the results which ignore the effects of the dynamic load.
- Reinforcement (steel and GFRP) was considered to be perfectly bonded to concrete with no slipping by taking into account the required development length and making the reinforcement passes through the support points. Moreover, all reinforcement parts were modeled to be embedded region constraints.
- From literature review and the past experiments and Finite Element Analysis, epoxy has no significant effect on the study results. So, epoxy can be neglected and considering Titanium is fully bonded to concrete.

3.5 Building and verification of model data

To start this study, beams should be simulated started by creating parts with the predefined dimensions and adding materials' definitions, then creating new sections by assigning every part and the corresponding material. There is an additional part called "Steel Plate" was added to apply the load on and to support the beam. To make sure that this part will not affect the results, modulus of elasticity of this part was assigned as 10 times the normal steel's modulus to be 2,000,000 MPa with relatively small dimensions. Assembling the parts together is a very important step to finalize with the model shaped as the experiment. There were two load points each with distance 305 mm from the middle of the beam with two supports, a roller and a pin.

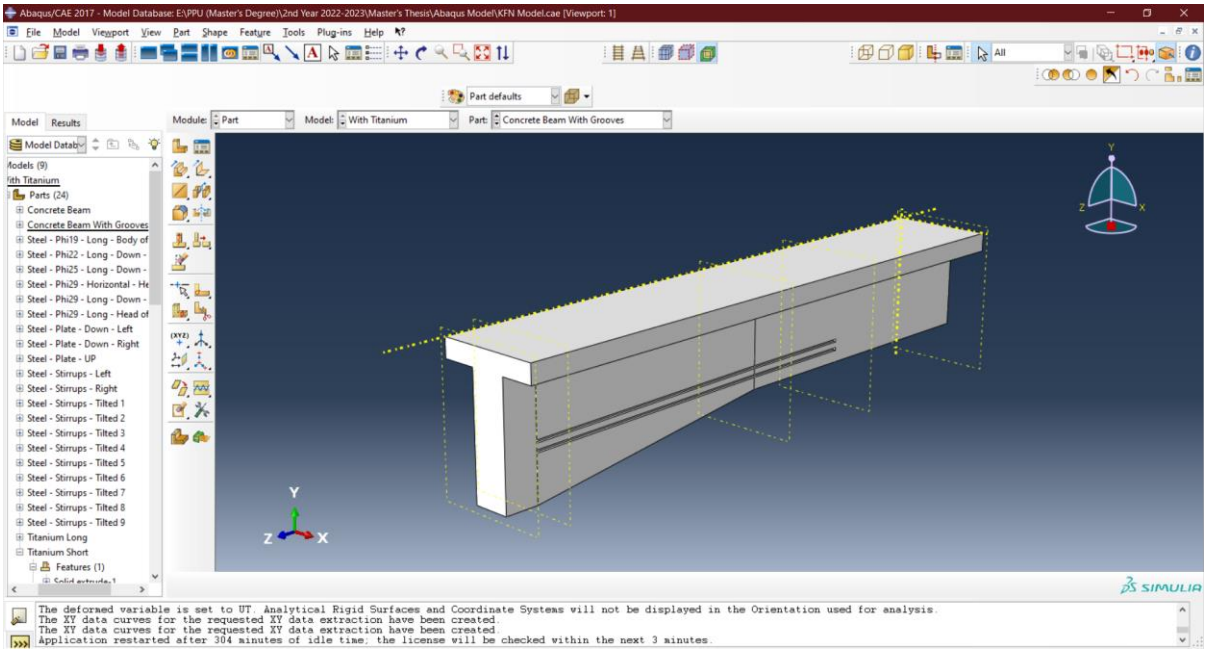

Figure 17: Parts menu and showing Concrete Beam with grooves

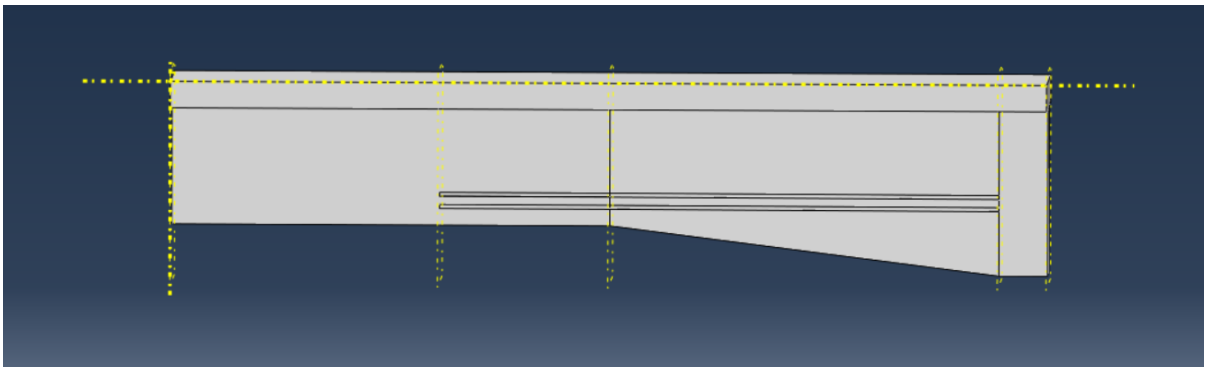

Figure 18: Second side of beam

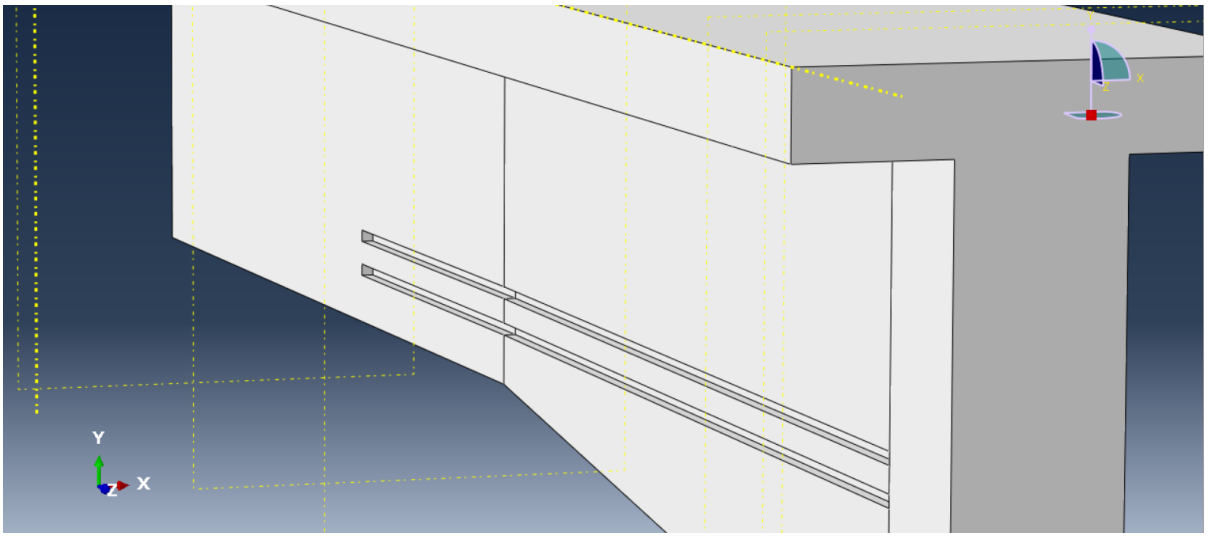

Figure 19: Illustrating Grooves on the two sides of concrete

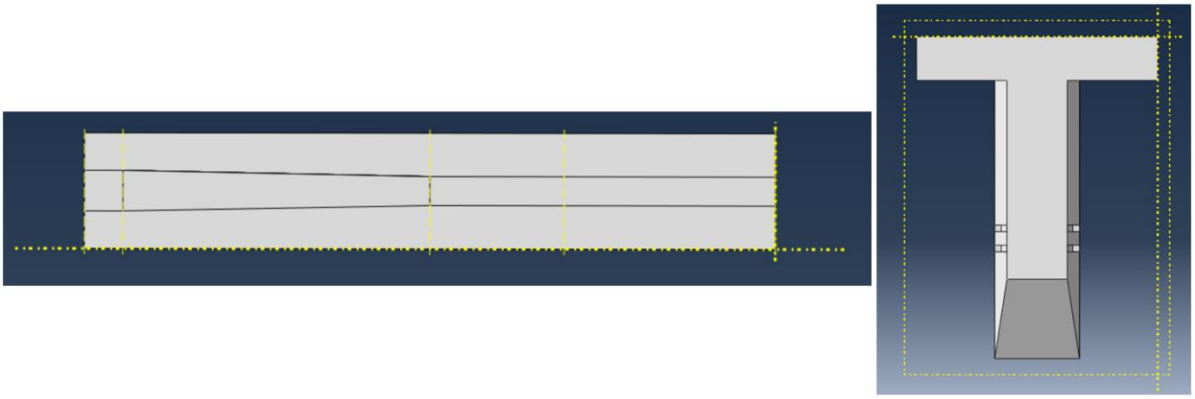

Figure 20: showing the difference in sizes between two sides of beam

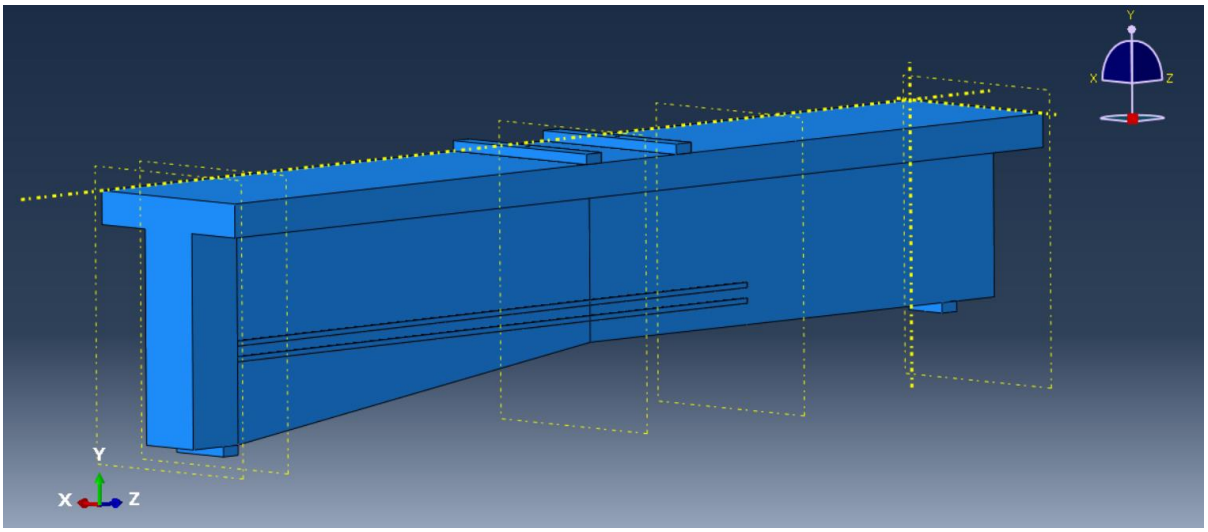

Figure 21: The assembled shape for the beam

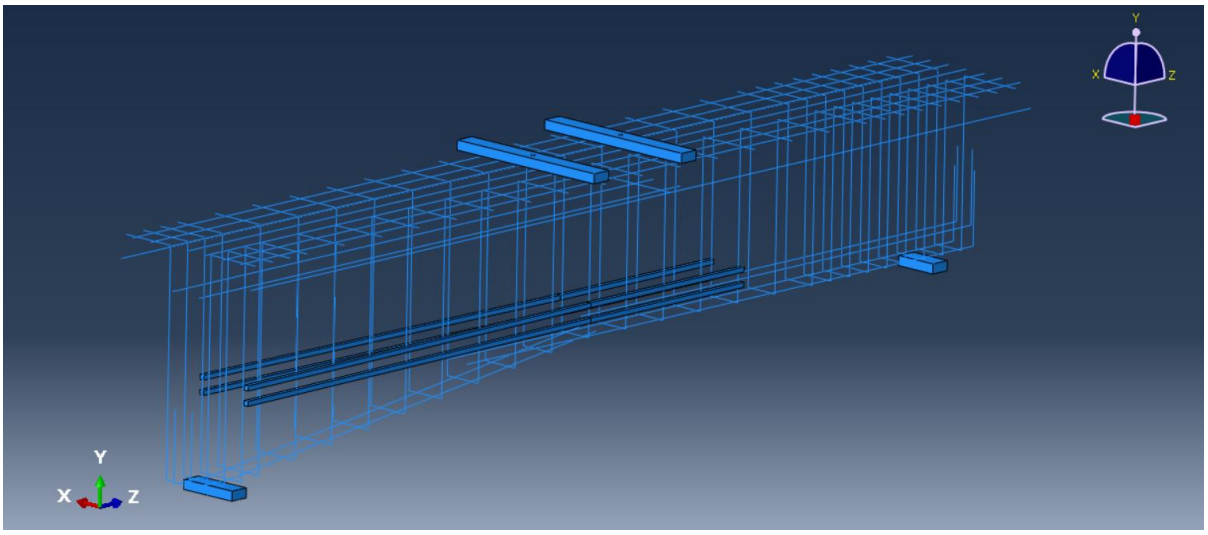

Figure 22: Showing the reinforcement (steel+TiABs)

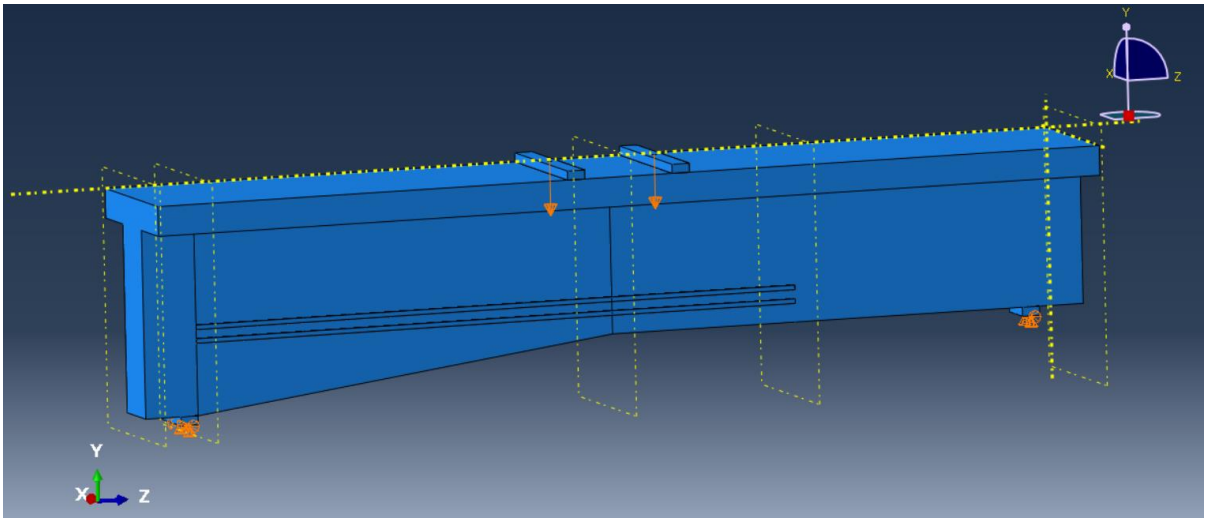

Figure 23: Load and supports' locations

To start the Finite Element (F.E) analysis, all elements should be meshed so each element is divided to very small parts to study the behavior of each part alone.

Table 6: Elements' mesh types

Material	Family	Description	Code	Notes
Concrete	3D Stress	8-node	C3D8R	-
Concrete with Grooves	3D Stress	10-node	C3D10	Meshed as tet
Steel Plates	3D Stress	8-node	C3D8R	-
Steel Reinforcement	Truss	2-node	T3D2	Wire / Embedded
SMA (Titanium)	3D Stress	8-node	C3D8R	-

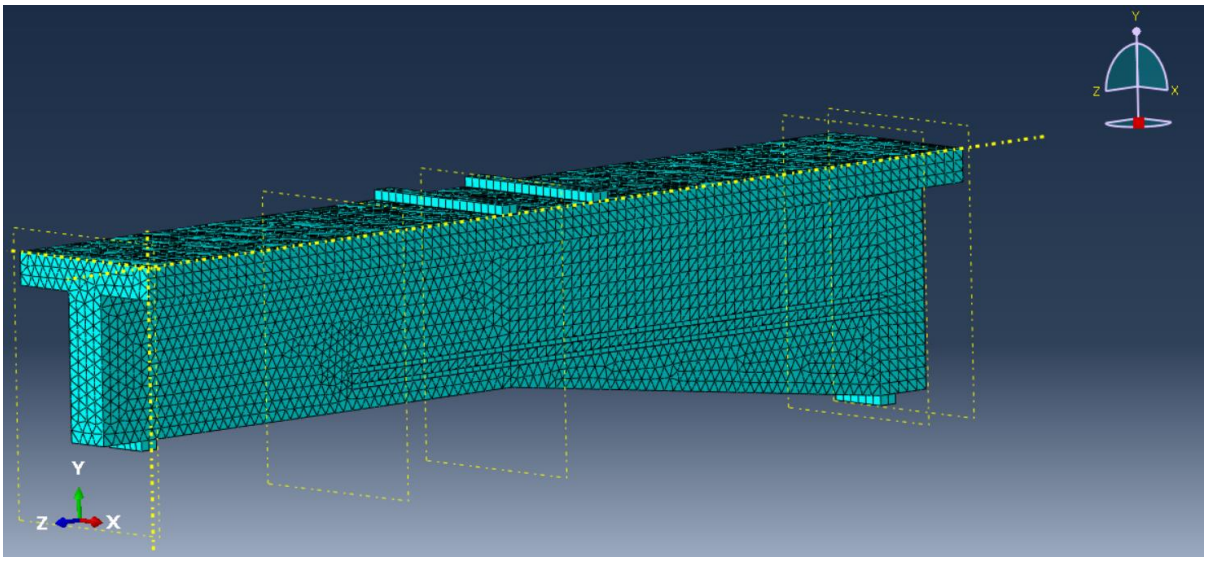

Figure 24: Meshing the whole model

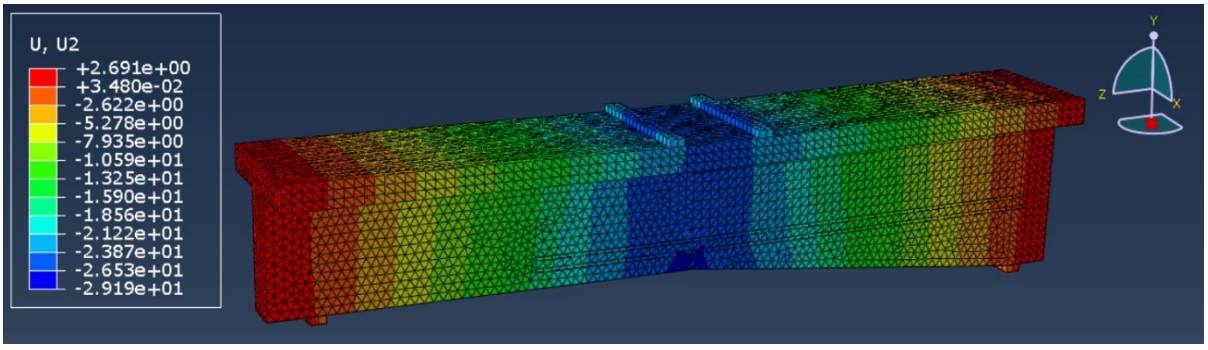

Figure 25: With Titanium Model - U2 (Vertical Displacement)

`

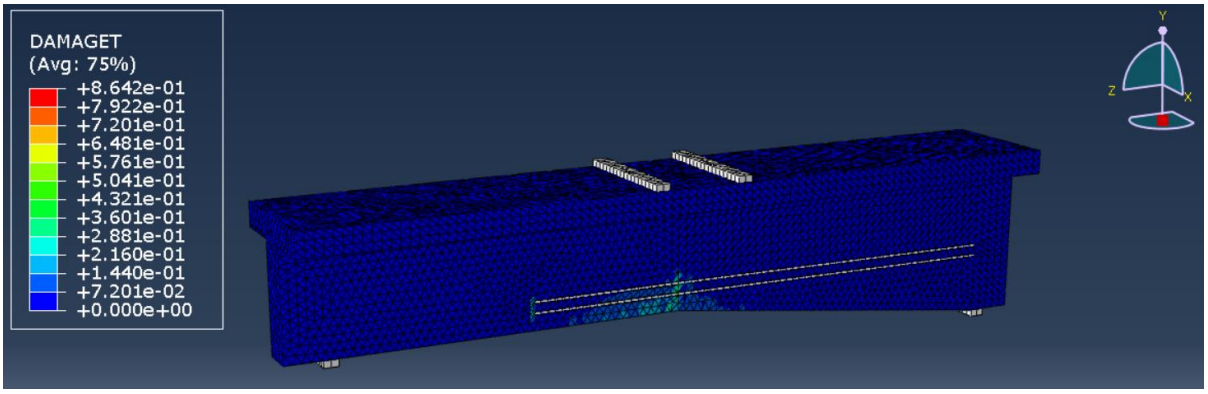

Figure 26: With Titanium Model - First Tension Crack

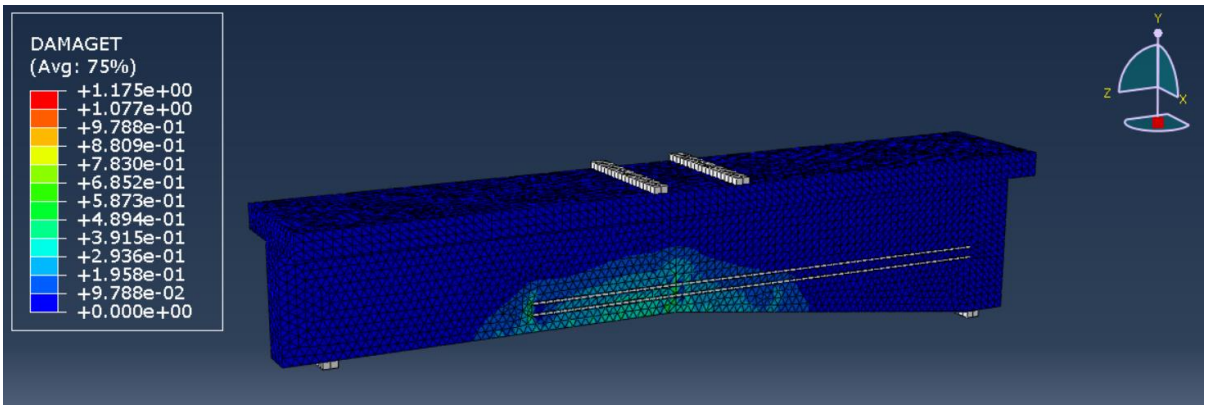

Figure 27: With Titanium Model - Cracks' Propagation (1)

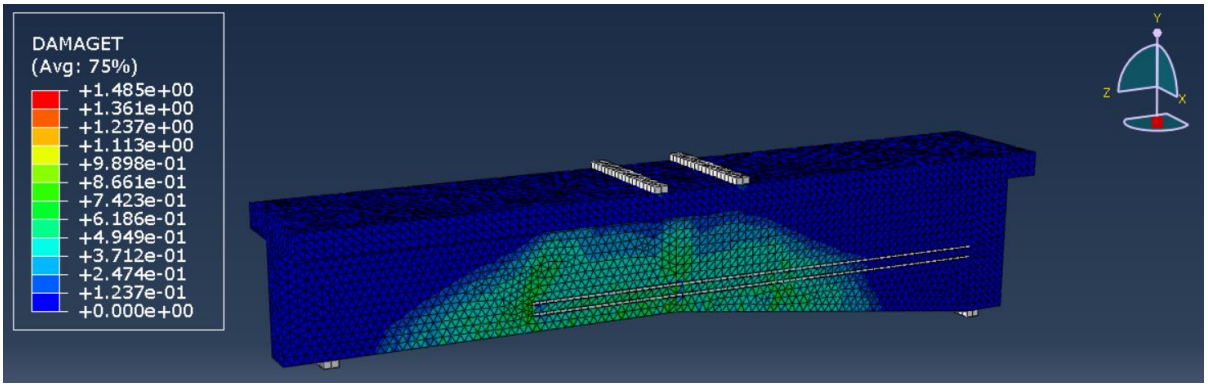

Figure 28: With Titanium Model - Cracks' Propagation (2)

As noticed from figures above, cracks firstly appeared in the mid-span of the beam which permits the Titanium to start to act as tension reinforcement in parallel with steel.

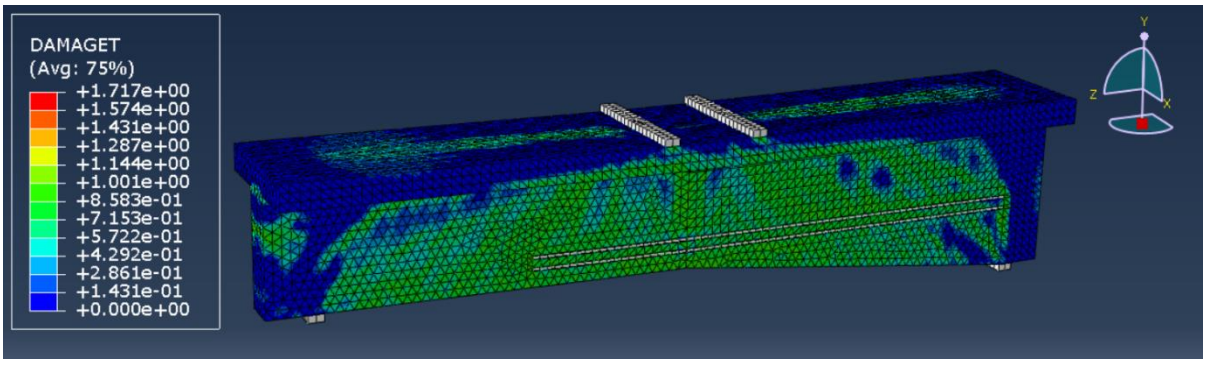

Figure 29: With Titanium Model - Damage Tension

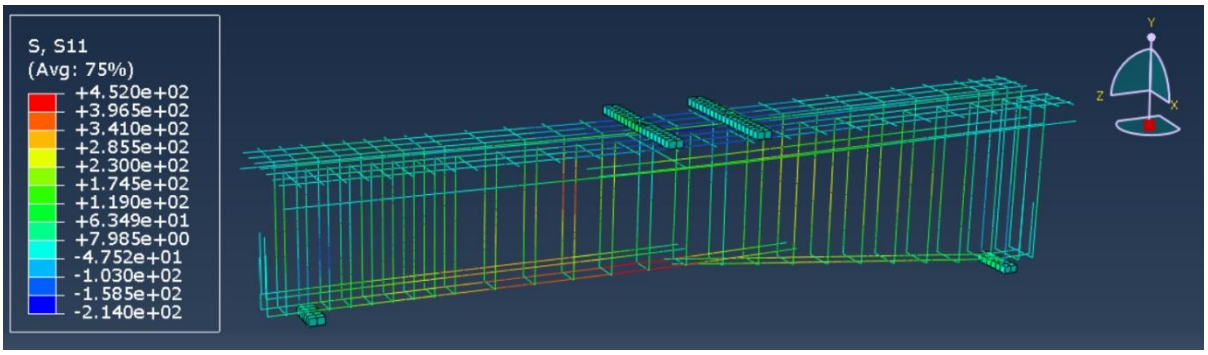

Figure 30: With Titanium Model - Steel Normal Stress

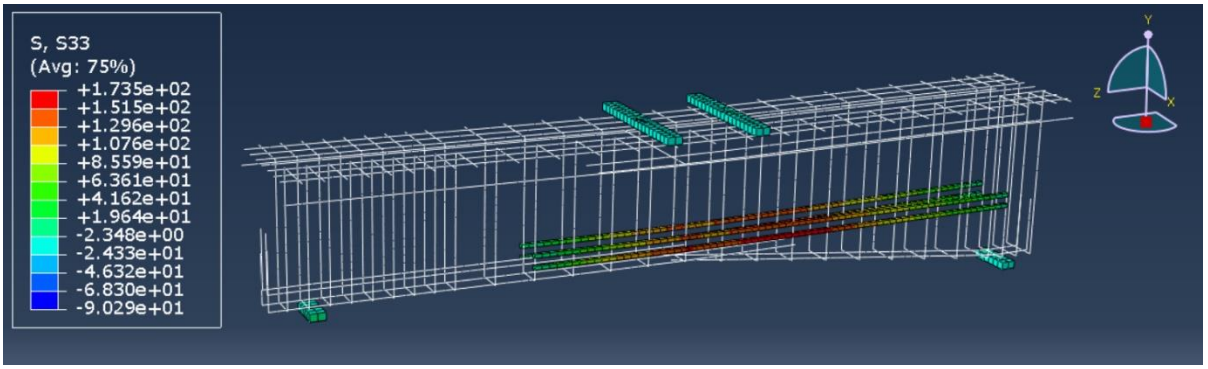

Figure 31: With Titanium Model - S33 for Titanium Bars

The figure below shows the relation between moment and displacement on the midspan of the beam (the converting point of the size of the beam) both given by the paper (Higgins et al., 2017) and obtained from the Abaqus software. Abaqus model showed a very similar behavior and reaction of the experimental beam. Maximum moment capacities were approximately 748kN.m and 711kN.m in Abaqus model and experiment respectively at midspan displacement of 26.5mm. The difference of the maximum moment capacity obtained from Abaqus is incrementation about 5% which is acceptable percentage.

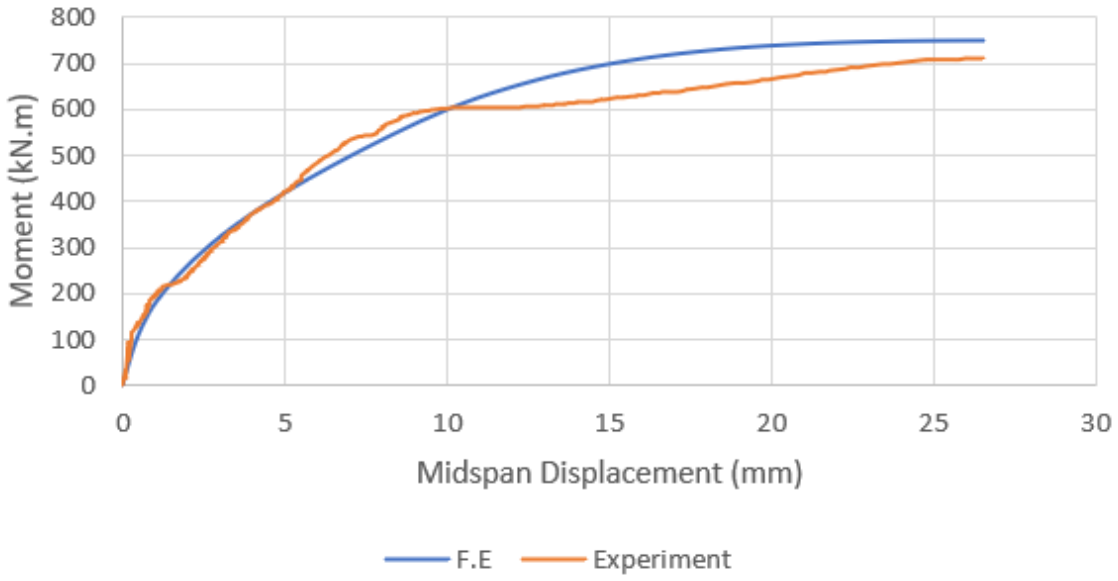

Figure 32: Moment - Displacement Curve for original model

A new model was made to be as control to compare the result of the parametric study with. This model was not containing any Titanium bars. Just containing reinforced concrete using steel bars.

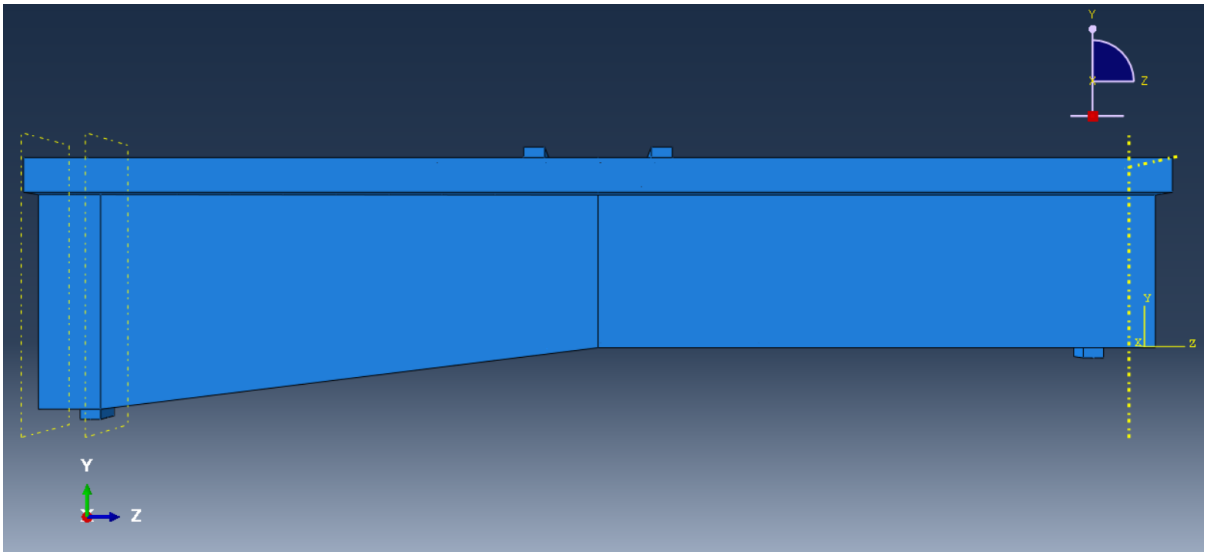

Figure 33: Side view for the control beam (without Titanium)

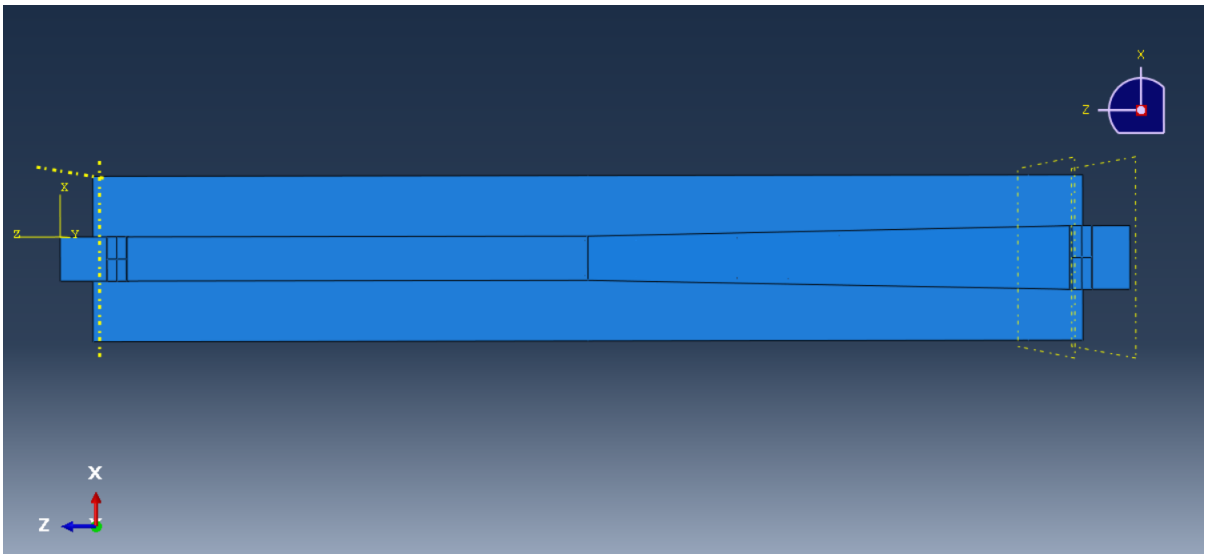

Figure 34: Bottom view for the control beam (without Titanium)

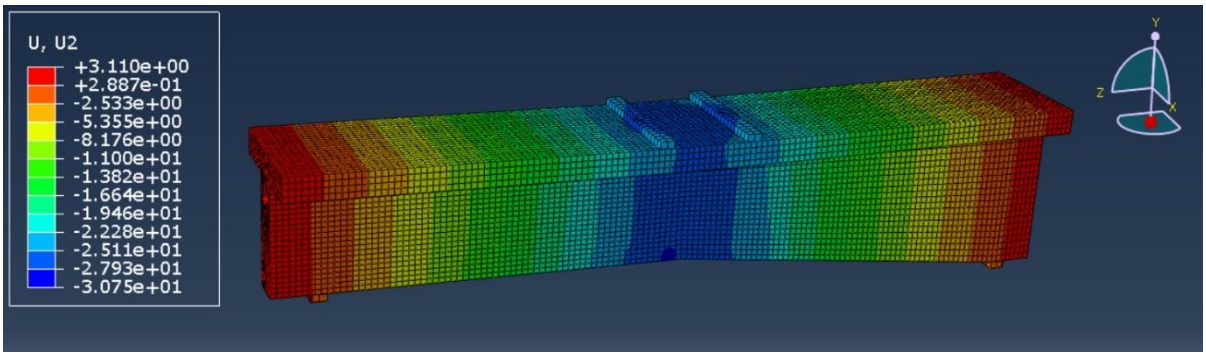

Figure 35: Without Titanium Model - U2 (Vertical Displacement)

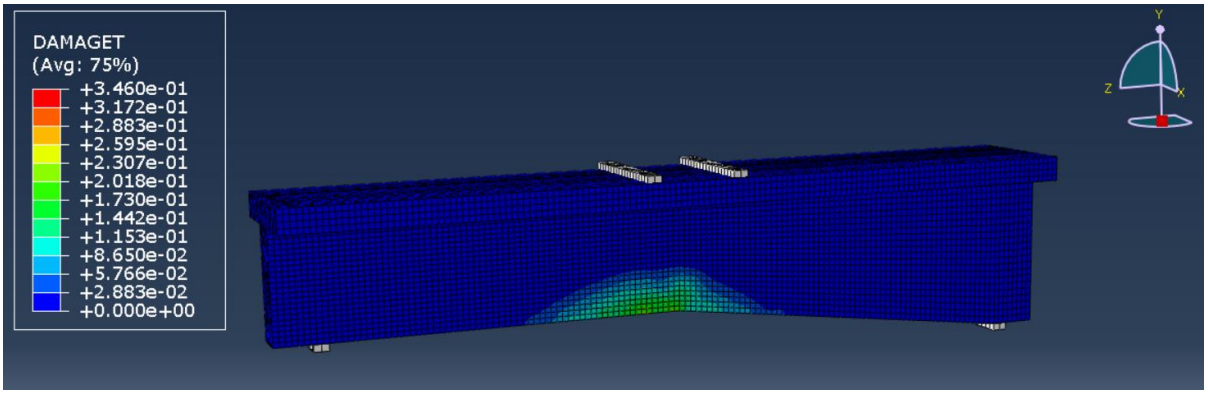

Figure 36: Without Titanium Model - First Tension Crack

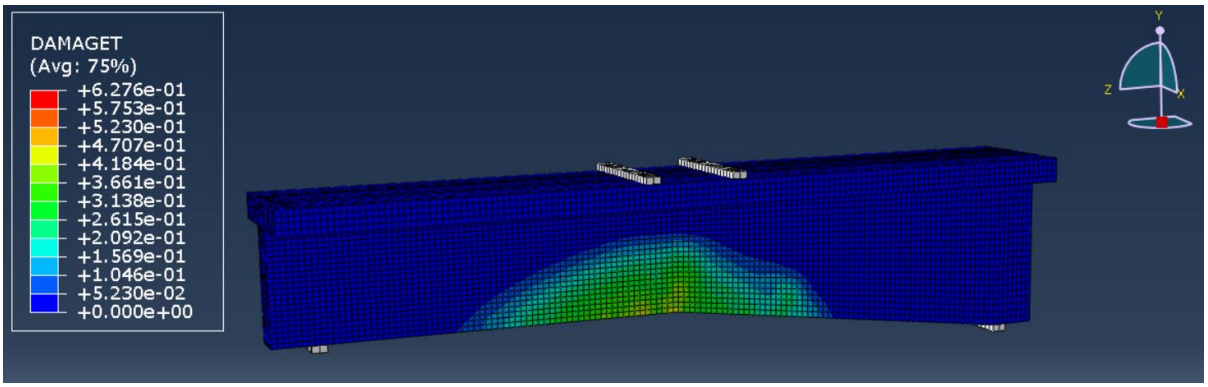

Figure 37: Without Titanium Model - Cracks' Propagation

The tension damage in model without Titanium is propagated faster and larger than the tension damage appeared in model with the usage of Titanium bars.

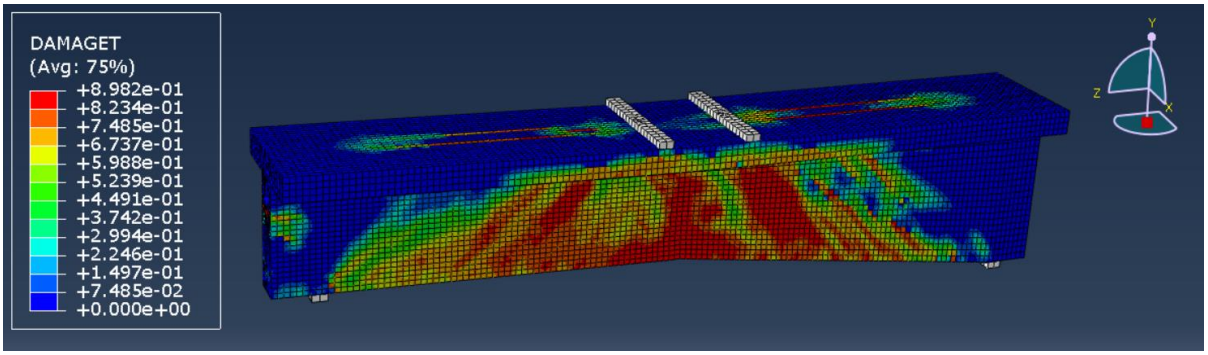

Figure 38: Without Titanium Model - Damage Tension

As Finite Element showed, the values in DAMAGET are approximately close for with and without Titanium models. But the difference will be best shown in the strength curve.

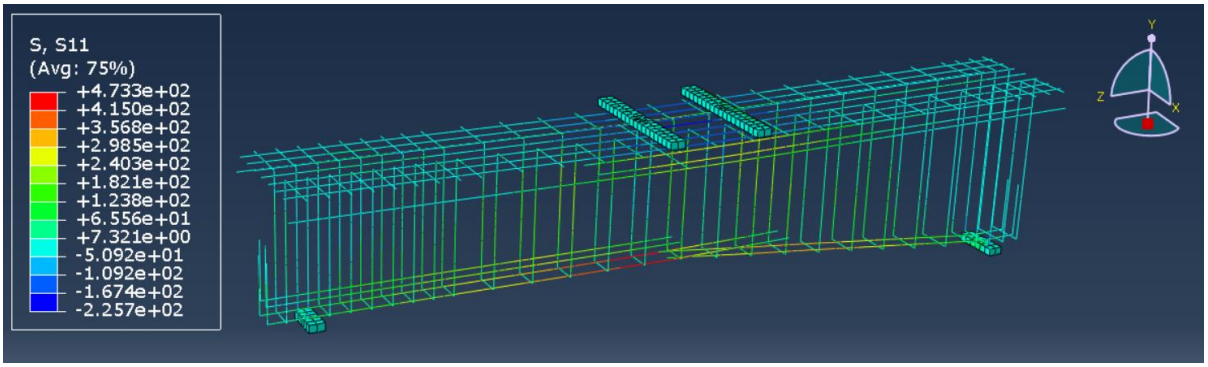

Figure 39: Without Titanium Model - Steel Normal Stress

This control beam showed a maximum moment capacity of 536 kN.m at the midspan displacement of 26.5 mm. Using Titanium alloy bars - like in the previous model - can increase the maximum moment capacity up to 748 kN.m as shown in results from Finite Element "Abaqus", which means a development of more than 39% while maintaining the midspan displacement.

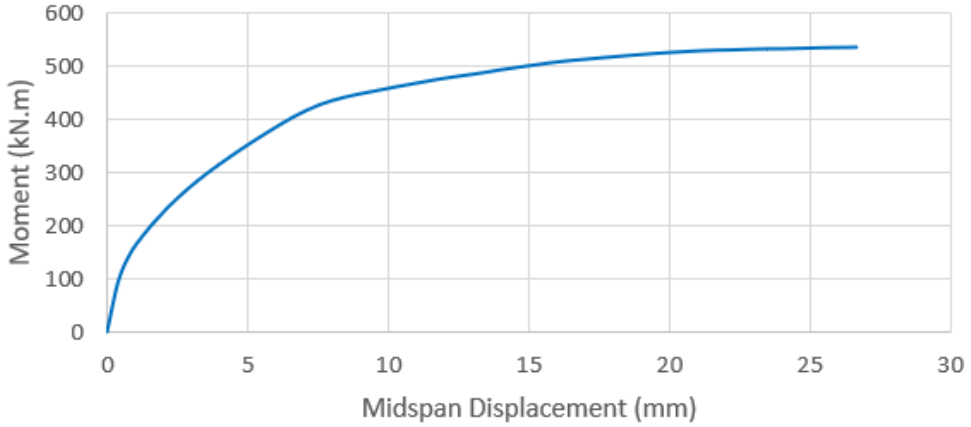

Figure 40: Moment-Displacement curve for the control beam (without Titanium)

3.6 Parametric study

Parametric study is conducted to investigate the behavior of R.C beam strengthened by SMA (TiAB) in different cases. This study will be done while fixing properties of the whole model and changing some parameters. These parameters are chosen due to the easy of the application and implanting SMA near the surface of beams without affecting the structural design to explore the best method, location, and the number of Titanium bars used to strengthen T-beam with having a transitional point in which the T-beam becomes larger as follows:

3.6.1 Strengthening beam from bottom

The Titanium bars applied on the bottom of the beam. There are 3 models developed in this area:

3.6.1.1 Strengthening beam with one bar

The Titanium is limited to be one bar on the bottom side and with the same dimensions of the original beam. The bar is centered as illustrated in the following picture:

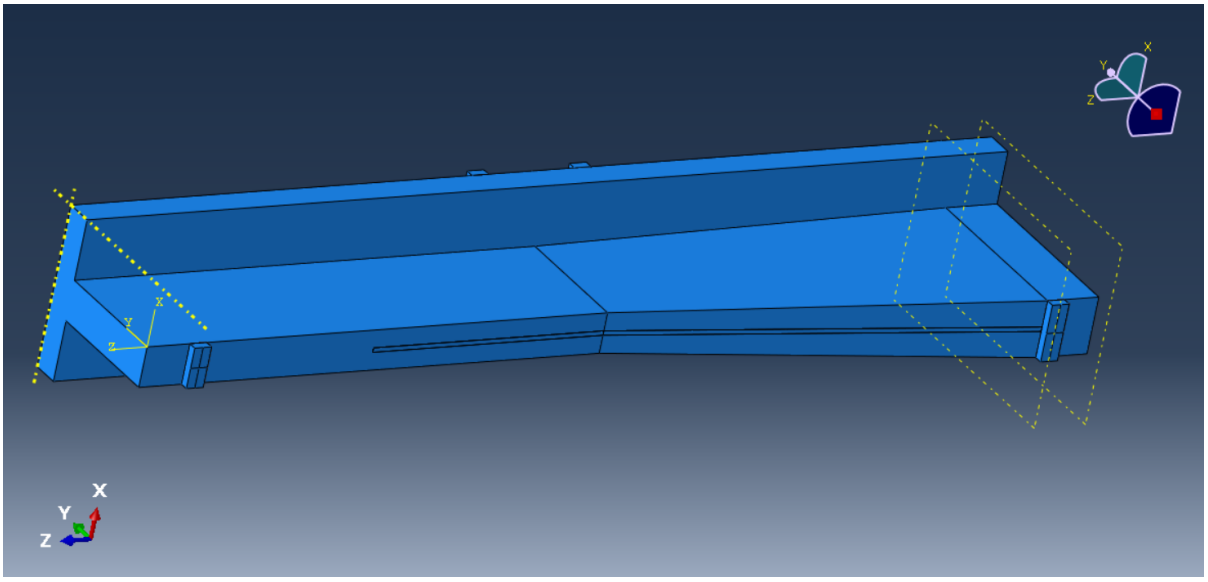

Figure 41: With Titanium-1BG Model - Bottom

3.6.1.2 Strengthening beam with two bars

There is another Titanium bar added to the beam to obtain a total of two bars on the bottom side. The bars were put inside grooves made in the one and two third of the width of the web as shown in the following picture:

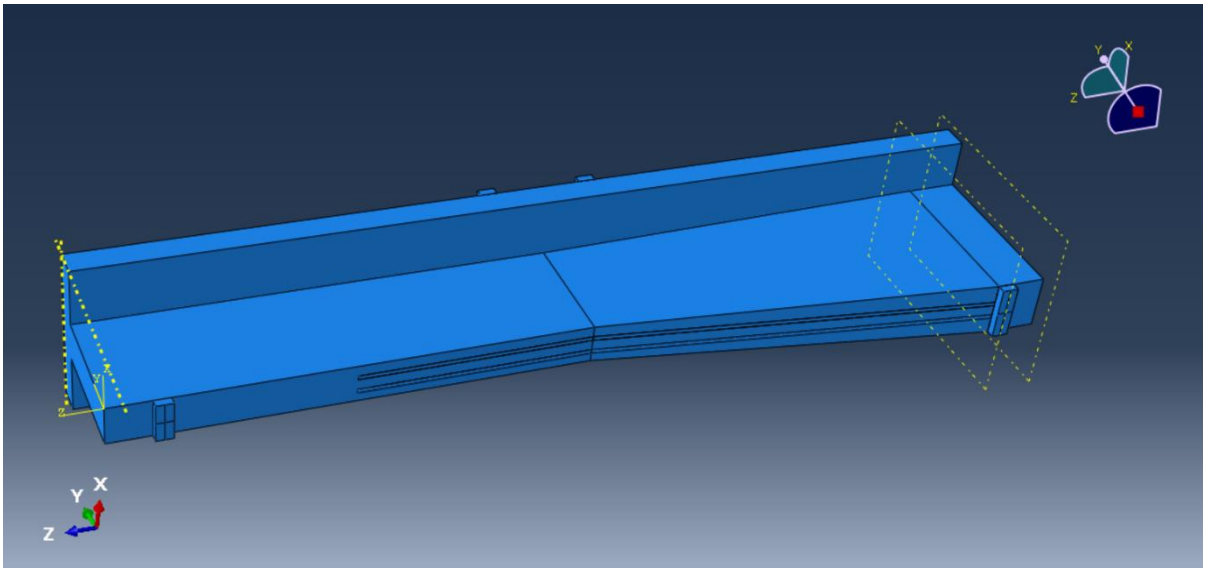

Figure 42: With Titanium-2BG Model - Bottom

3.6.1.3 Strengthening beam with three bars

There is another Titanium bar added to the beam to obtain a total of three bars on the bottom side. The bars were put inside grooves made in the one fourth, half, and three fourth of the width of the web as shown in the following picture:

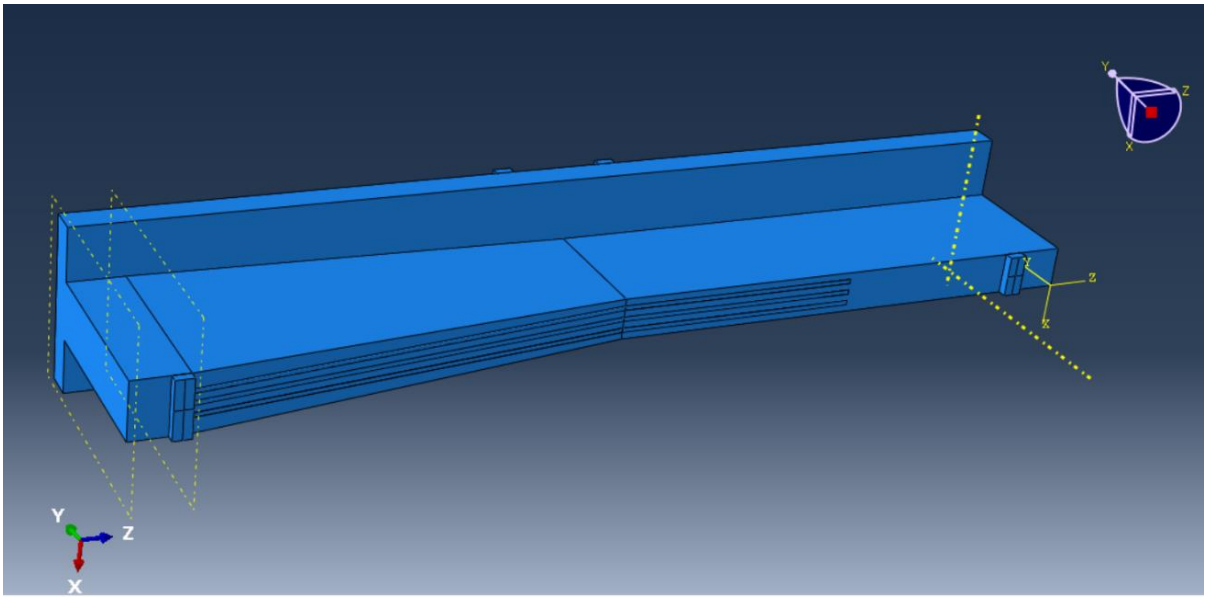

Figure 43: With Titanium-3BG Model - Bottom

3.6.2 Strengthening beam from sides

The Titanium bars applied on the two sides of the beam. There are 3 models developed in this area:

3.6.2.1 Strengthening beam with one bar on each side

In this model, two grooves are made on the two sides of the beam (one groove on each side):

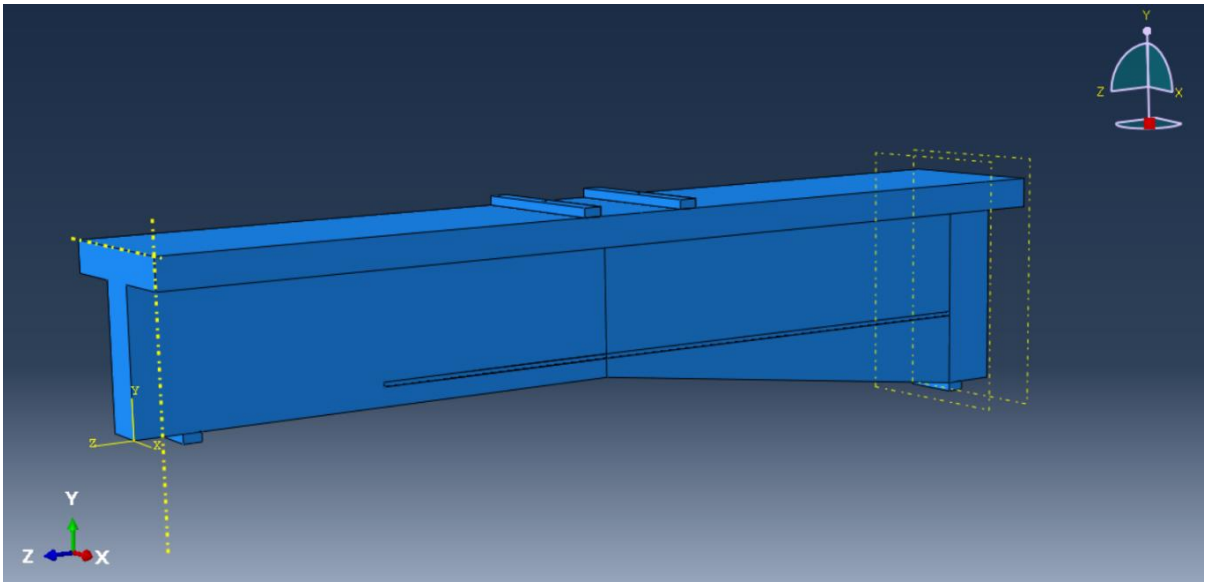

Figure 44: With Titanium-1SG Model - Side 1

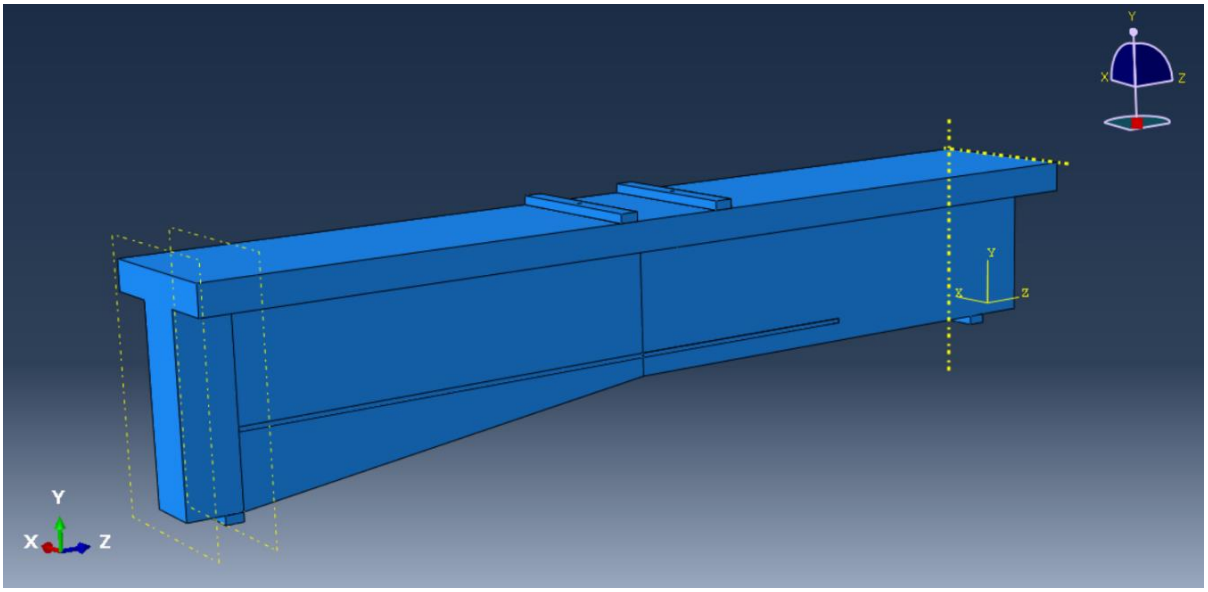

Figure 45: With Titanium-1SG Model - Side 2

3.6.2.2 Strengthening beam with two bars on each side

This model is exactly the original beam which was modelled first to verify the data obtained from Abaqus.

3.6.2.3 Strengthening beam with three bars on each side

In this model, six grooves are made on the two sides of the beam (three groove on each side):

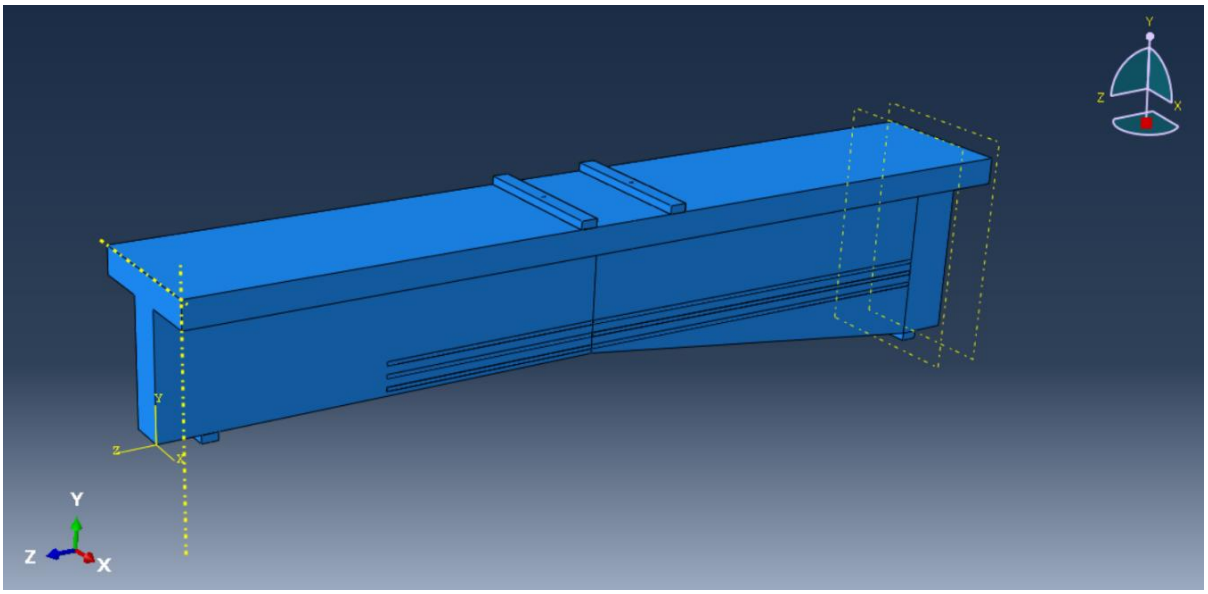

Figure 46: With Titanium-3SG Model - Side 1

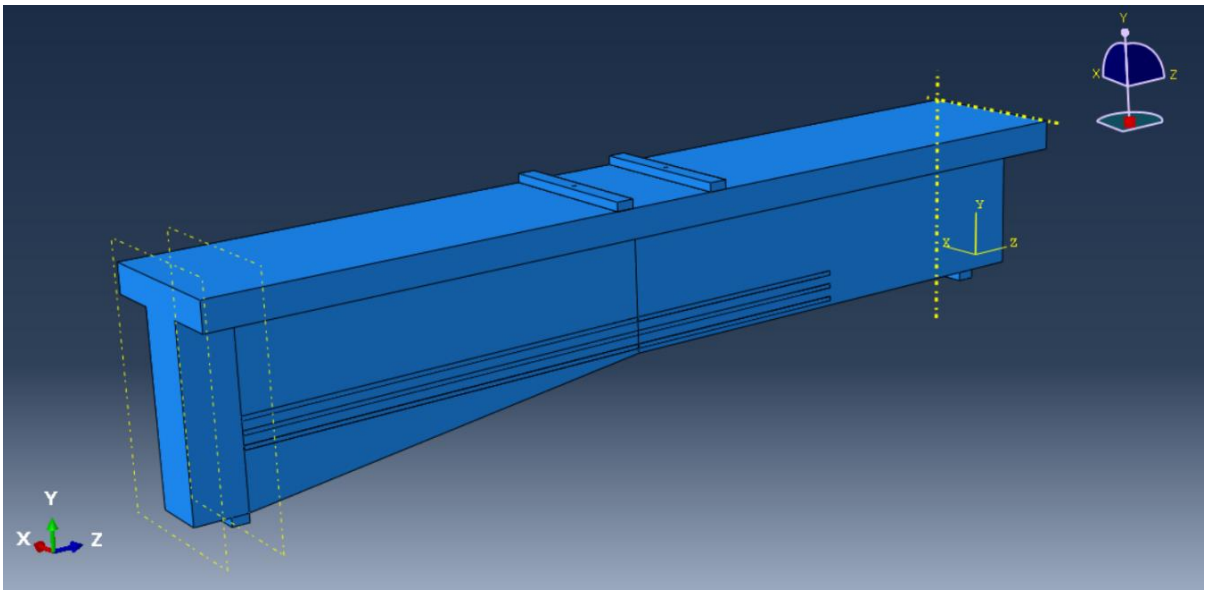

Figure 47: With Titanium-3SG Model - Side 2

3.6.3 Strengthening beam with different alloy bars' sizes

While fixing the number of the Titanium bars to be four (two on each side), the effect of the Titanium section sizes will be studied. Three different sizes were considered:

3.6.3.1 Strengthening beam with two (15×15) mm Titanium bars on each side

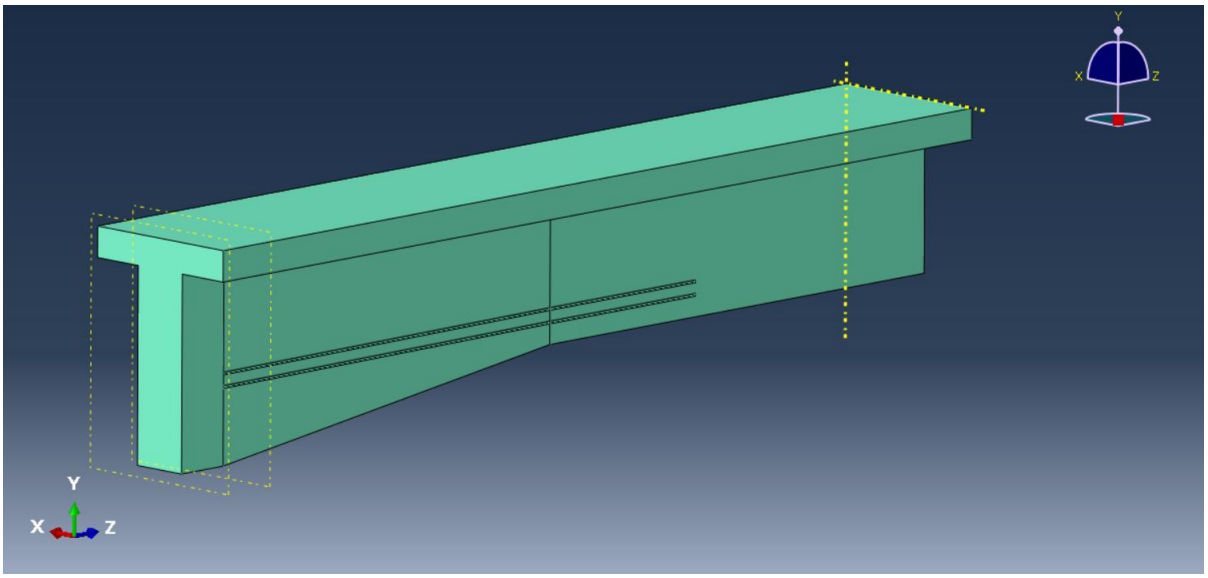

Figure 48: With Titanium-2SG-15 Model - Concrete Side 1

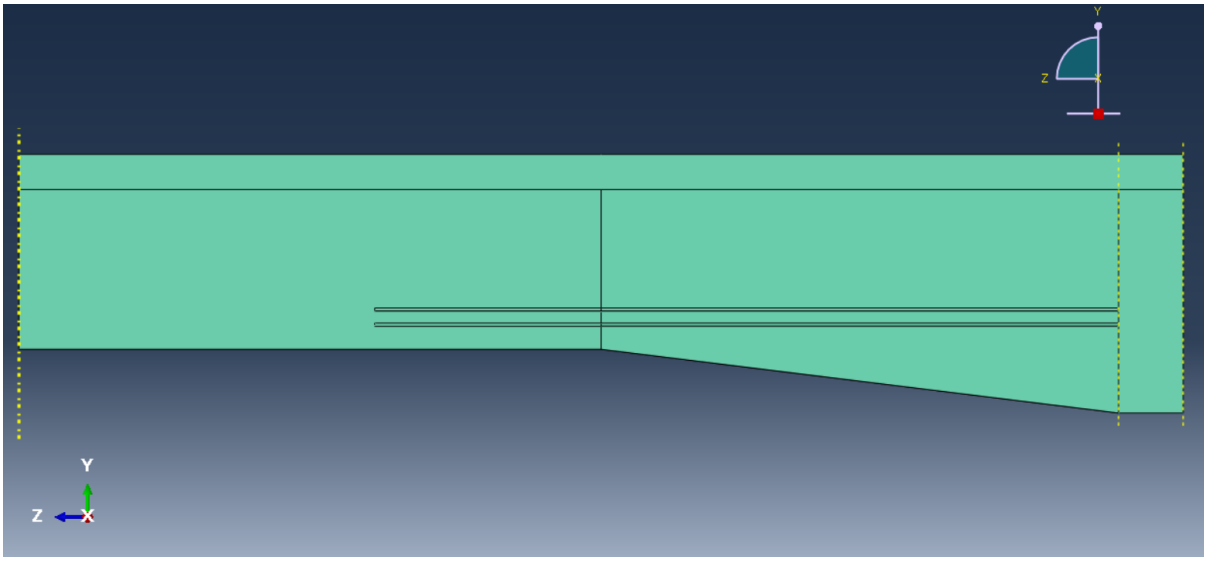

Figure 49: With Titanium-2SG-15 Model - Concrete Side 2

3.6.3.2 Strengthening beam with two (25×25) mm Titanium bars on each side

This model is also exactly the original beam which was modelled first to verify the data obtained from Abaqus.

3.6.3.3 Strengthening beam with two (35×35) mm Titanium bars on each side

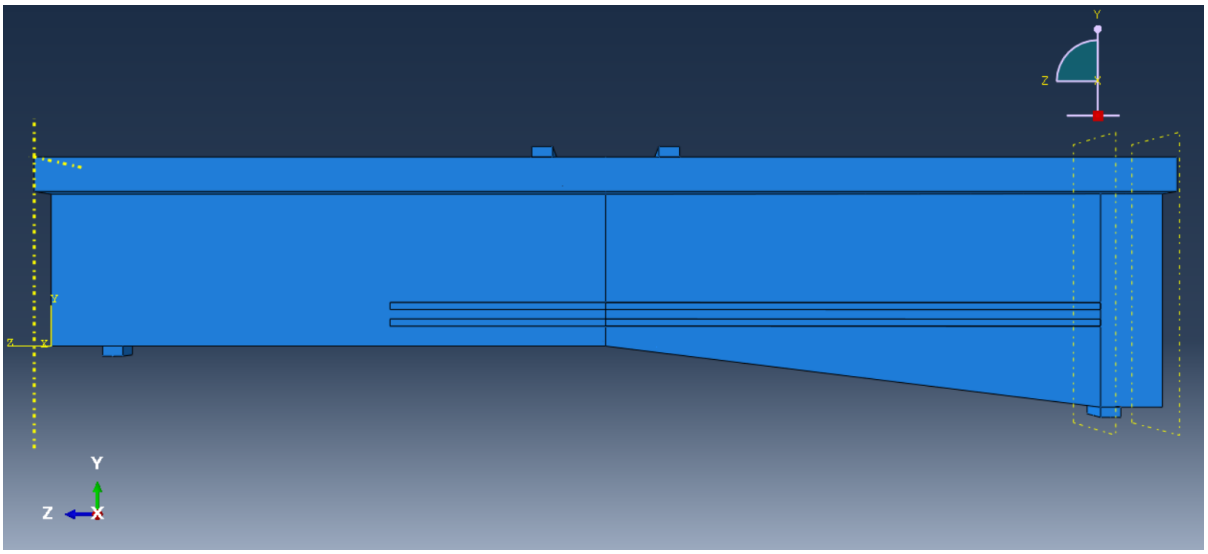

Figure 50: With Titanium-2SG-35 Model - Side 1

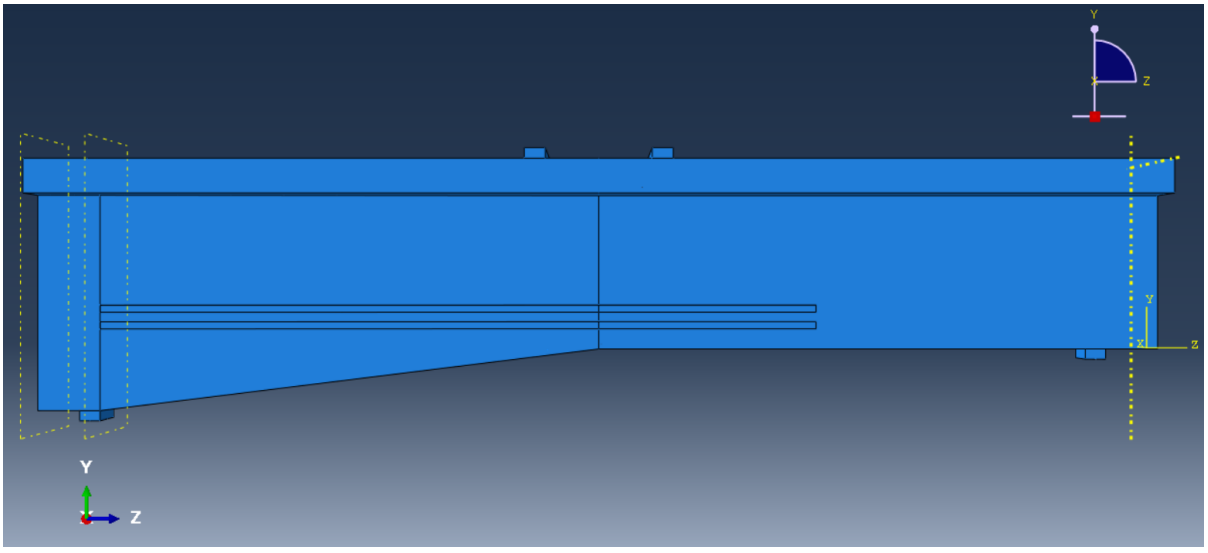

Figure 51: With Titanium-2SG-35 Model - Side 2

3.6.4 Strengthening beam with inclined Titanium bars

The Titanium bars applied on the two sides of the beam with inclination on the enlarging half of the beam. There are 3 models developed in this area:

3.6.4.1 Strengthening beam with one bar on each side

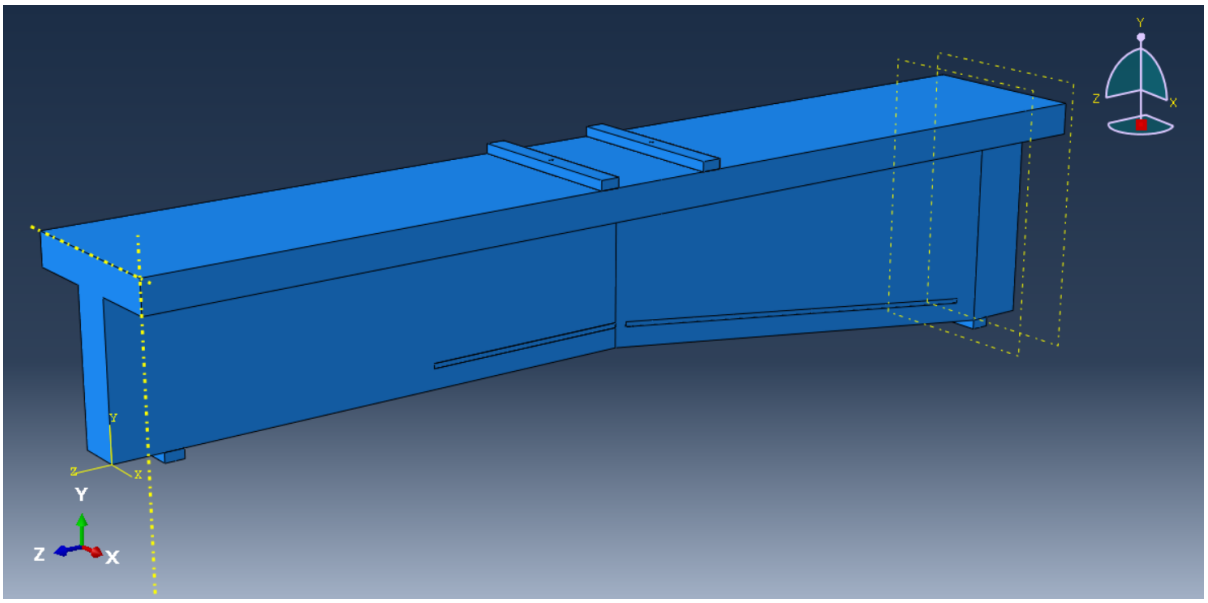

Figure 52: With Titanium-1ISG Model - Side 1

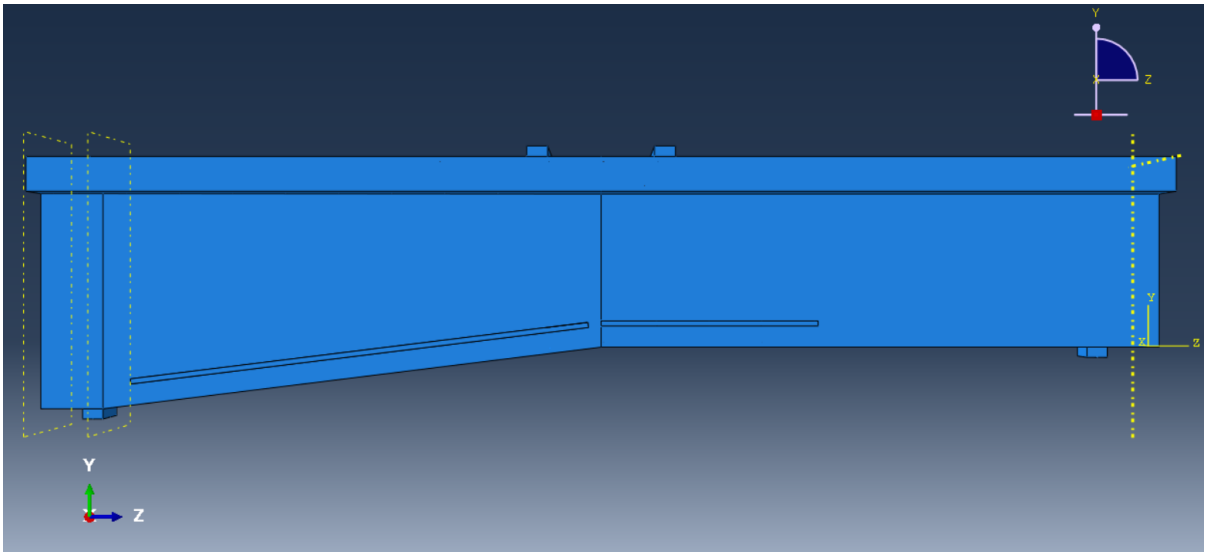

Figure 53: With Titanium-1ISG Model - Side 2

3.6.4.2 Strengthening beam with two bars on each side

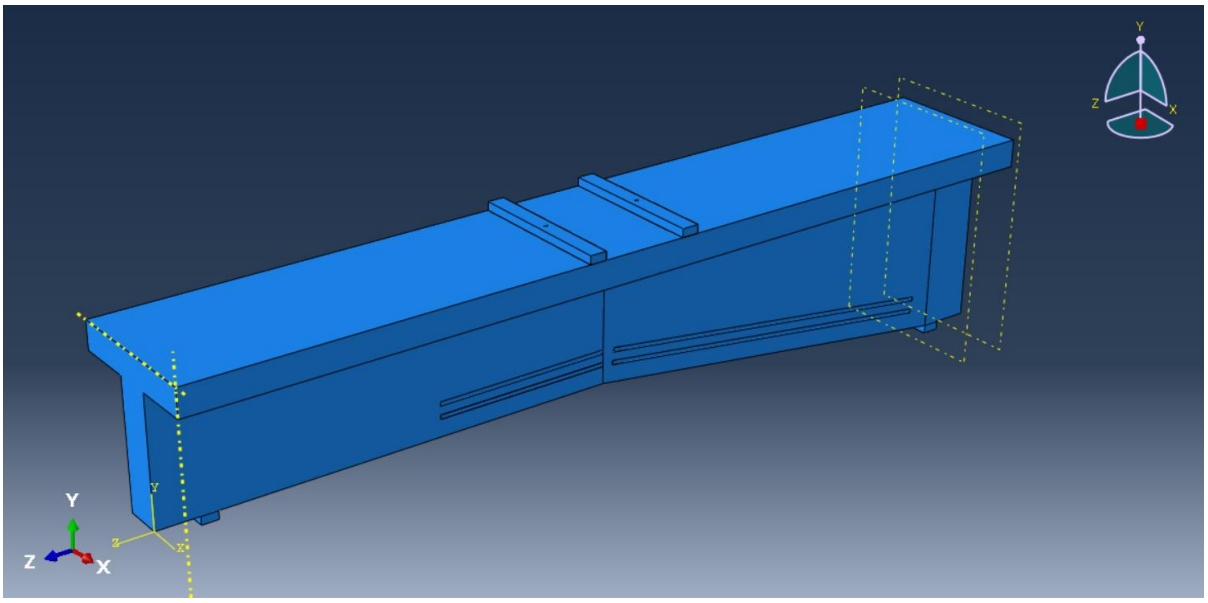

Figure 54: With Titanium-2ISG Model - Side 1

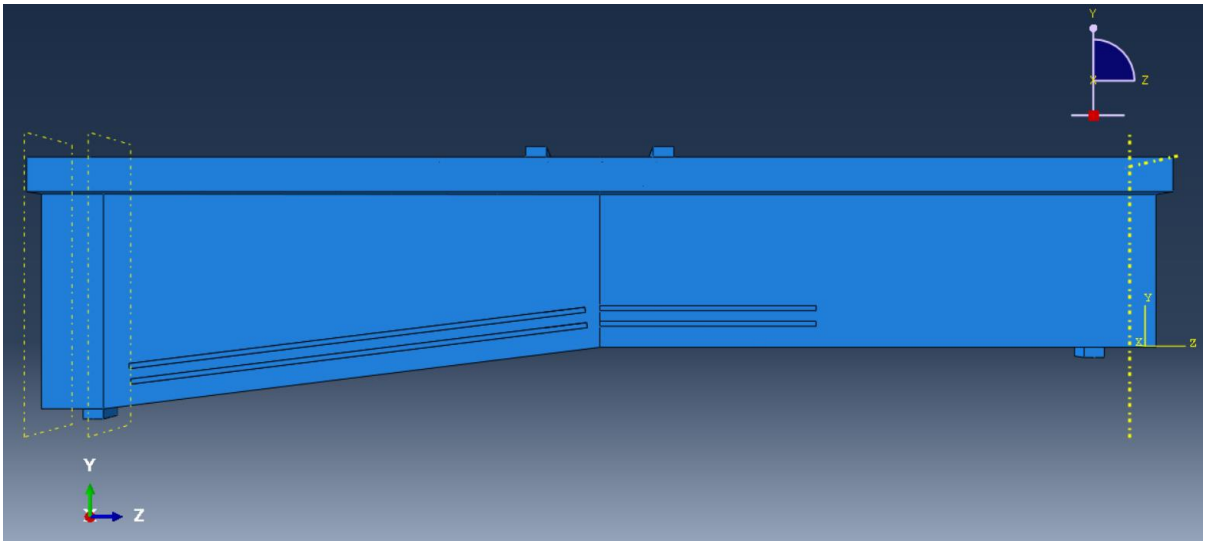

Figure 55: With Titanium-2ISG Model - Side 2

3.6.4.3 Strengthening beam with three bars on each side

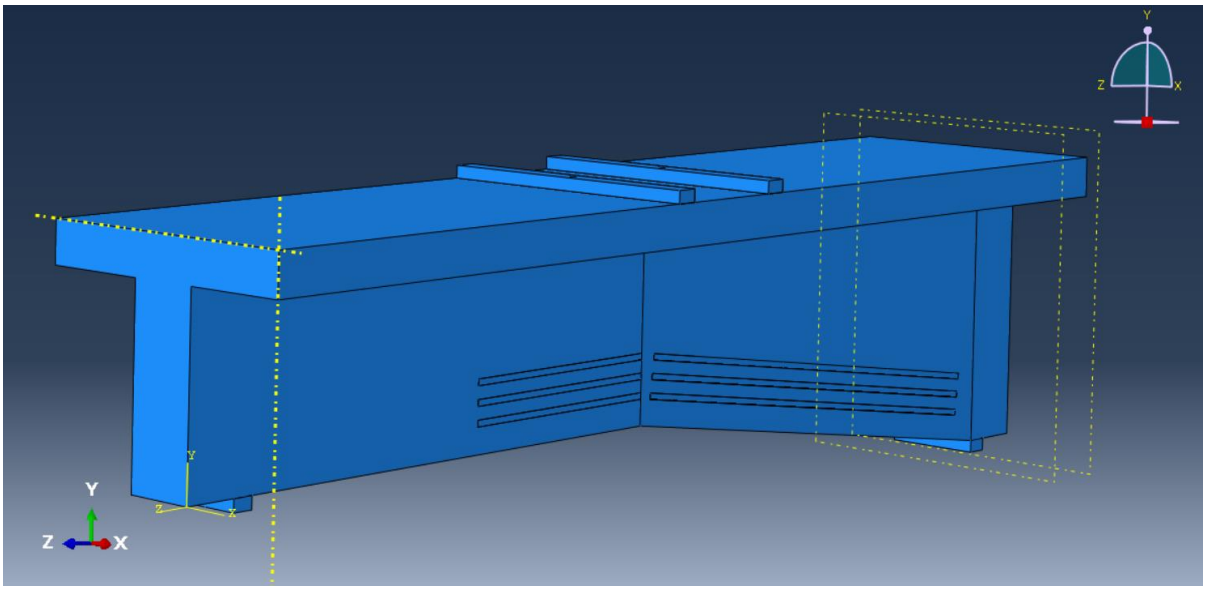

Figure 56: With Titanium-3ISG Model - Side 1

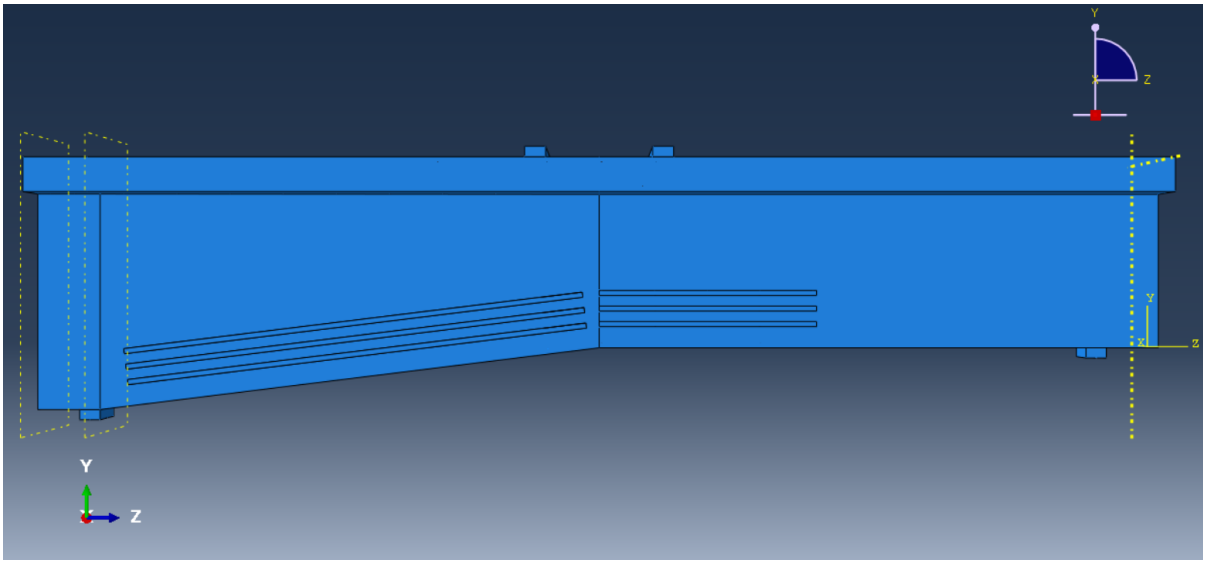

Figure 57: With Titanium-3ISG Model - Side 2

Chapter 4: Results

In this chapter, the main results of all parameters studied that were mentioned in Chapter 3 (3.5.1 to 3.5.4) will be presented. Moment-deflection curves will be shown for all cases and will be discussed.

4.1 Strengthening beam from bottom

4.1.1 Strengthening beam with one bar

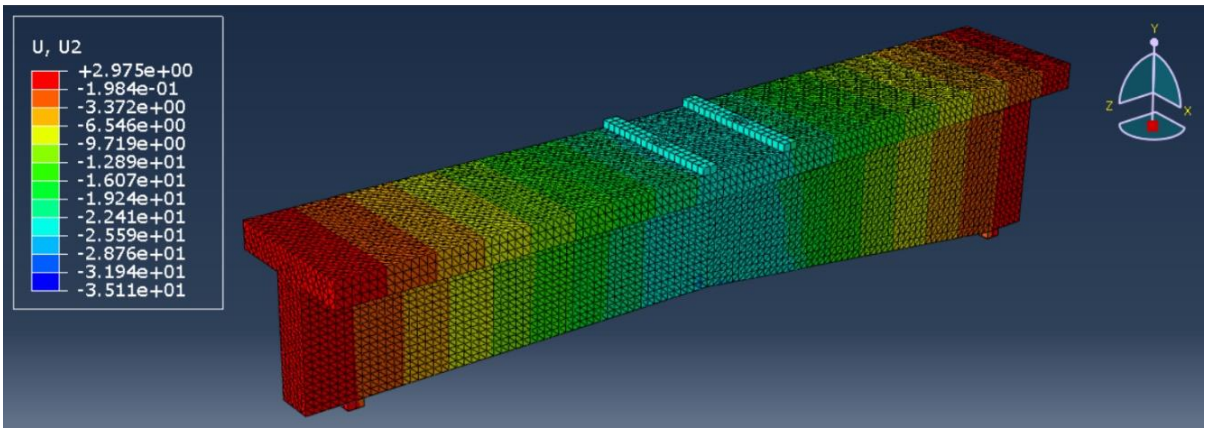

Figure 58: With Titanium-1BG Model - U2 (Vertical Displacement)

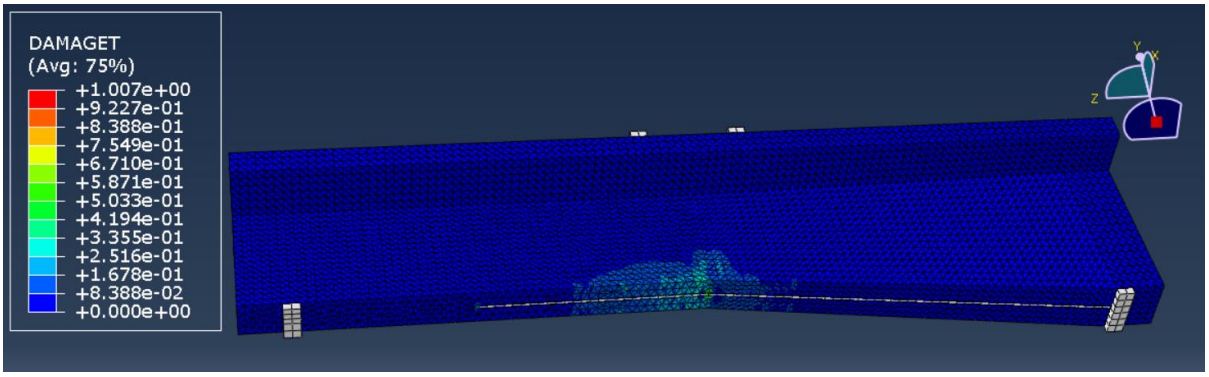

Figure 59: With Titanium-1BG Model - First Tension Crack

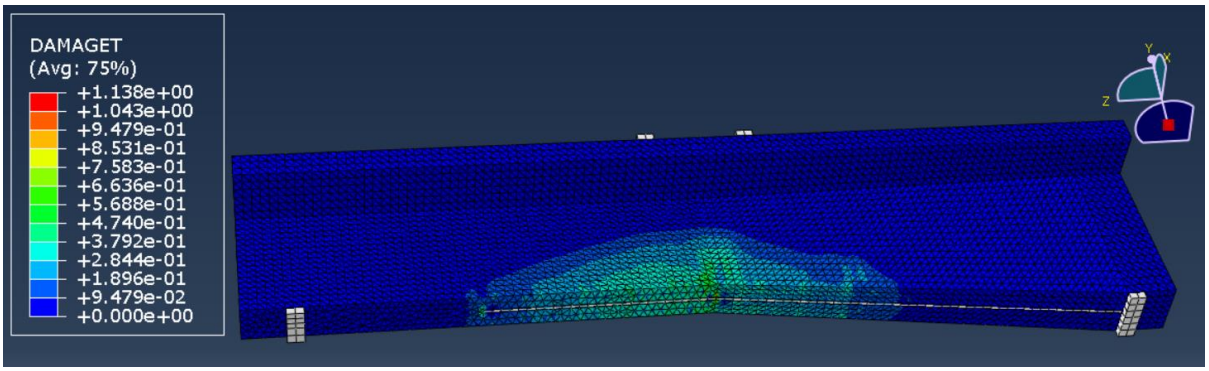

Figure 60: With Titanium-1BG Model - Cracks' Propagation

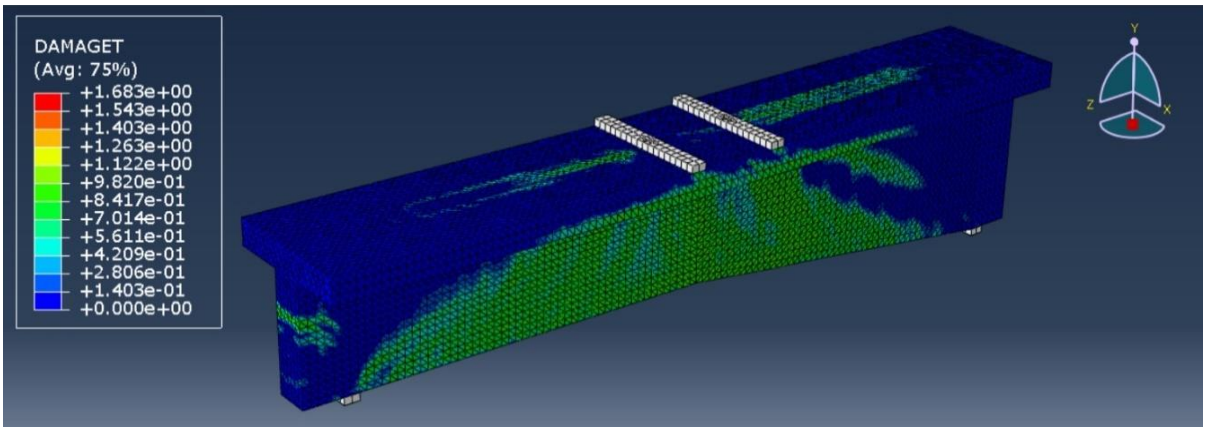

Figure 61: With Titanium-1BG Model - Damage Tension

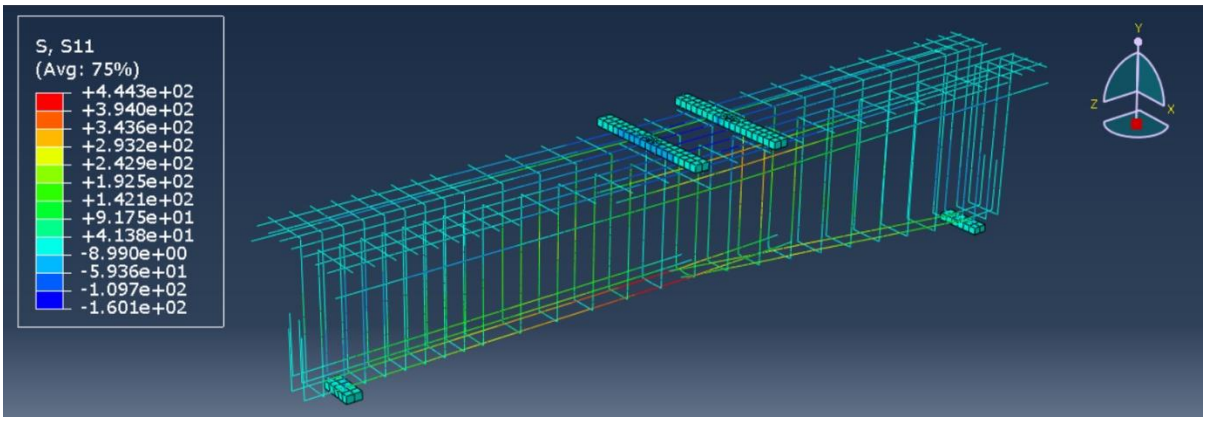

Figure 62: With Titanium-1BG Model - Steel Normal Stress

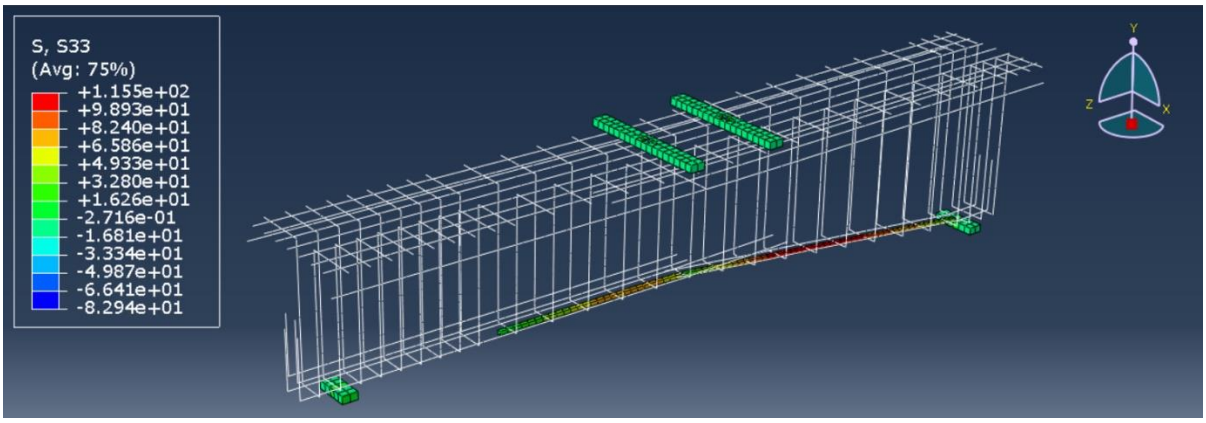

Figure 63: With Titanium-1BG Model - S33 for Titanium Bars

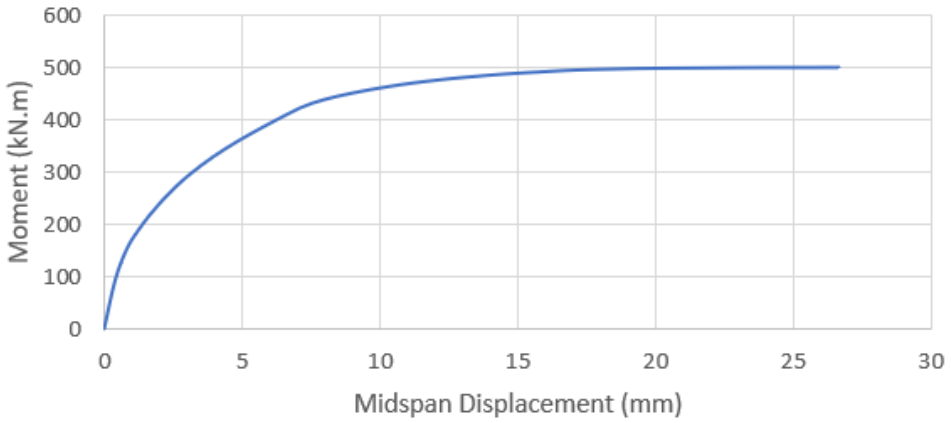

Figure 64: Moment-Displacement curve for With Titanium-1BG Model

As shown in the figure above, the maximum moment capacity was about 500 kN.m.

4.1.2 Strengthening beam with two bars

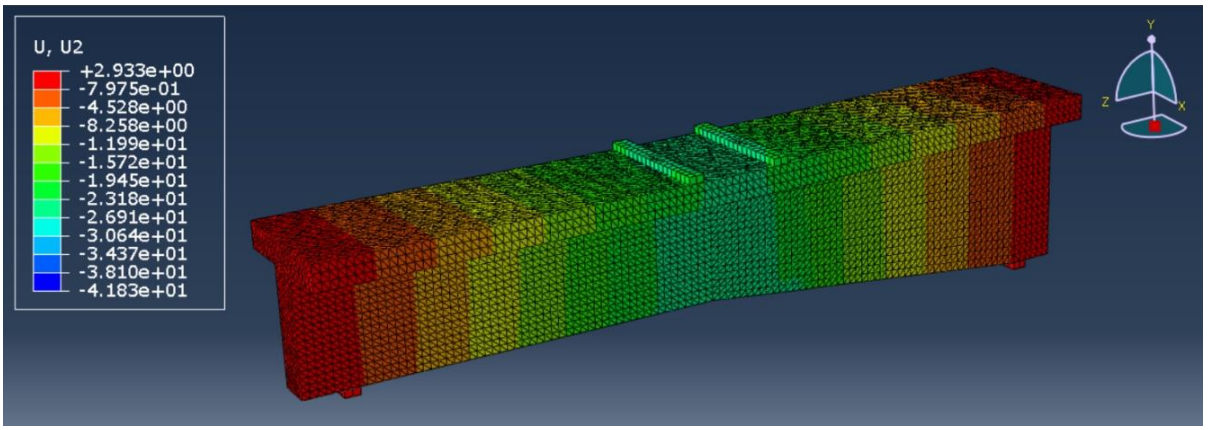

Figure 65: With Titanium-2BG Model - U2 (Vertical Displacement)

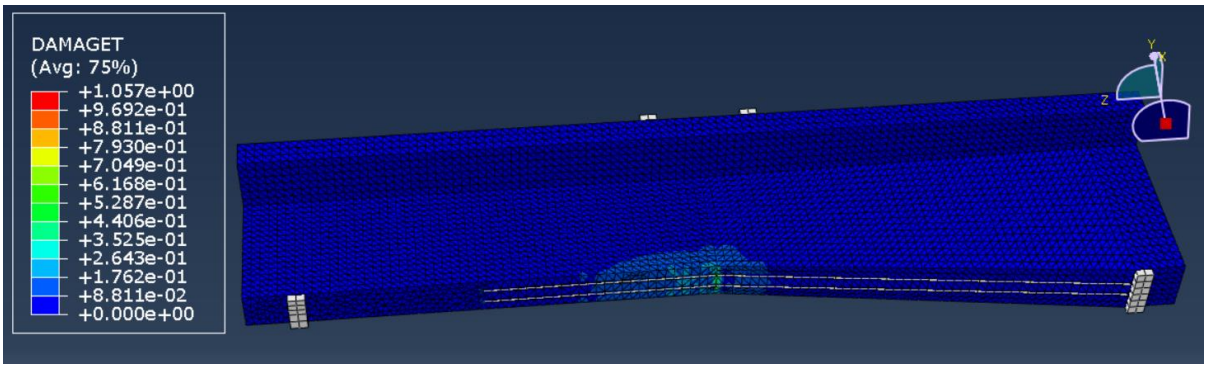

Figure 66: With Titanium-2BG Model - First Tension Crack

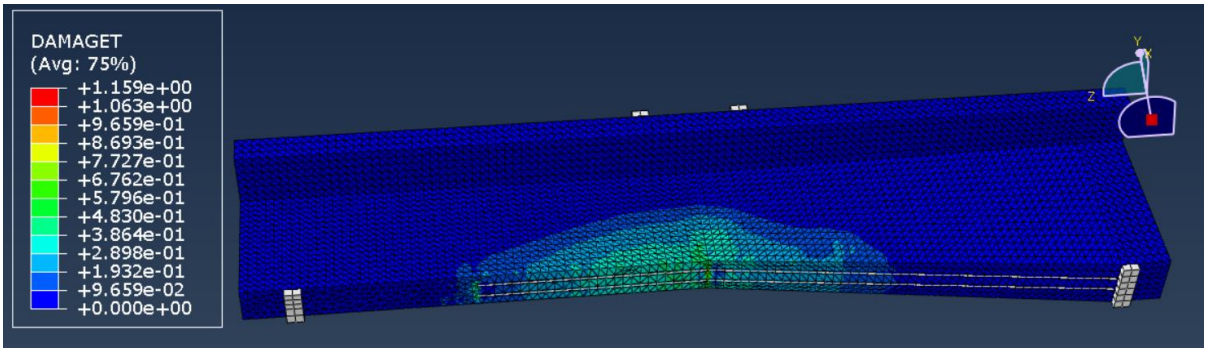

Figure 67: With Titanium-2BG Model - Cracks' Propagation

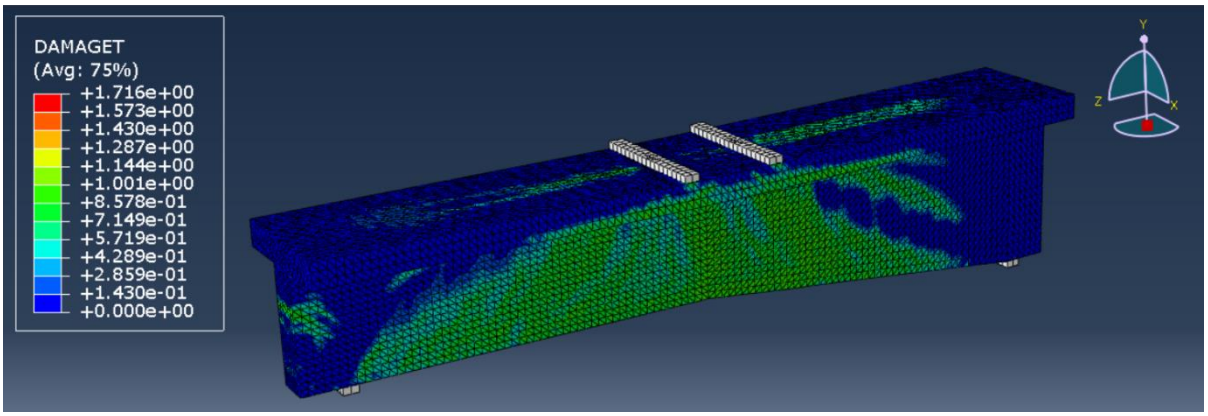

Figure 68: With Titanium-2BG Model - Damage Tension

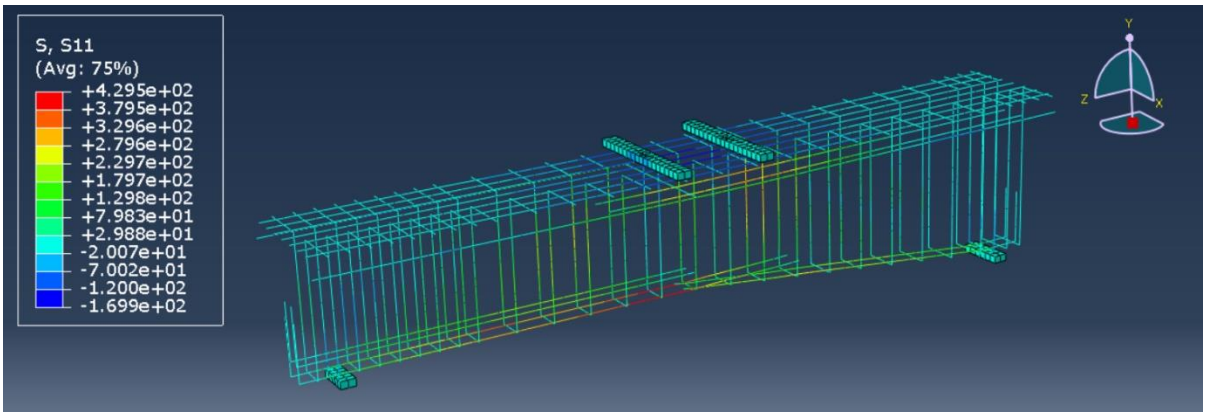

Figure 69: With Titanium-2BG Model - Steel Normal Stress

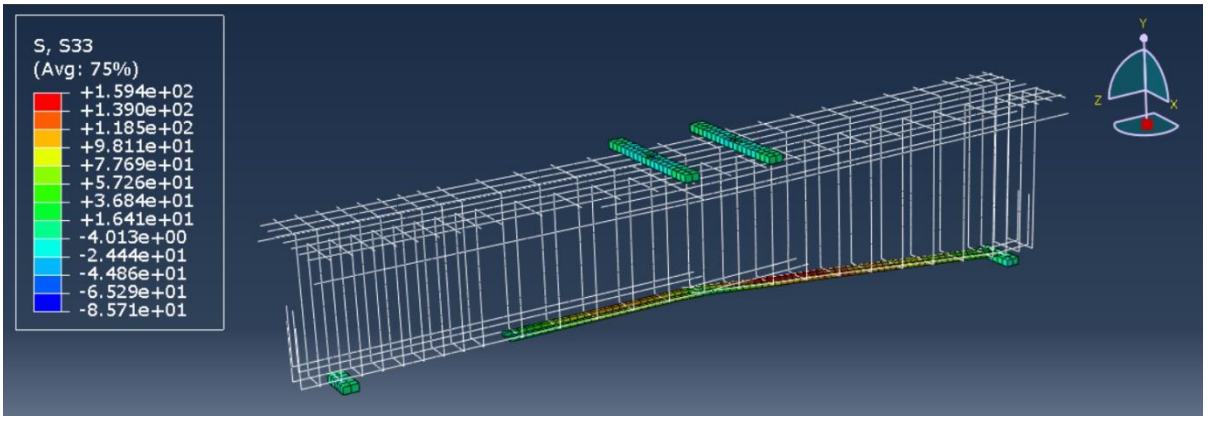

Figure 70: With Titanium-2BG Model - S33 for Titanium Bars

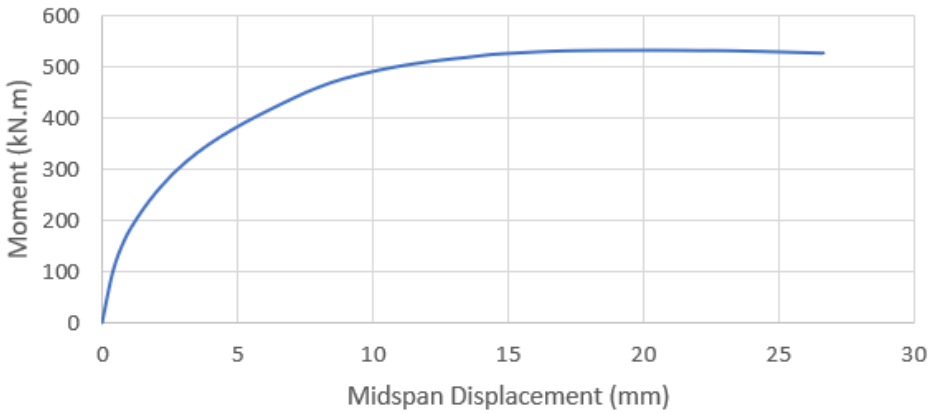

Figure 71: Moment-Displacement curve for With Titanium-2BG Model

As illustrated in the figure above, the maximum moment capacity was about 530 kN.m.

4.1.3 Strengthening beam with three bars

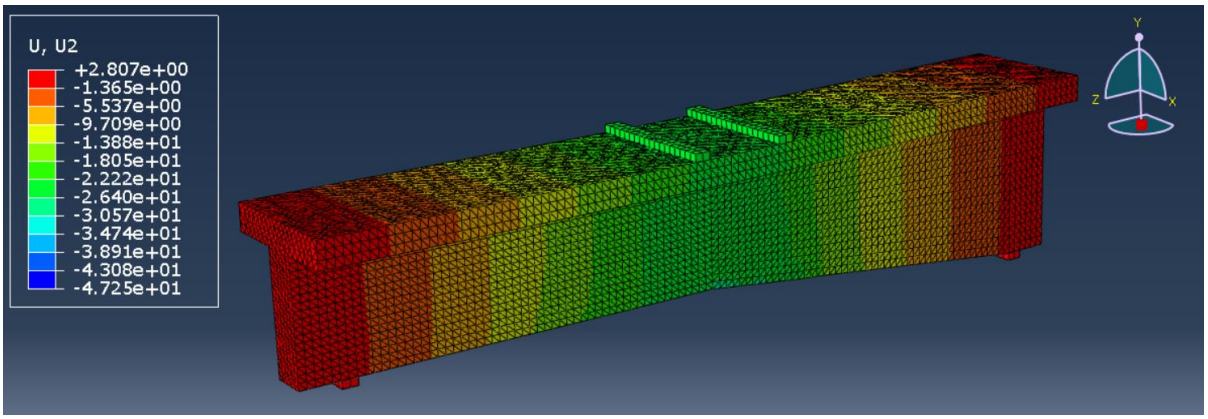

Figure 72: With Titanium-3BG Model - U2 (Vertical Displacement)

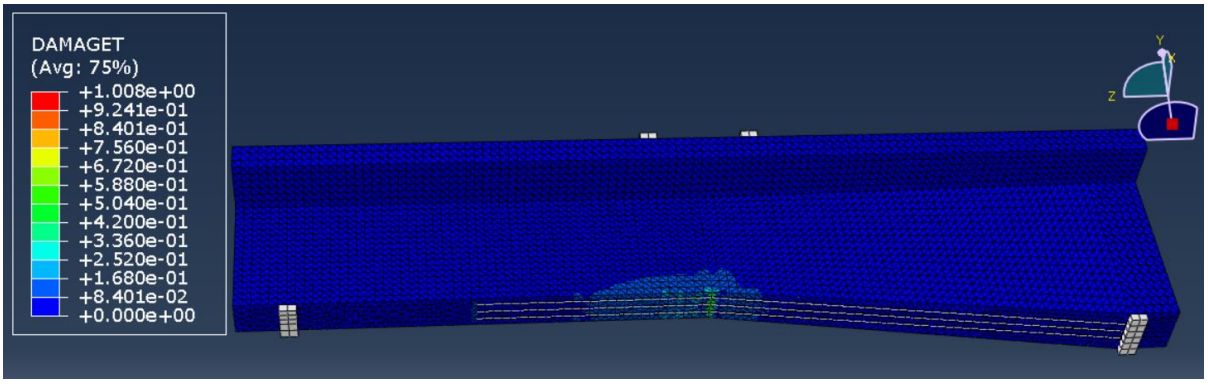

Figure 73: With Titanium-3BG Model - First Tension Crack

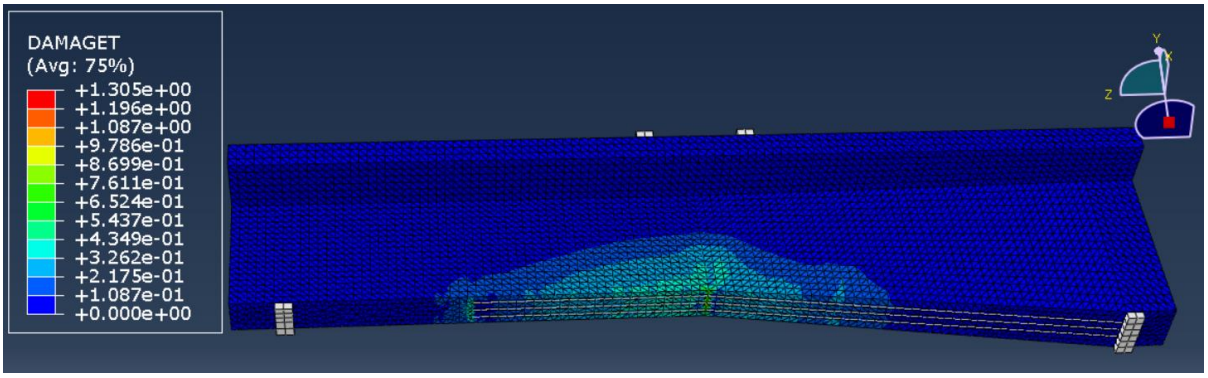

Figure 74: With Titanium-3BG Model - Cracks' Propagation

The propagation for last three models (1BG, 2BG, and 3BG) is more moving horizontally than vertically due to the length of the Titanium bars used with comparing to model without Titanium.

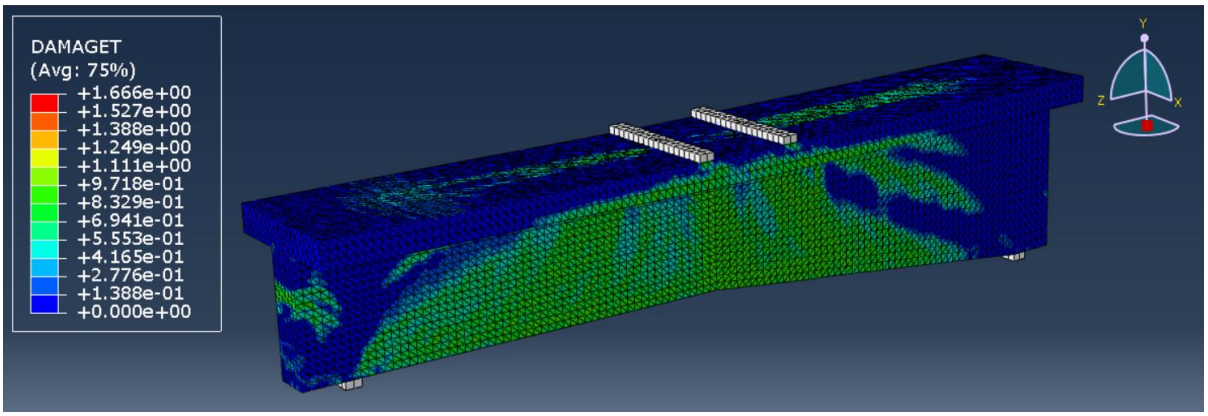

Figure 75: With Titanium-3BG Model - Damage Tension

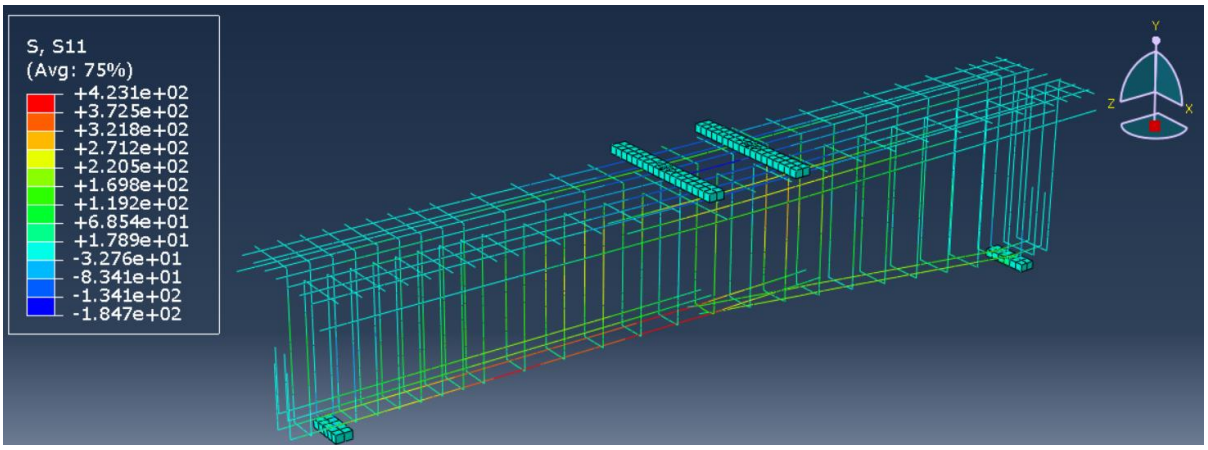

Figure 76: With Titanium-3BG Model - Steel Normal Stress

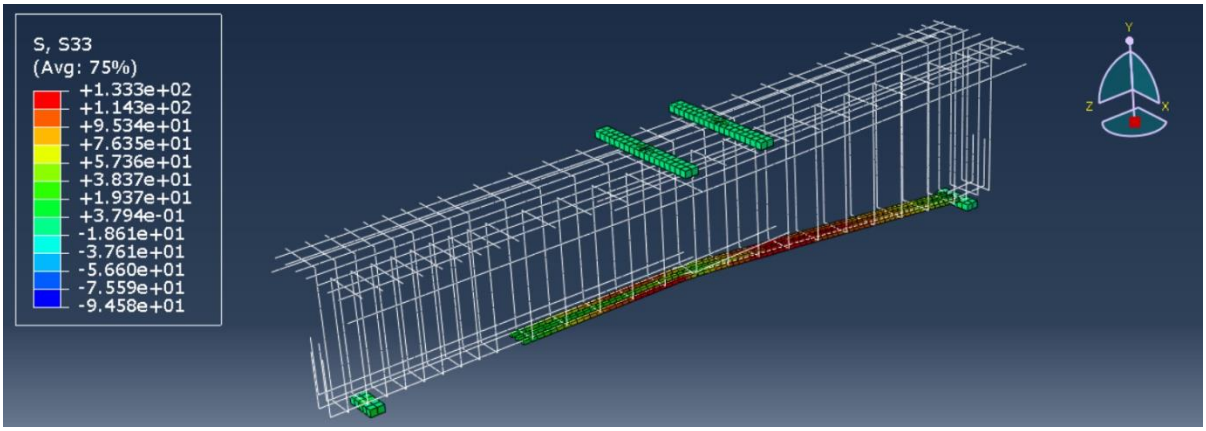

Figure 77: With Titanium-3BG Model - S33 for Titanium Bars

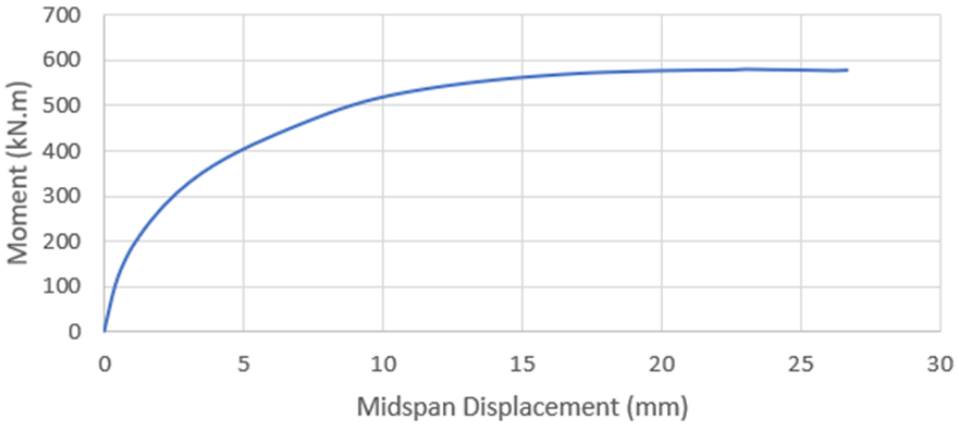

Figure 78: Moment-Displacement curve for With Titanium-3BG Model

As shown above, the maximum moment capacity was about 580 kN.m.

4.2 Strengthening beam from sides

4.2.1 Strengthening beam with one bar on each side

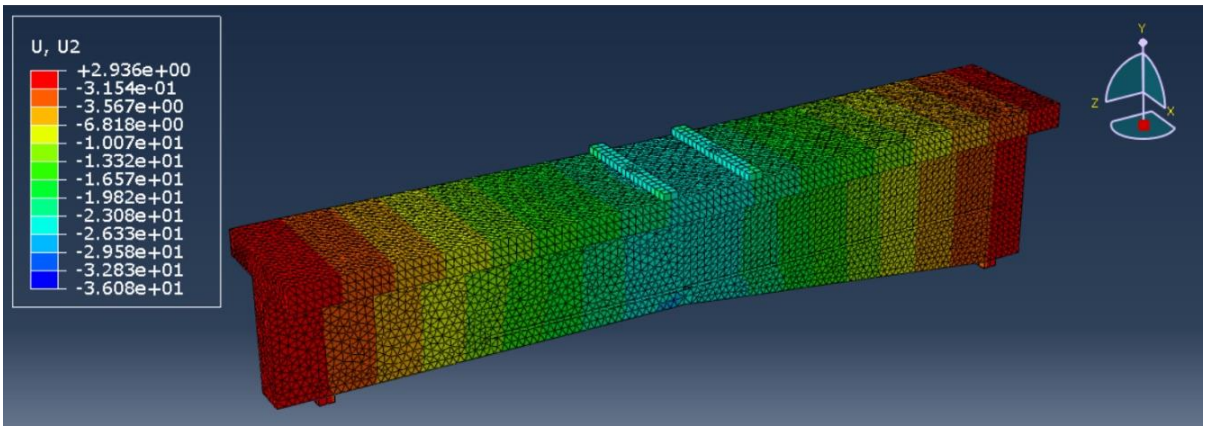

Figure 79: With Titanium-1SG Model - U2 (Vertical Displacement)

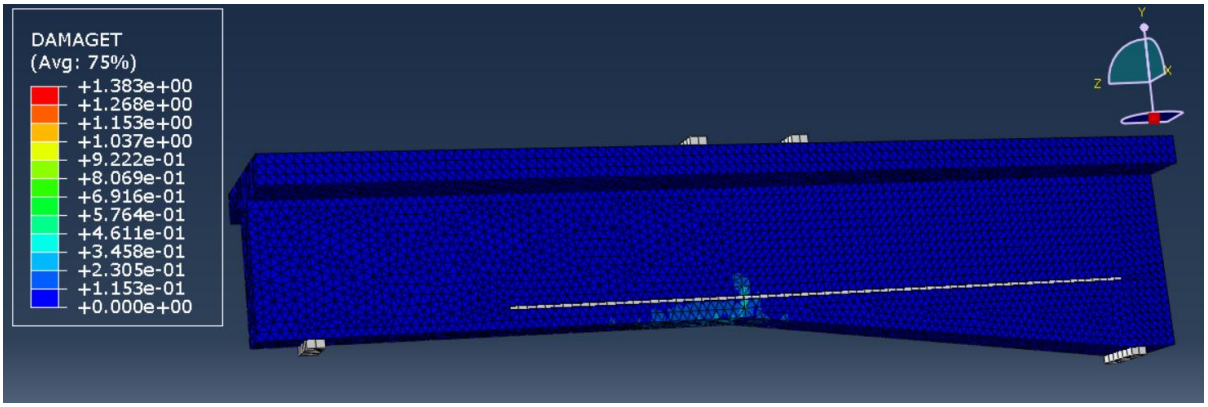

Figure 80: With Titanium-1SG Model - First Tension Crack

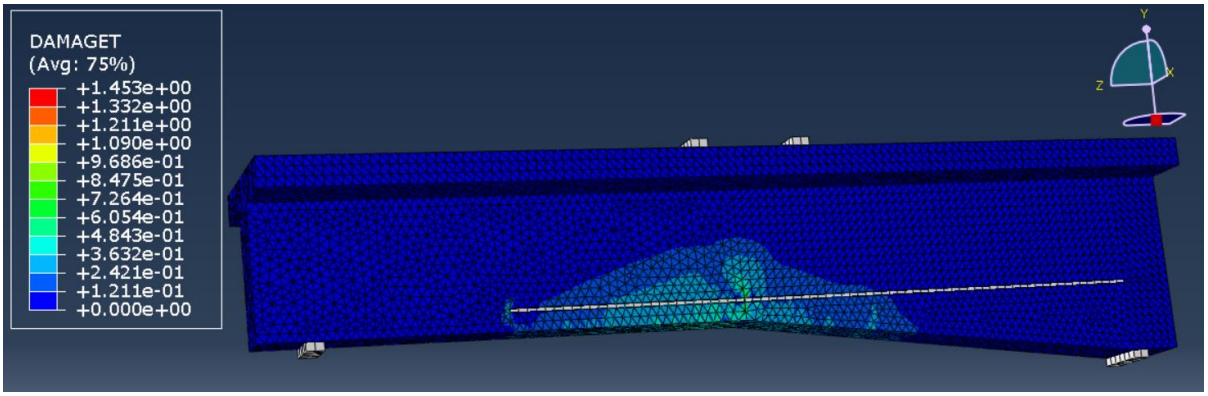

Figure 81: With Titanium-1SG Model - Cracks' Propagation

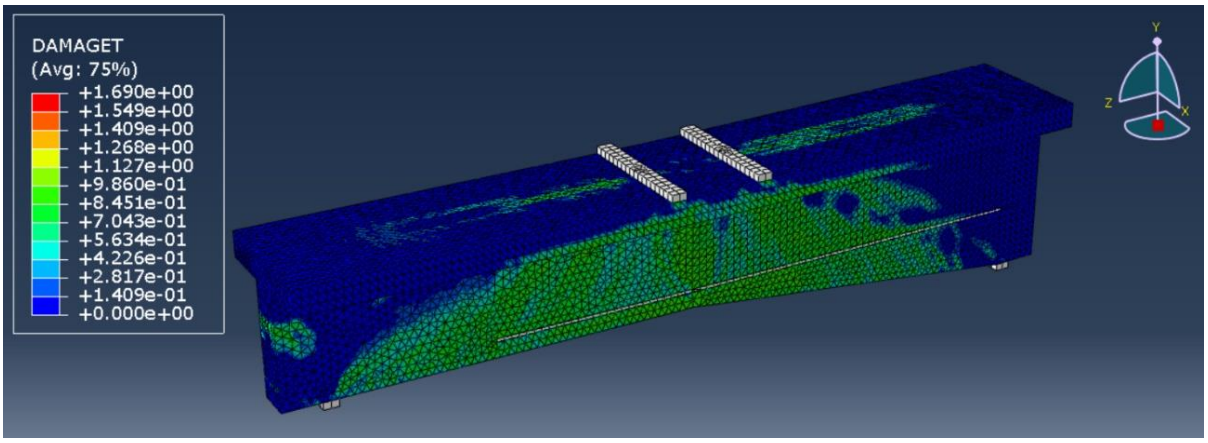

Figure 82: With Titanium-1SG Model - Damage Tension

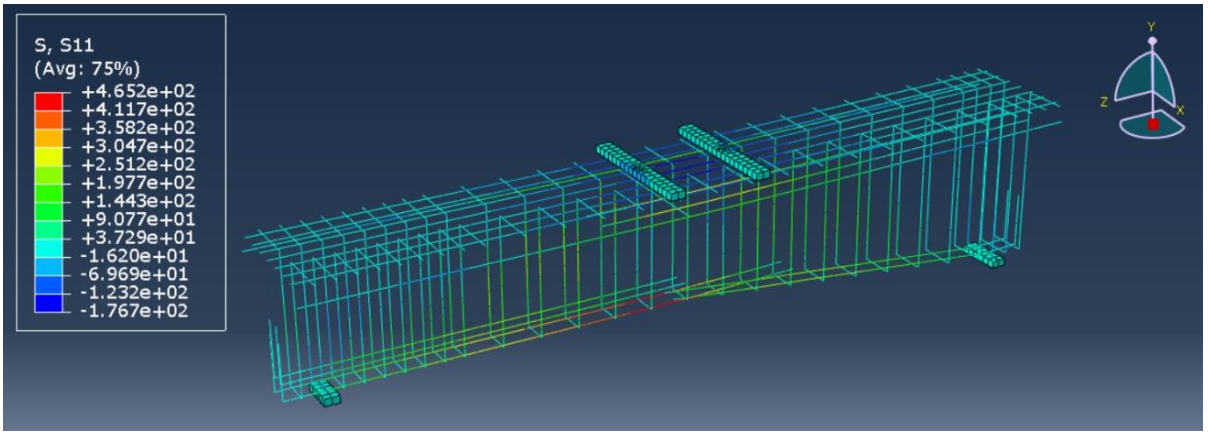

Figure 83: With Titanium-1SG Model - Steel Normal Stress

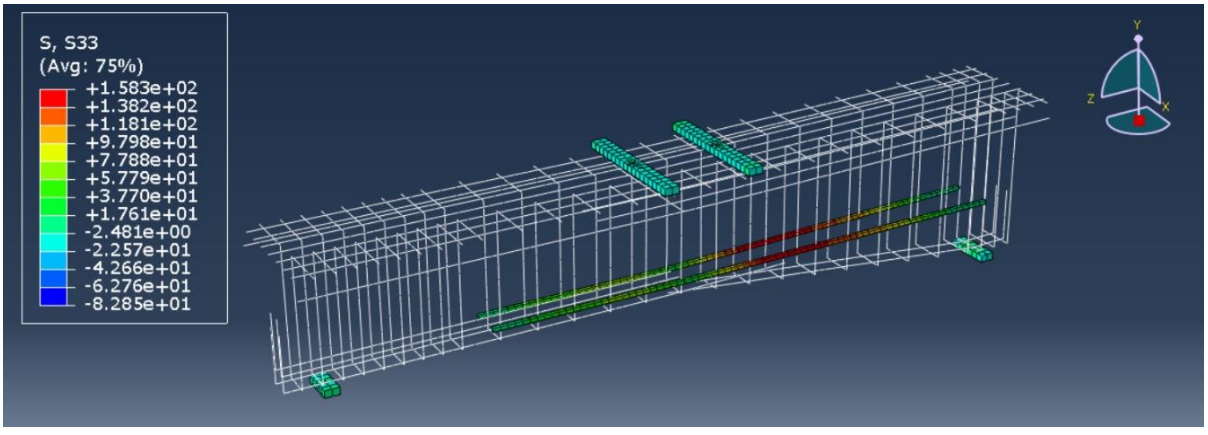

Figure 84: With Titanium-1SG Model - S33 for Titanium Bars

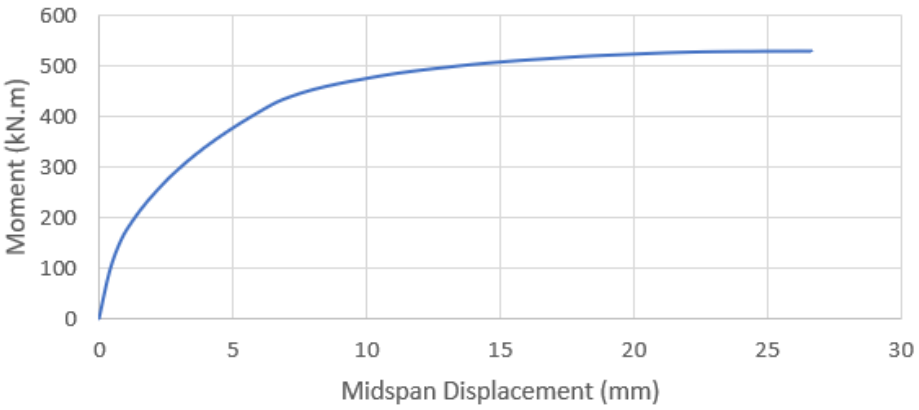

Figure 85: Moment-Displacement curve for With Titanium-1SG Model

As the figure above illustrates, the maximum moment capacity was about 530 kN.m.

4.2.2 Strengthening beam with two bars on each side

This model is exactly the original beam which was modelled first to verify the data obtained from Abaqus. So, the same results will be obtained as mentioned before.

4.2.3 Strengthening beam with three bars on each side

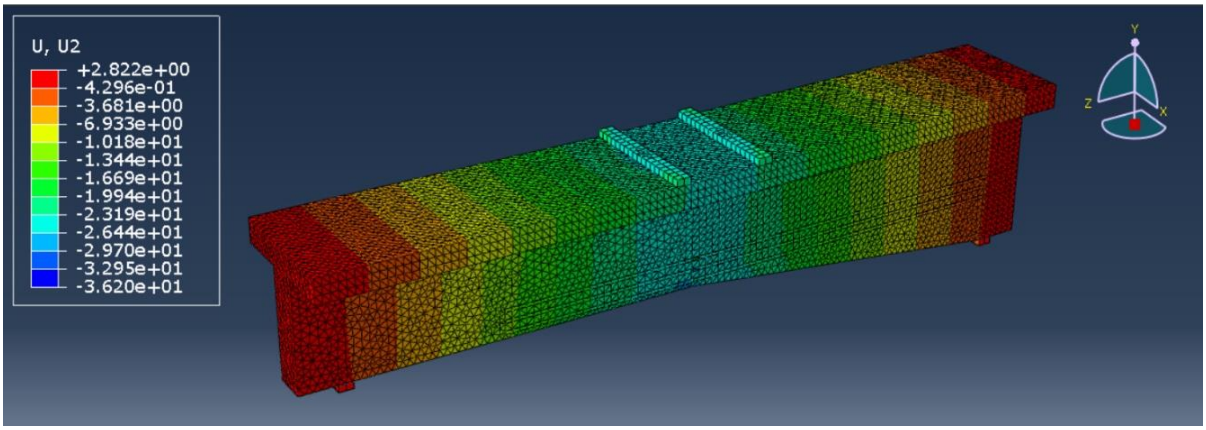

Figure 86: With Titanium-3SG Model - U2 (Vertical Displacement)

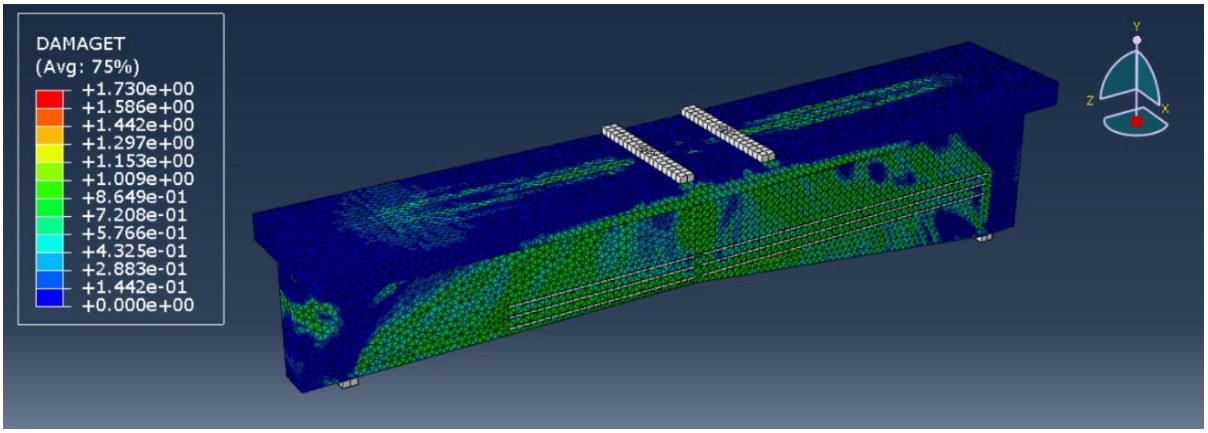

Figure 87: With Titanium-3SG Model - Damage Tension

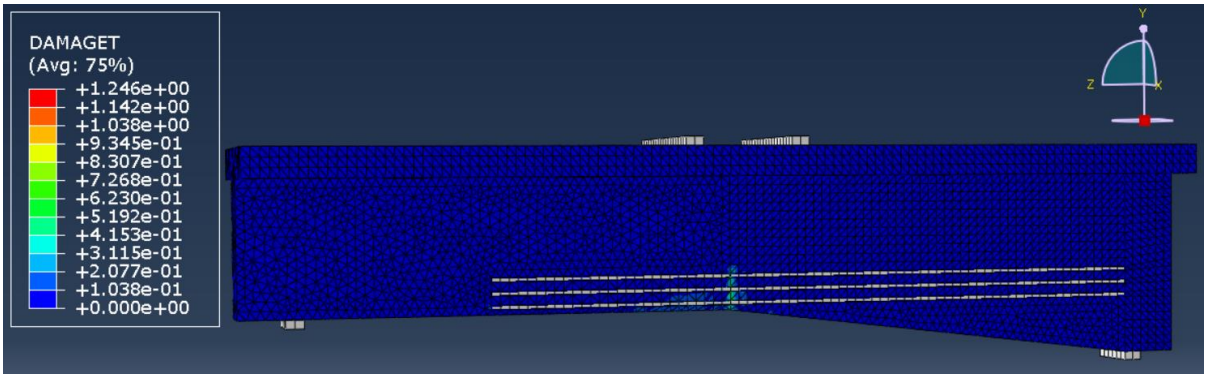

Figure 88: With Titanium-3SG Model - First Tension Crack

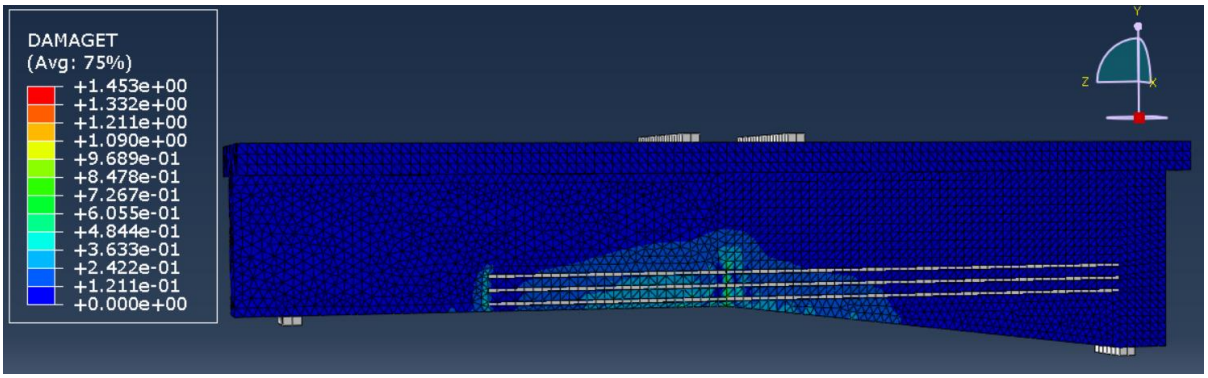

Figure 89: With Titanium-3SG Model - Cracks' Propagation

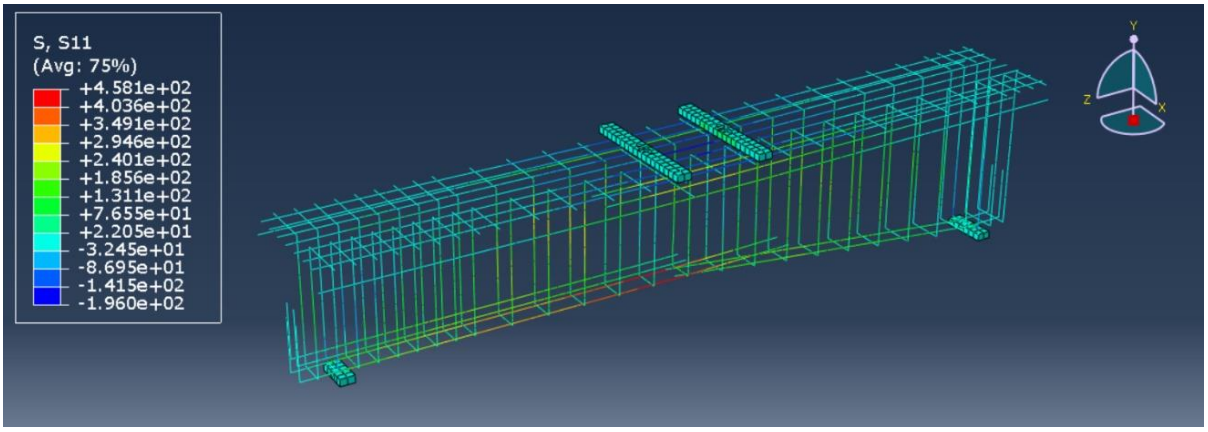

Figure 90: With Titanium-3SG Model - Steel Normal Stress

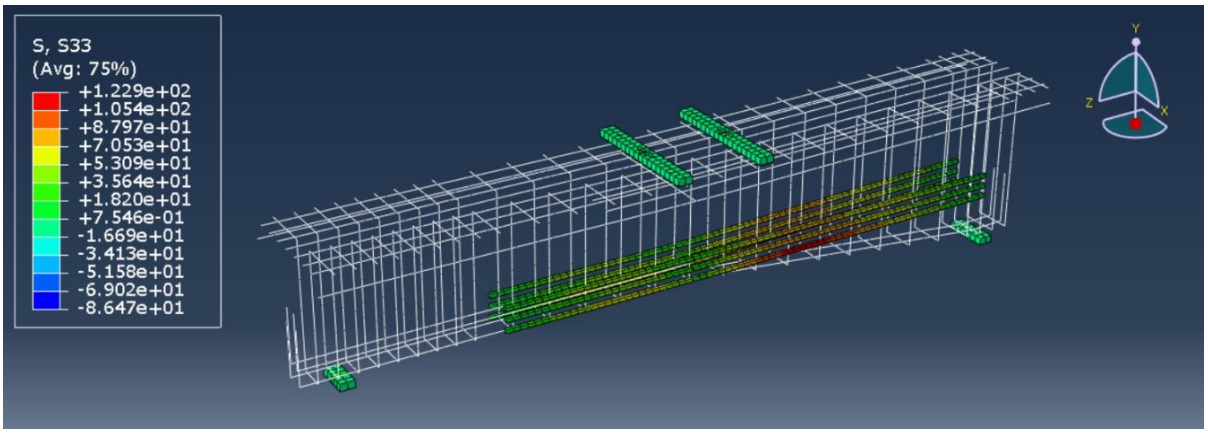

Figure 91: With Titanium-3SG Model - S33 for Titanium Bars

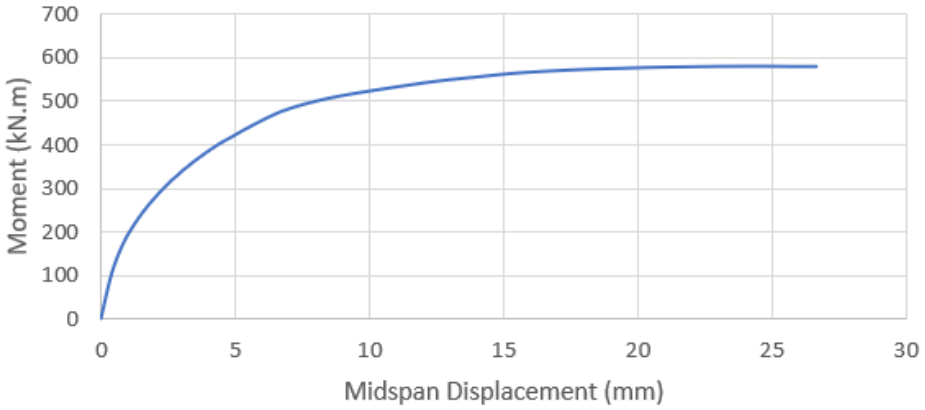

Figure 92: Moment-Displacement curve for With Titanium-3SG Model

As demonstrated in the figure above, the maximum moment capacity was about 580 kN.m.

4.3 Strengthening beam with different alloy bars' sizes

4.3.1 Strengthening beam with two (15×15) mm Titanium bars on each side

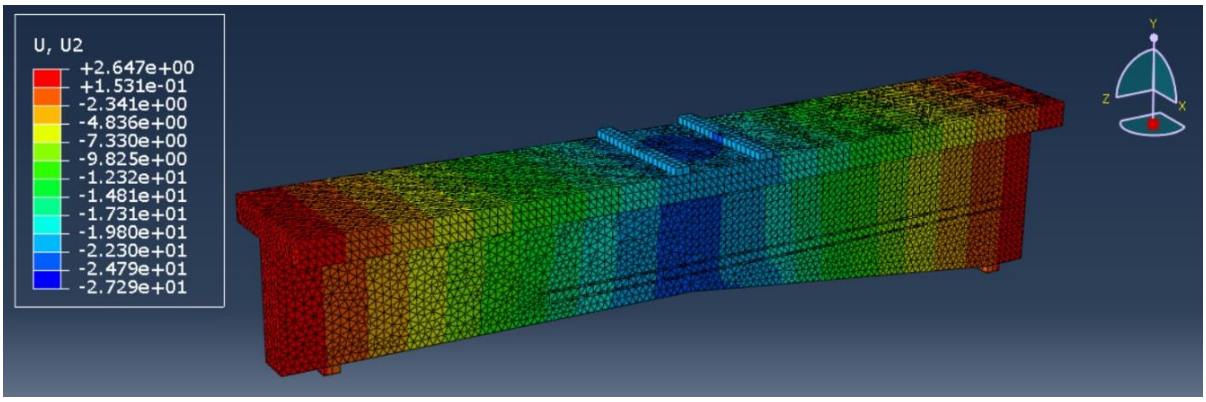

Figure 93: With Titanium-2SG-15 Model - U2 (Vertical Displacement)

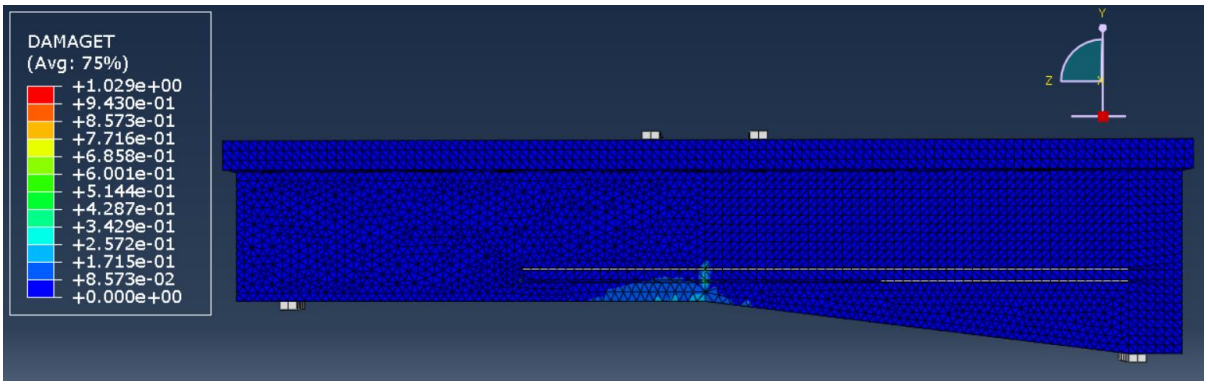

Figure 94: With Titanium-2SG-15 Model - First Tension Crack

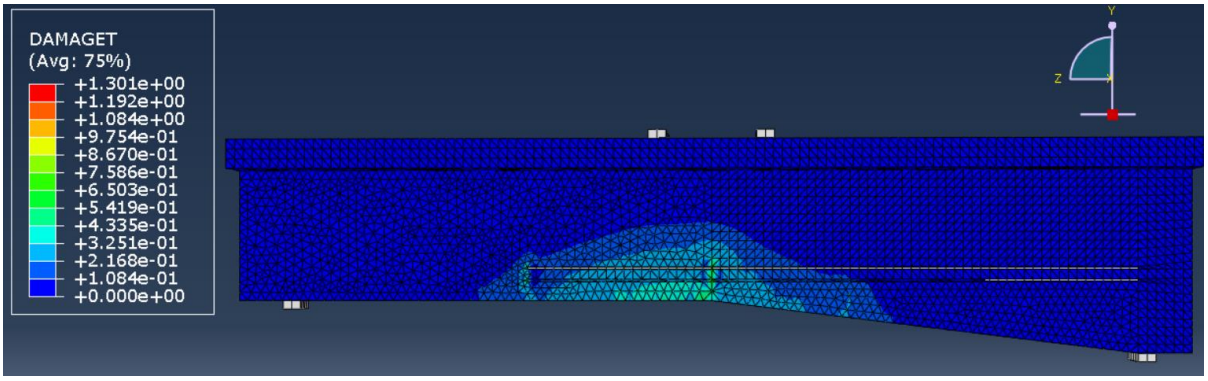

Figure 95: With Titanium-2SG-15 Model - Cracks' Propagation

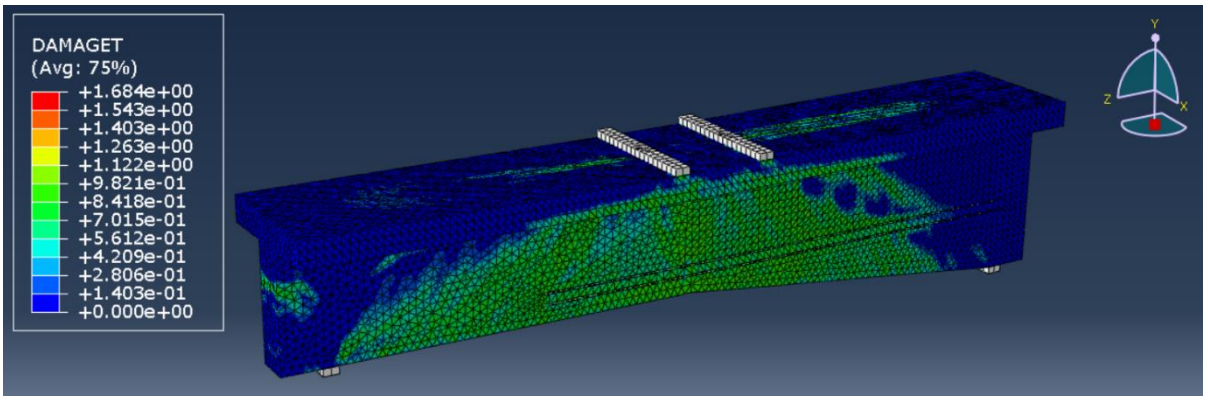

Figure 96: With Titanium-2SG-15 Model - Damage Tension

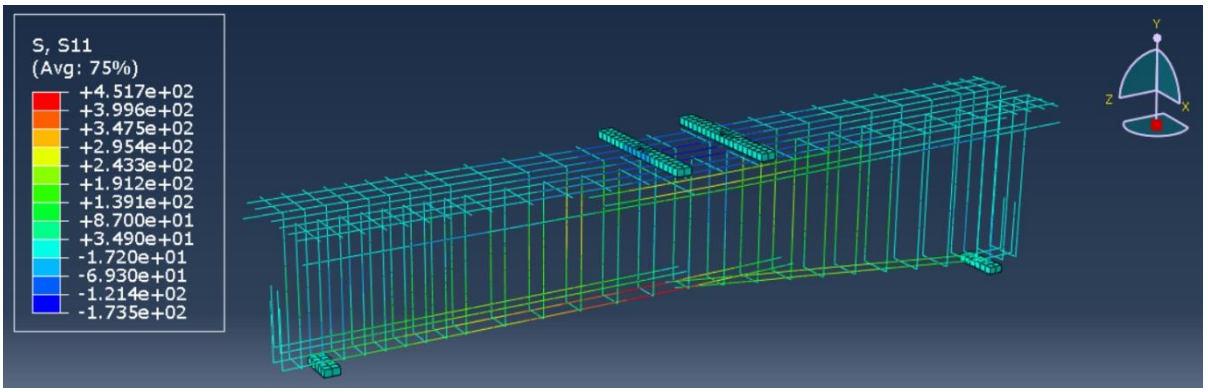

Figure 97: With Titanium-2SG-15 Model - Steel Normal Stress

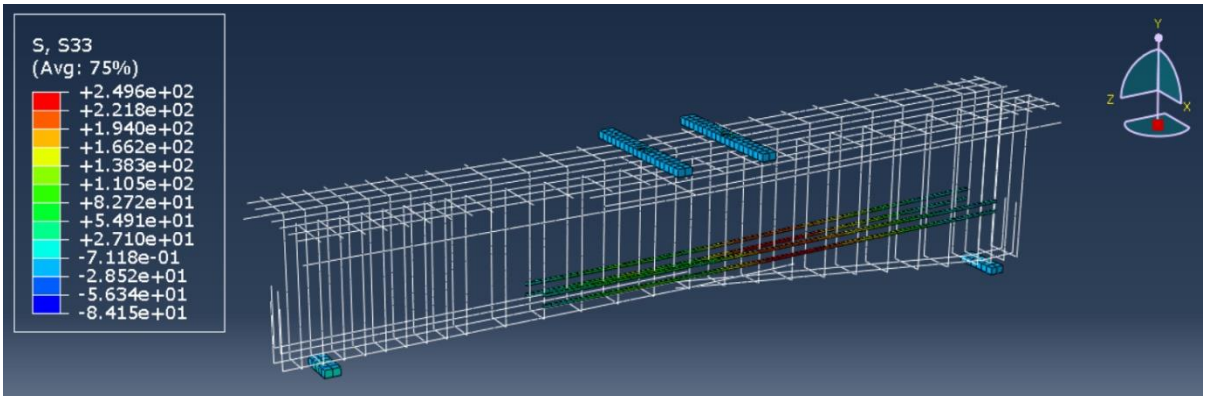

Figure 98: With Titanium-2SG-15 Model - S33 for Titanium Bars

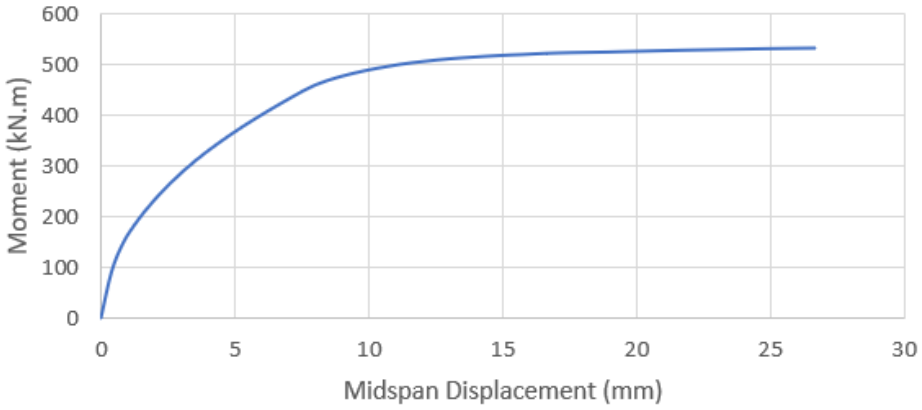

Figure 99: Moment-Displacement curve for With Titanium-2SG-15 Model

The figure above shows that the maximum moment capacity was about 532 kN.m.

4.3.2 Strengthening beam with two (25×25) mm Titanium bars on each side

This model is exactly the original beam which was modelled first to verify the data obtained from Abaqus. So, the same results will be obtained as mentioned before.

4.3.3 Strengthening beam with two (35×35) mm Titanium bars on each side

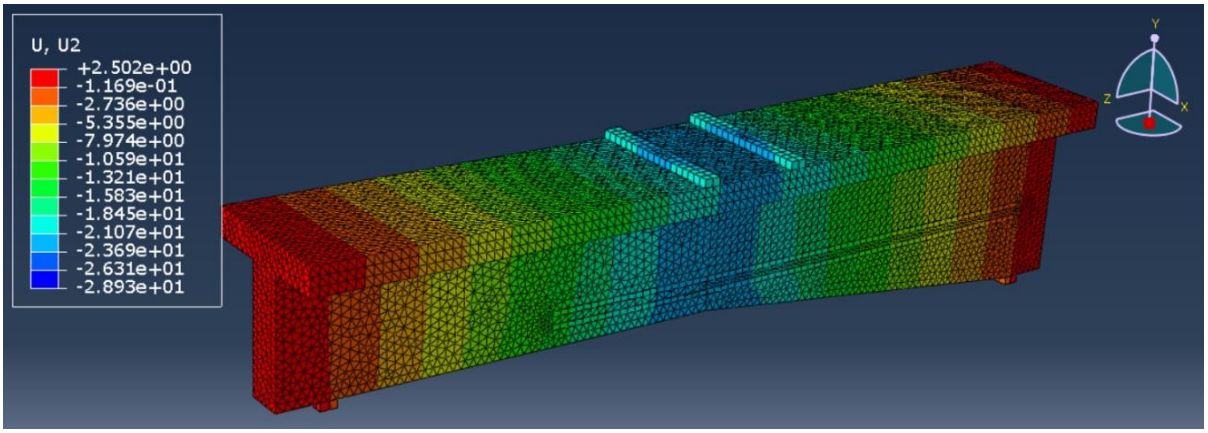

Figure 100: With Titanium-2SG-35 Model - U2 (Vertical Displacement)

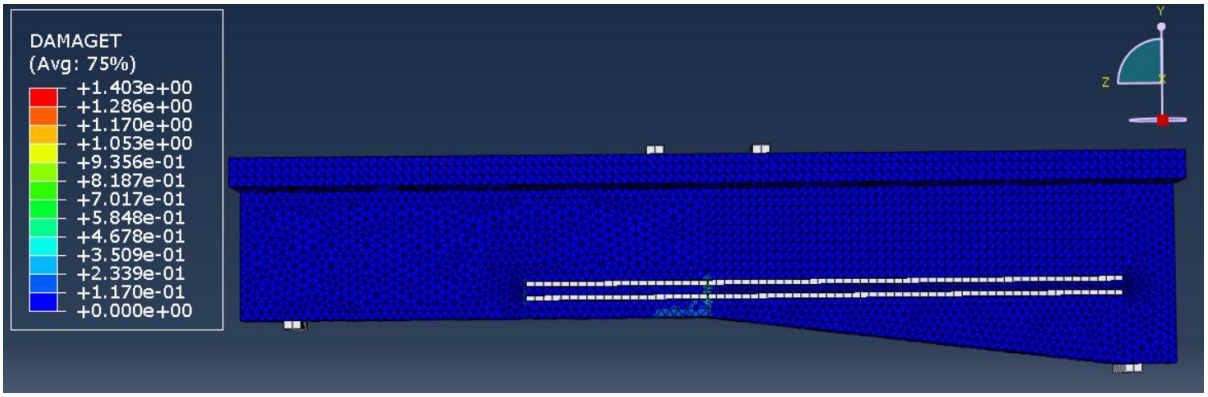

Figure 101: With Titanium-2SG-35 Model - First Tension Crack

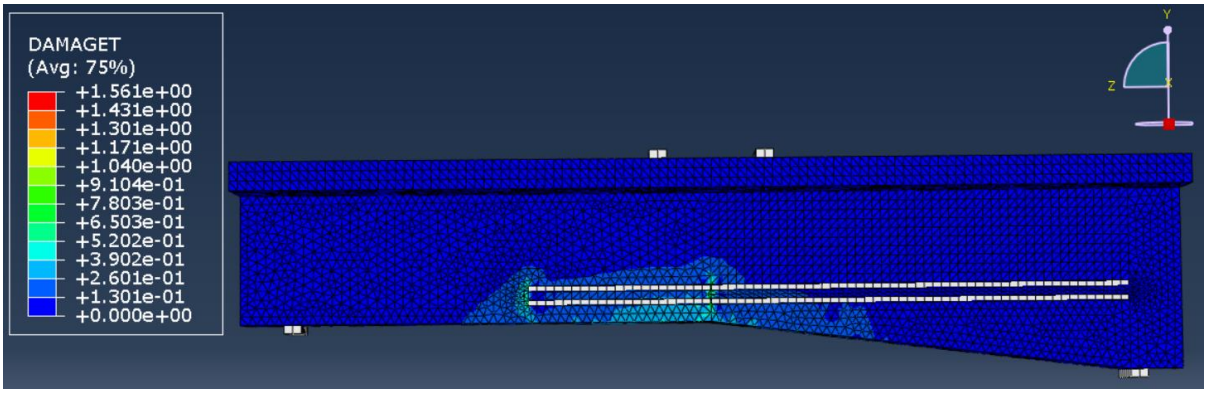

Figure 102: With Titanium-2SG-35 Model - Cracks' Propagation

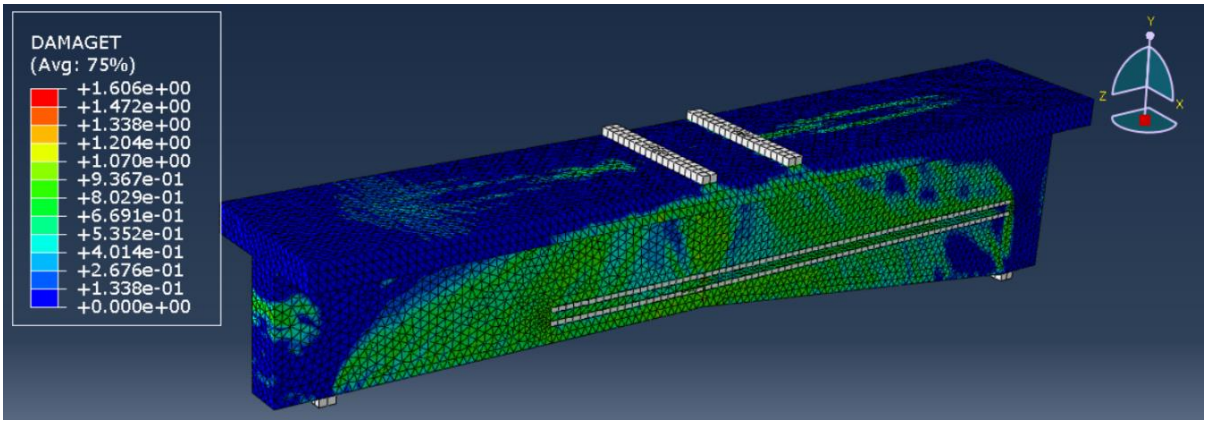

Figure 103: With Titanium-2SG-35 Model - Damage Tension

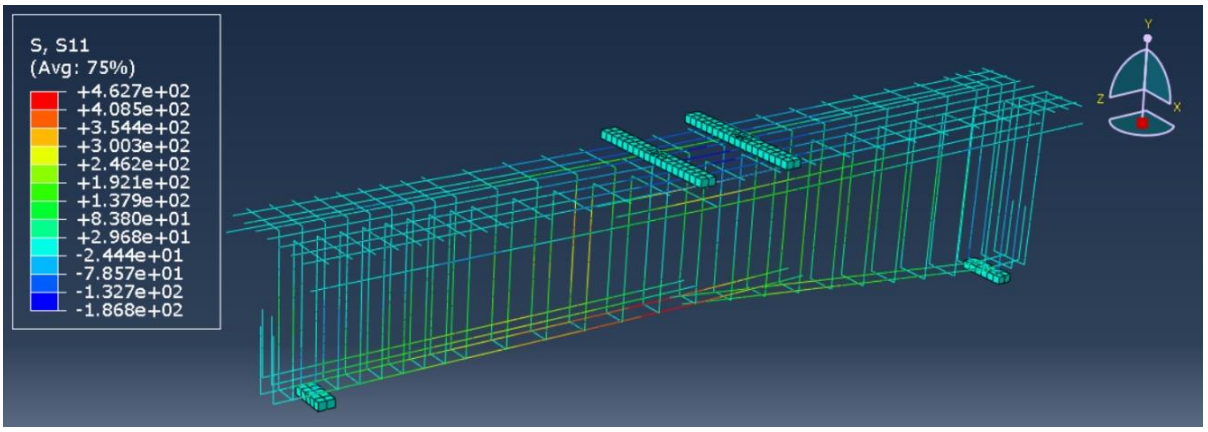

Figure 104: With Titanium-2SG-35 Model - Steel Normal Stress

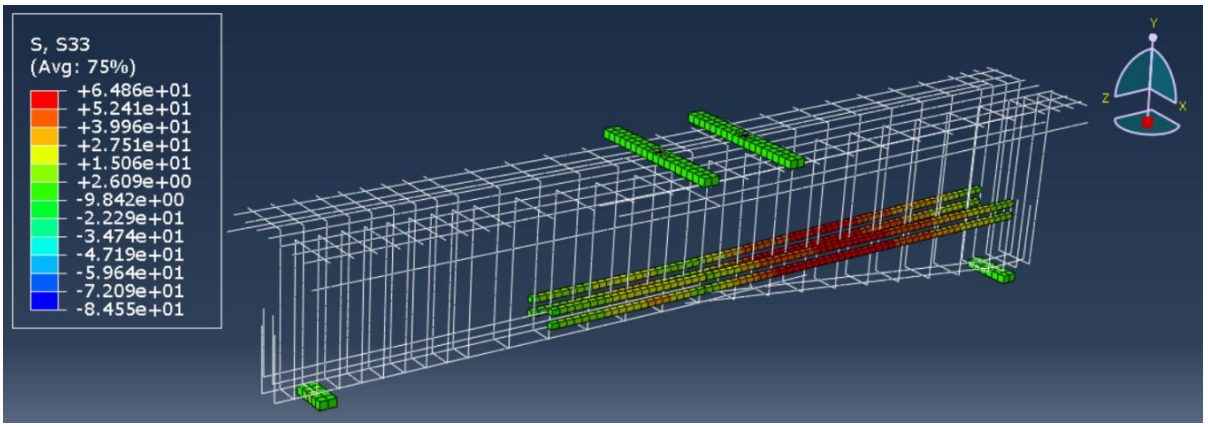

Figure 105: With Titanium-2SG-35 Model - S33 for Titanium Bars

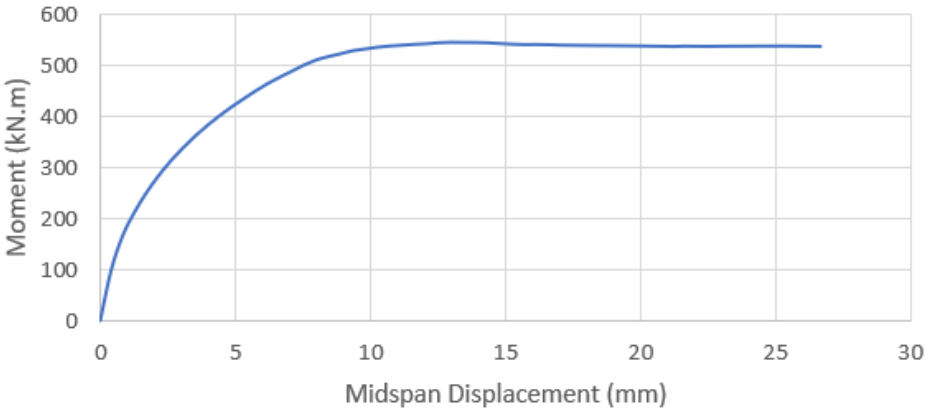

Figure 106: Moment-Displacement curve for With Titanium-2SG-35 Model

As shown above, the maximum moment capacity was about 540 kN.m.

4.4 Strengthening beam with inclined Titanium bars

4.4.1 Strengthening beam with one bar on each side

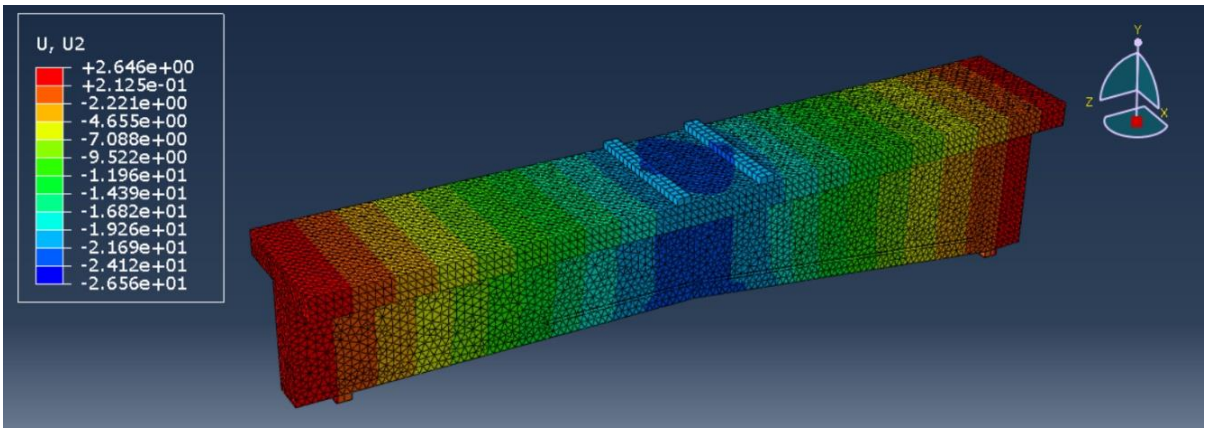

Figure 107: With Titanium-1ISG Model - U2 (Vertical Displacement)

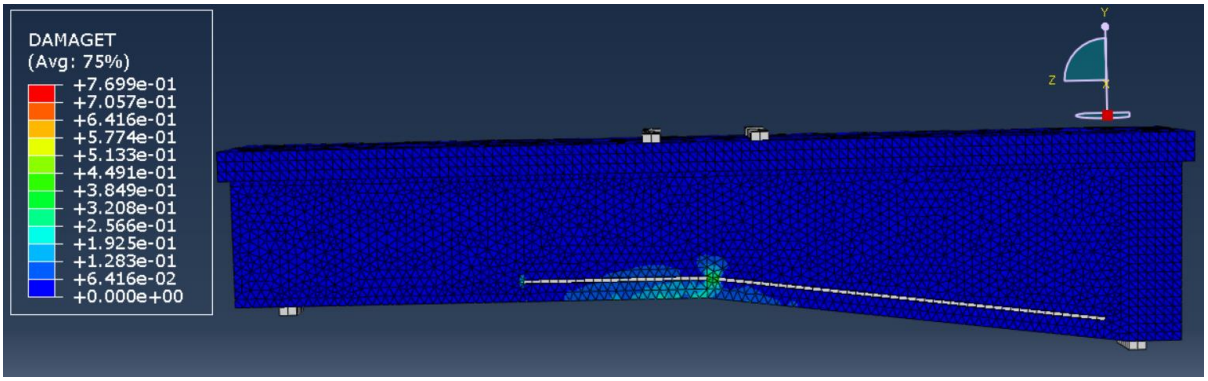

Figure 108: With Titanium-1ISG Model - First Tension Crack

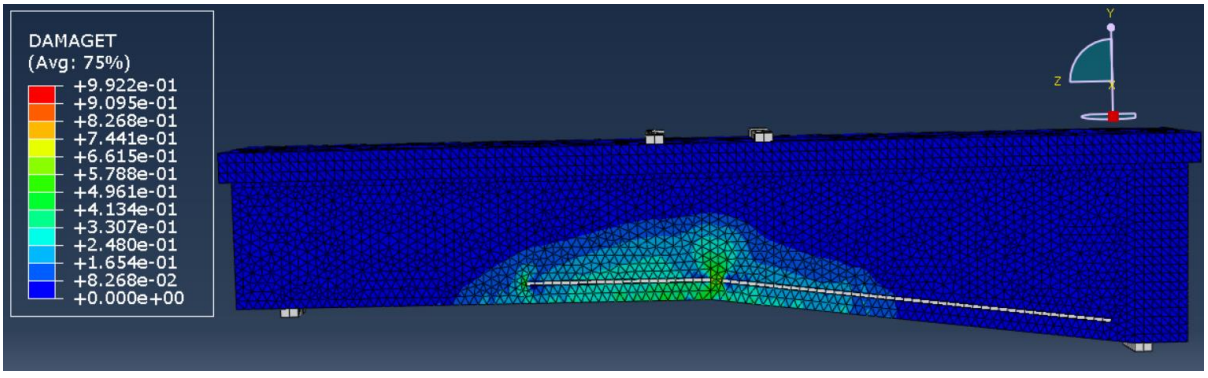

Figure 109: With Titanium-1ISG Model - Cracks' Propagation

As shown above, the cracks started from the point that there is no effect for Titanium bars which represents a weakness point in the beam.

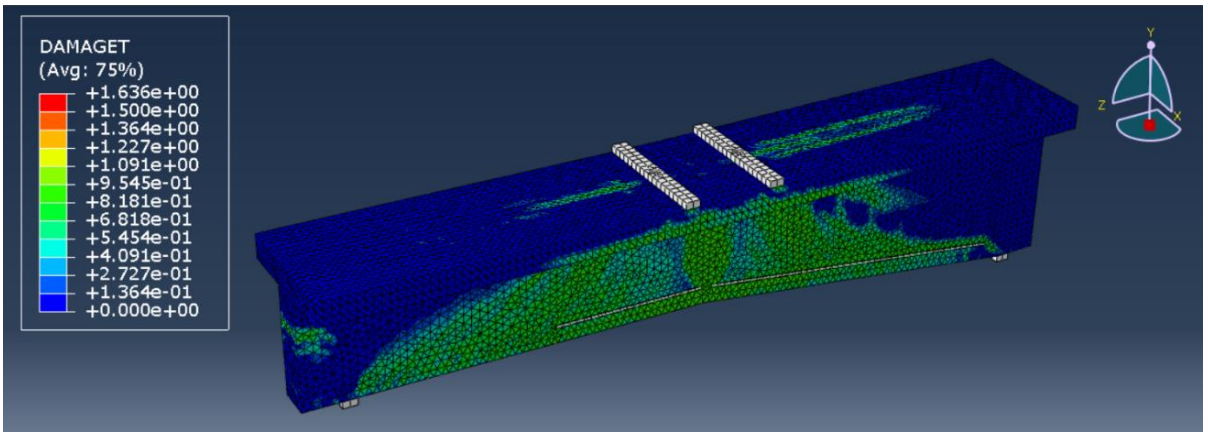

Figure 110: With Titanium-1ISG Model - Damage Tension

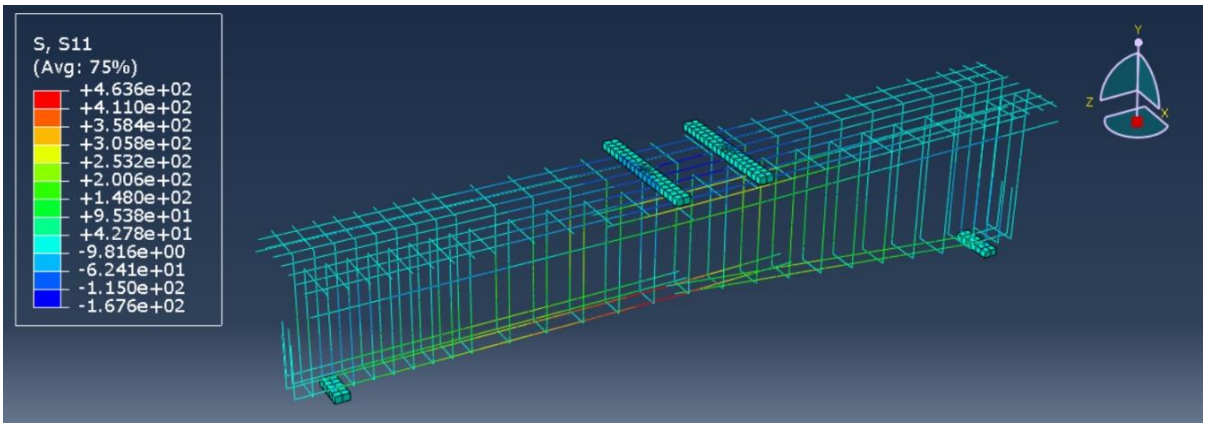

Figure 111: With Titanium-1ISG Model - Steel Normal Stress

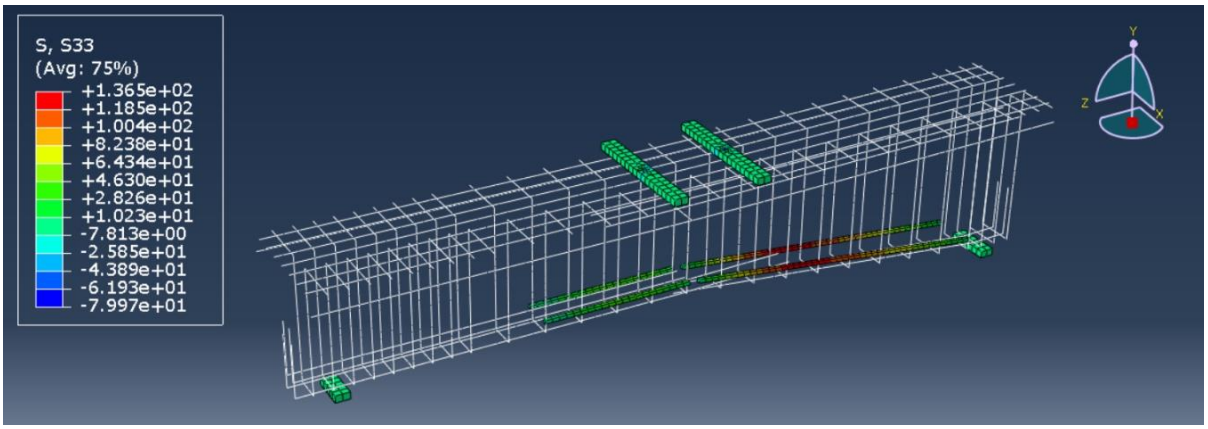

Figure 112: With Titanium-1ISG Model - S33 for Titanium Bars

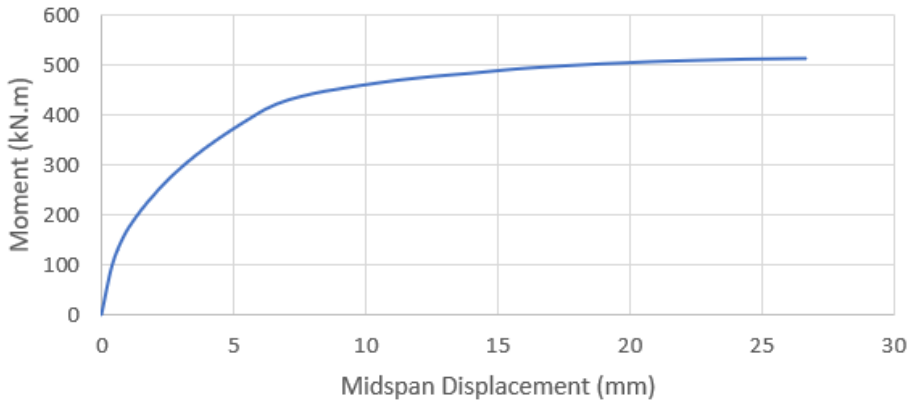

Figure 113: Moment-Displacement curve for With Titanium-1ISG Model

As data given in the above figure, the maximum moment capacity was about 511 kN.m.

4.4.2 Strengthening beam with two bars on each side

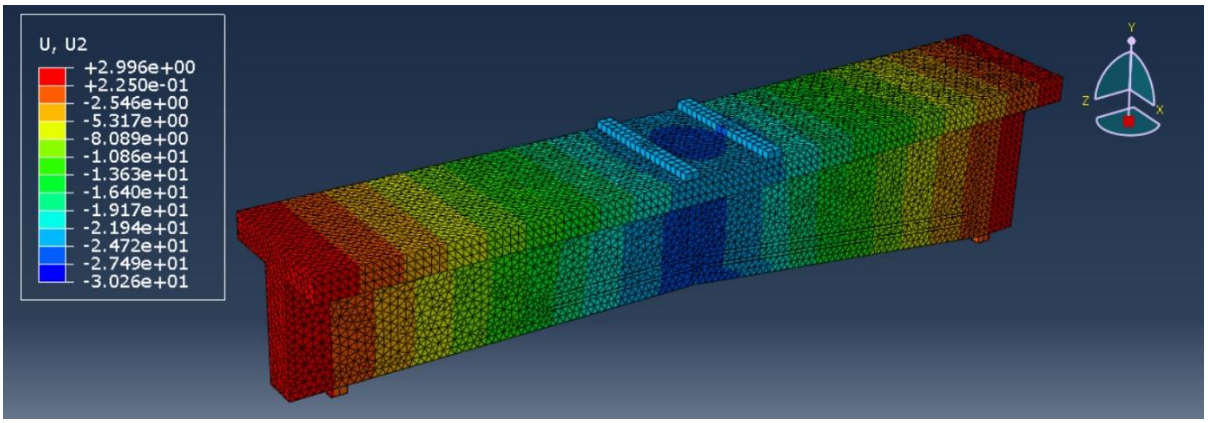

Figure 114: With Titanium-2ISG Model - U2 (Vertical Displacement)

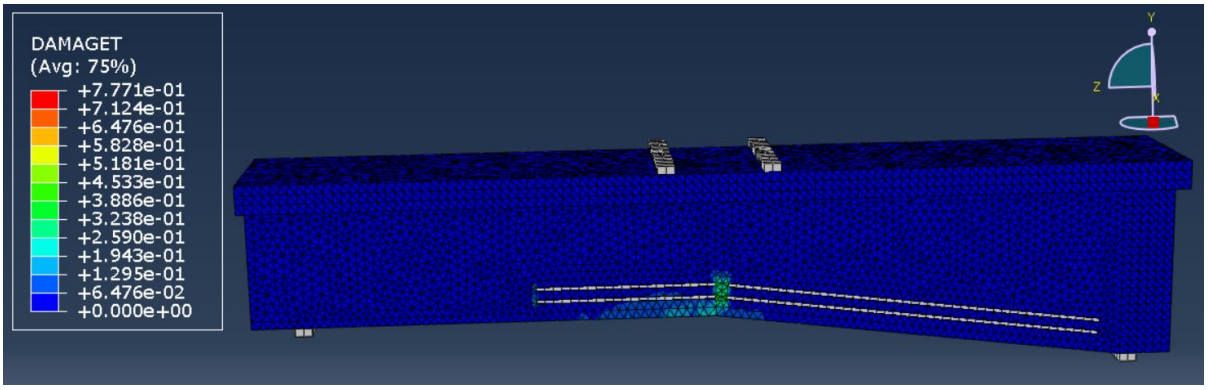

Figure 115: With Titanium-2ISG Model - First Tension Crack

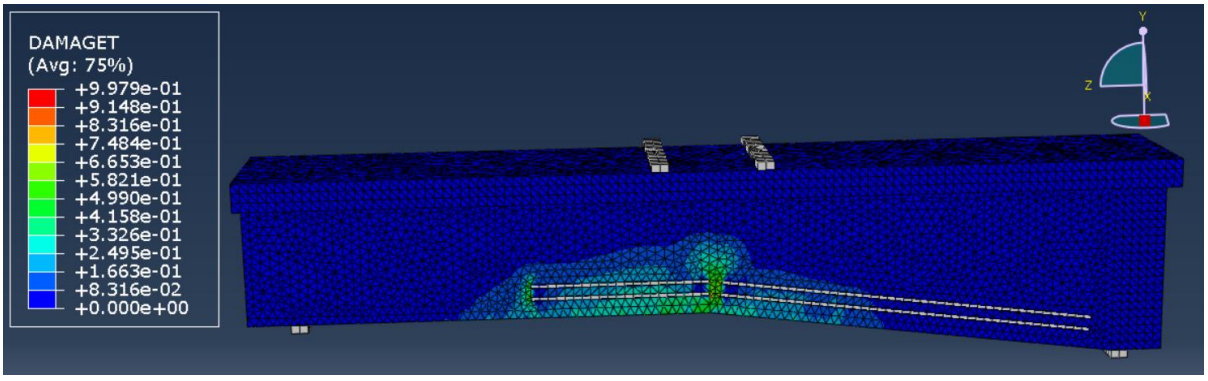

Figure 116: With Titanium-2ISG Model - Cracks' Propagation

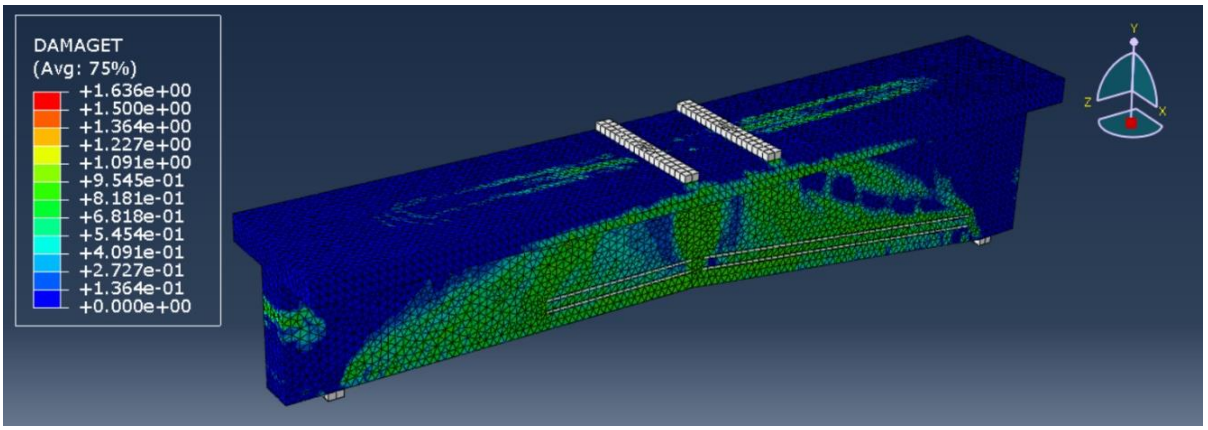

Figure 117: With Titanium-2ISG Model - Damage Tension

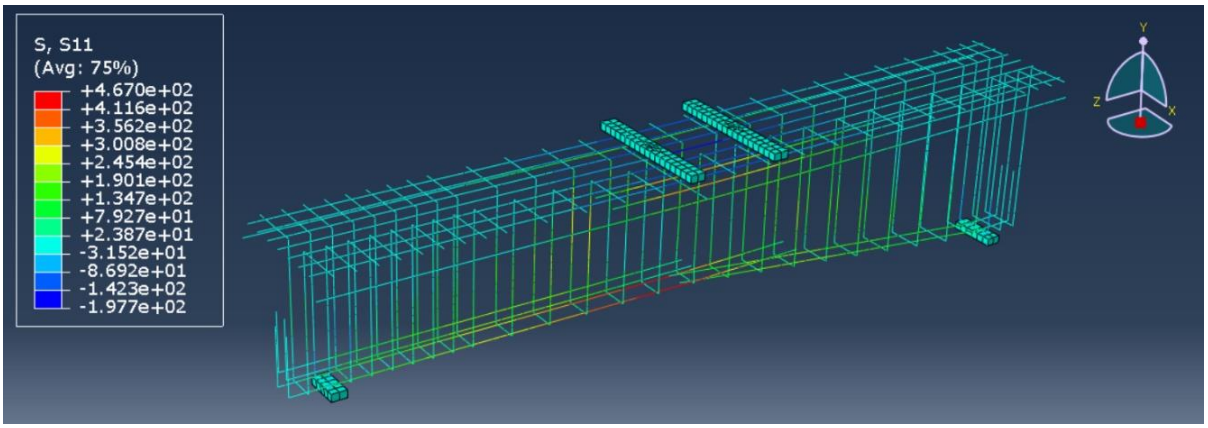

Figure 118: With Titanium-2ISG Model - Steel Normal Stress

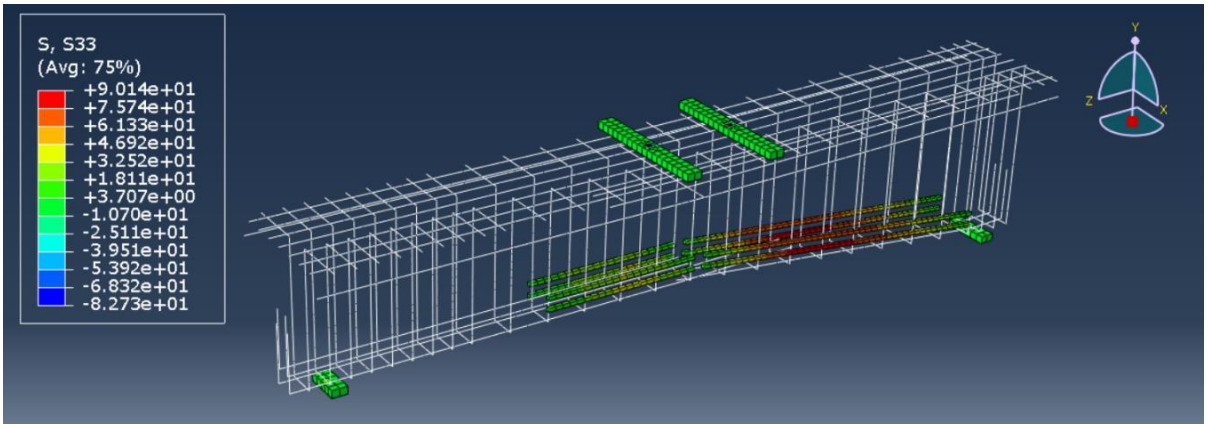

Figure 119: With Titanium-2ISG Model - S33 for Titanium Bars

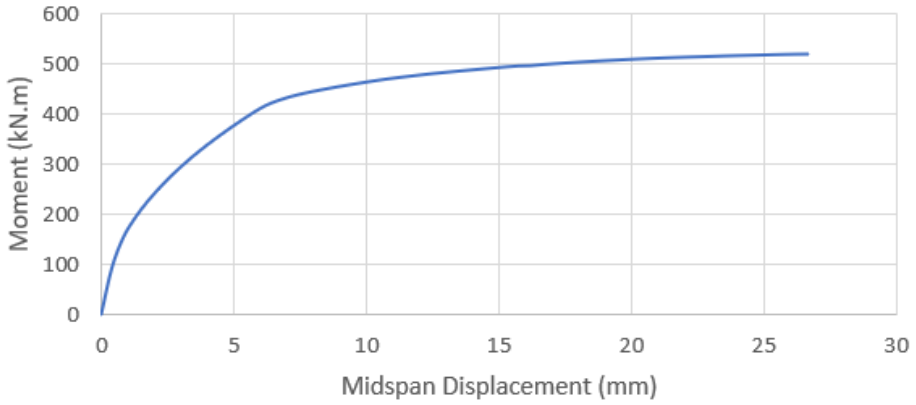

Figure 120: Moment-Displacement curve for With Titanium-2ISG Model

As demonstrated in the figure above, the maximum moment capacity was about 521 kN.m.

4.4.3 Strengthening beam with three bars on each side

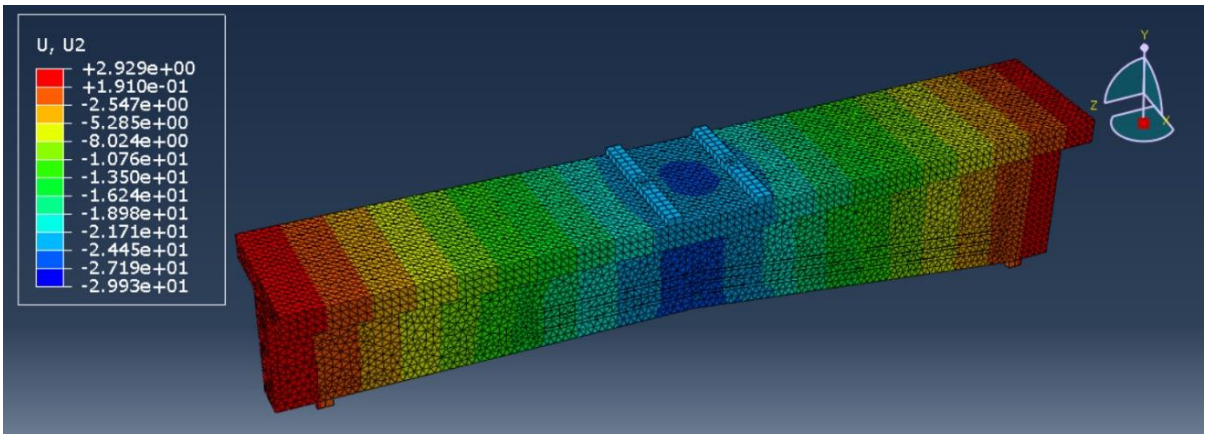

Figure 121: With Titanium-3ISG Model - U2 (Vertical Displacement)

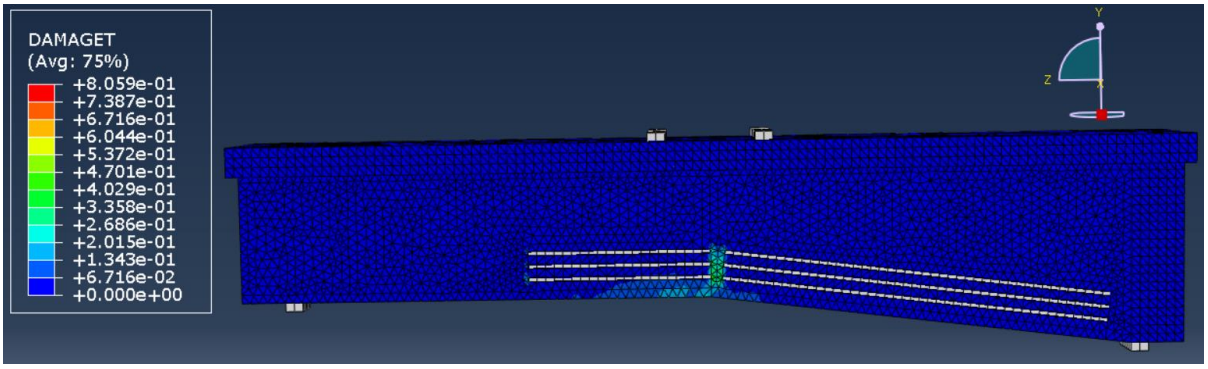

Figure 122: With Titanium-3ISG Model - First Tension Crack

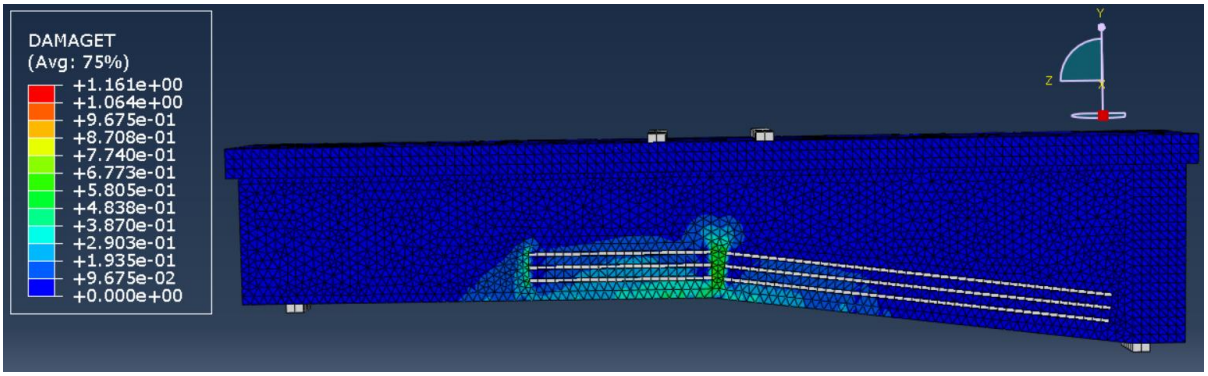

Figure 123: With Titanium-3ISG Model - Cracks' Propagation

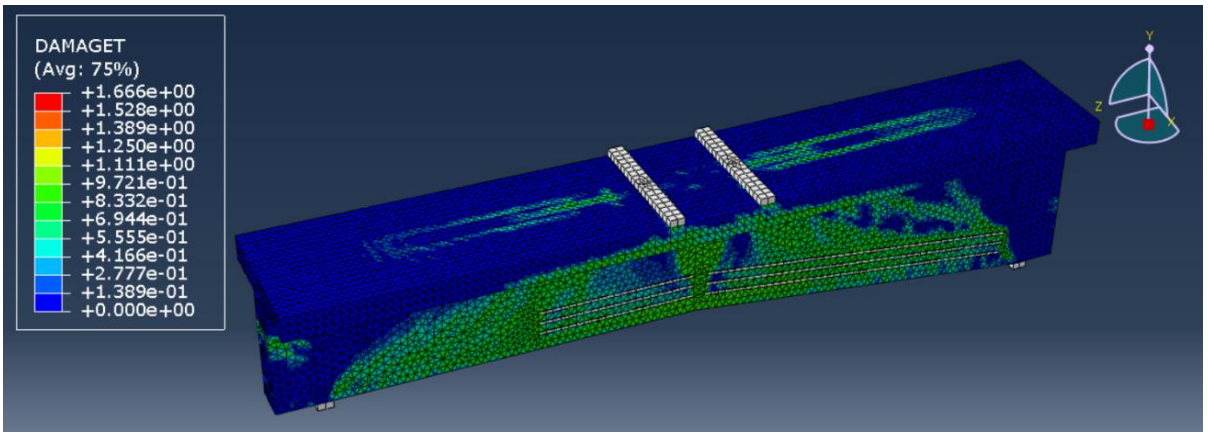

Figure 124: With Titanium-3ISG Model - Damage Tension

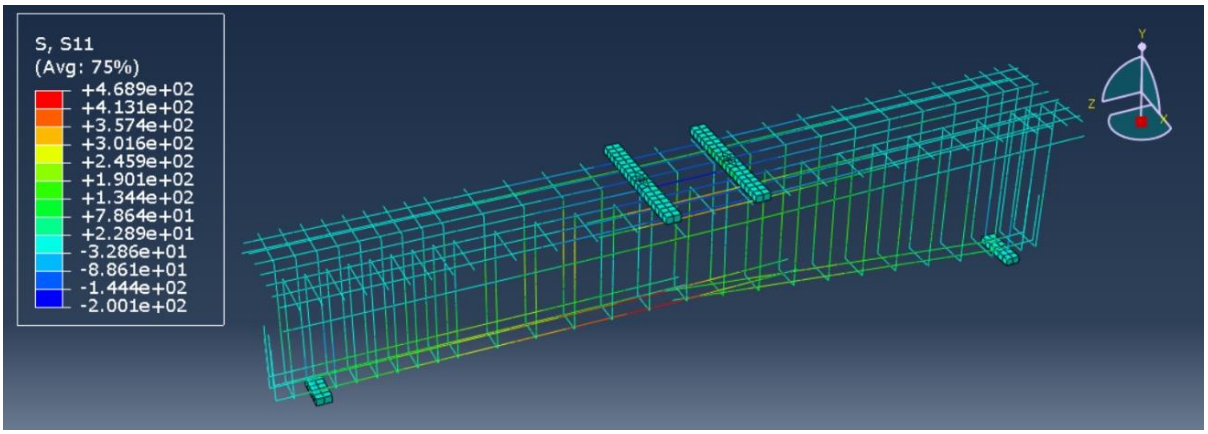

Figure 125: With Titanium-3ISG Model - Steel Normal Stress

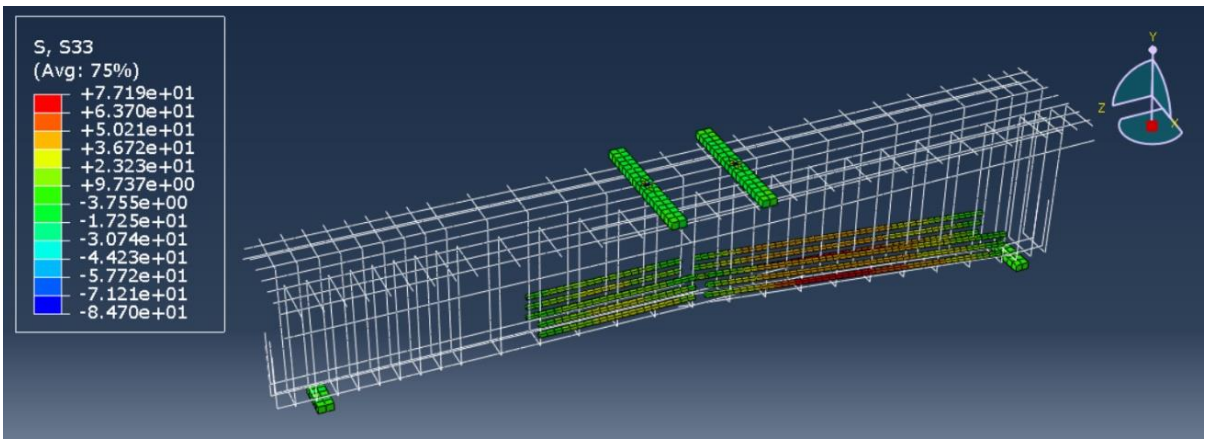

Figure 126: With Titanium-3ISG Model - S33 for Titanium Bars

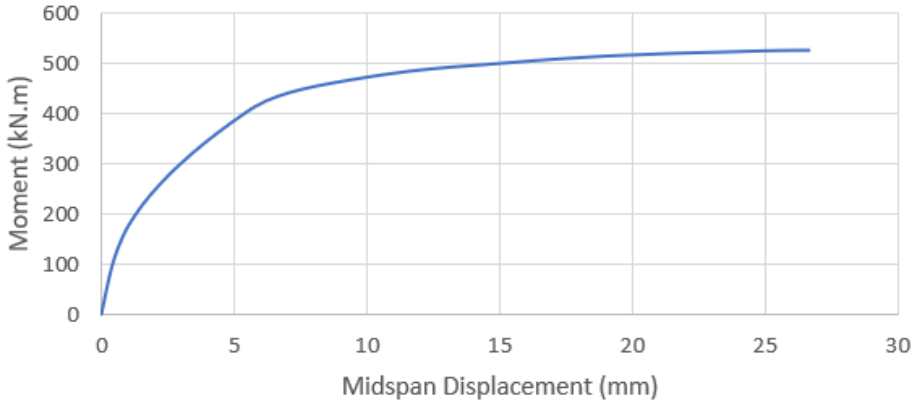

Figure 127: Moment-Displacement curve for With Titanium-3ISG Model

As demonstrated in the figure above, the maximum moment capacity was about 525 kN.m.

Chapter 5: Discussion

5.1 Strengthening beam from bottom

Depending on the results appeared after using finite element, and after comparing moment-displacement curves for “With Titanium-BG Models” (Bottom Grooves are applied) in the figure bellow, it is noticeable that using Titanium alloy bars with bottom grooves is not significantly altering the outcome. Using only one bottom Titanium bar resulting in a slight reduction in strength. The best result was while using three bottom Titanium alloy bars, that increases the strength by 8%.

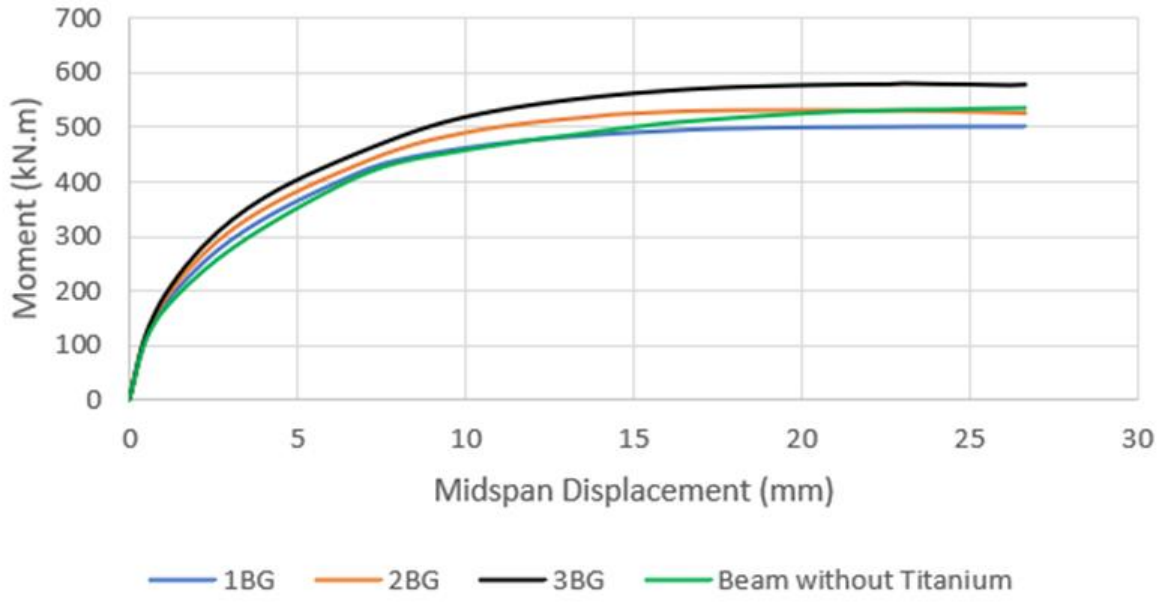

Figure 128: Moment-Displacement curve for With Titanium-BG Models

5.2 Strengthening beam from sides

Depending on the results appeared after using Abaqus, then comparing moment-displacement curves for “With Titanium-SG Models” (Side Grooves are applied) in the figure bellow, using Titanium alloy bars with one groove per side is not significantly affecting the strength. In contrast, using two grooves per side to be filled with Titanium bars resulting in a great moment strength development (as per work done in (Higgins et al., 2017)). The strength can reach the limit of 748 kN.m instead of 536 kN.m in beam without Titanium. A small strengthening done by using three grooves per side to reach 580 kN.m maximum moment strength.

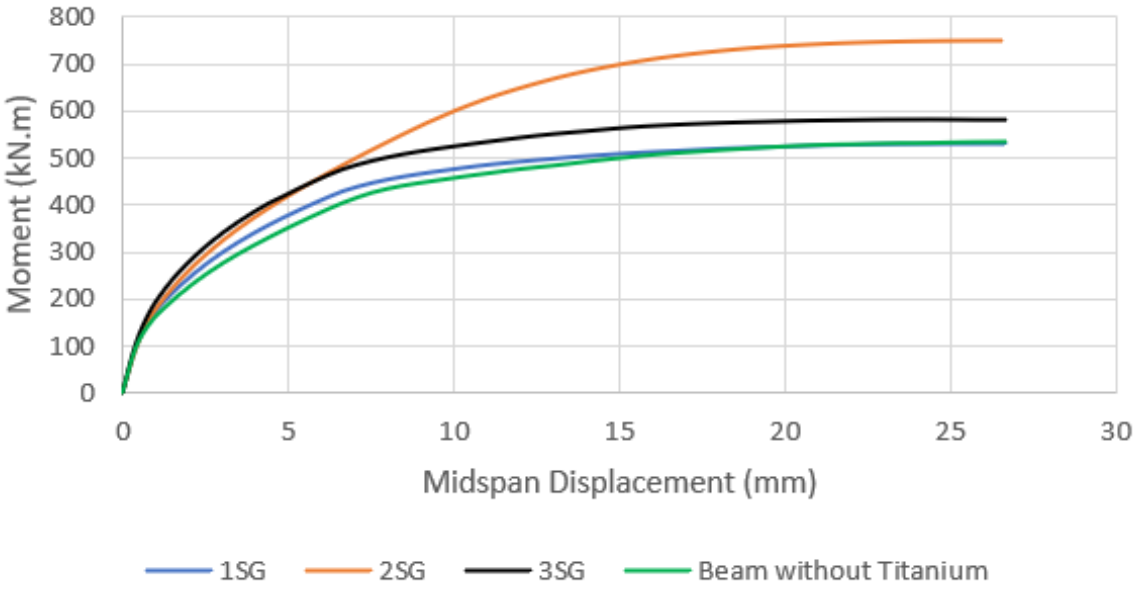

Figure 129: Moment-Displacement curve for With Titanium-SG Models

5.3 Strengthening beam with different alloy bars' sizes

Depending on the results appeared after using finite element, and after comparing moment-displacement curves for "WithTitanium-2SG Models" (two Side Grooves are applied with different dimensions) in the figure bellow, it seems that using Titanium alloy bars with two grooves per side with size (25×25) mm is significantly increasing the moment capacity till 749 kN.m. other cases are resulting in same capacity of non-strengthened beam.

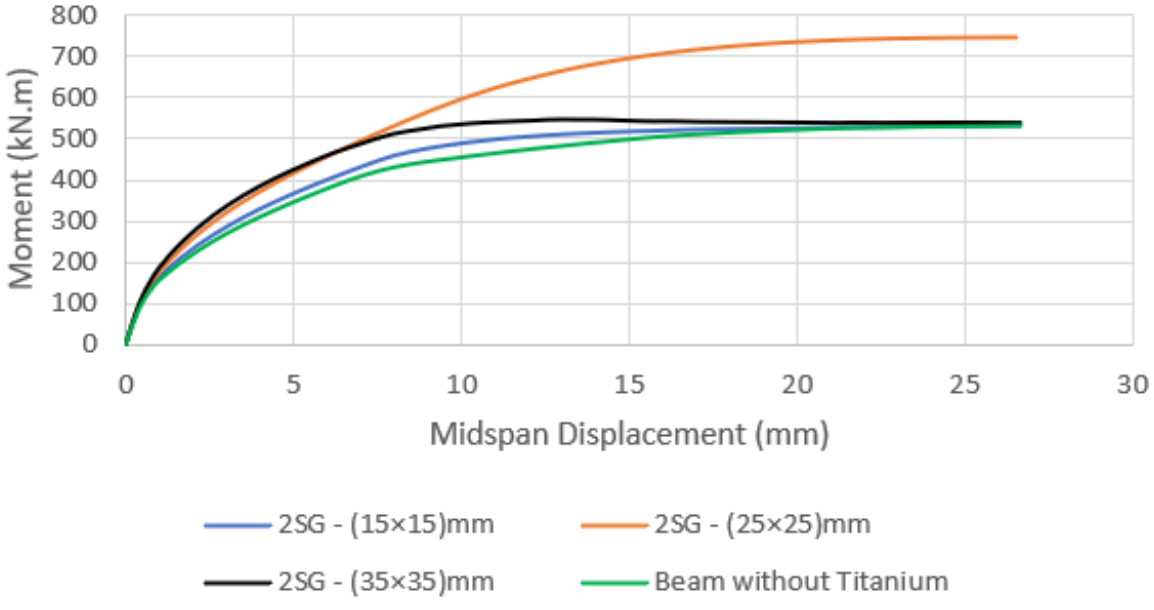

Figure 130: Moment-Displacement curve for WithTitanium-2SG Models

5.4 Strengthening beam with inclined Titanium bars

As per results from Abaqus for “With Titanium-ISG Models” (Inclined Side Grooves) in the figure bellow, there are very small effects that are neglected and cannot be considered as beam strengthening.

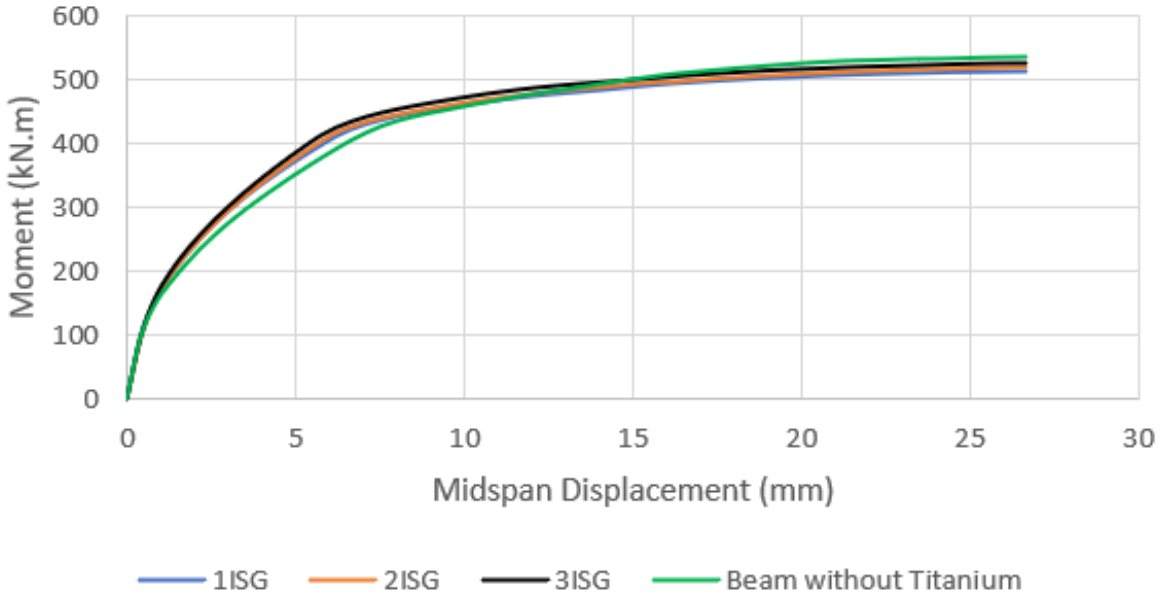

Figure 131: Moment-Displacement curve for With Titanium-ISG Models

5.5 Whole study

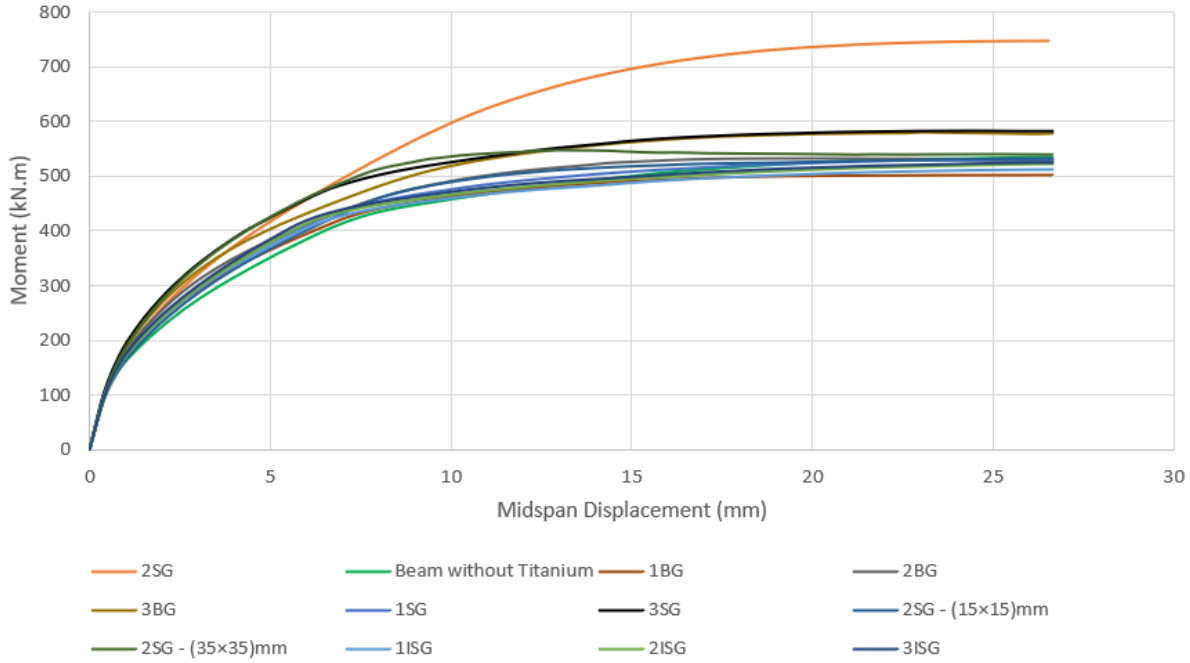

Figure 132: Moment-Displacement curve for all considered Models

The previous figure shows the moment capacities for all considered beams and parametric studies. It is obvious that the best way to strengthen a T beam with enlarging section dimensions from our parameters is to create two horizontal grooves on each side as presented in the first model (the model made for the verification of the data). Some other studies could increase the strength slightly, and the others showed no significant difference.

Table 7: Steel and Titanium stress' data

Model	Steel Yielding?	Midspan Moment at Steel Yielding	Titanium Yielding?	Maximum Titanium Stress / Bar
	Yes / No	kN.m	Yes / No	MPa
With Titanium	Yes	480.03*	No	177.40
Without Titanium		377.40**		No Titanium
With Titanium-1BG		399.76		114.80
With Titanium-2BG		416.67		161.30
With Titanium-3BG		448.98		133.90
With Titanium-1SG		394.76		155.90
With Titanium-3SG		440.93		122.40
With Titanium-2SG-15		421.34		249.00
With Titanium-2SG-35		472.41		63.86
With Titanium-1ISG		379.62		136.10
With Titanium-2ISG		381.14		89.16
With Titanium-3ISG		379.64		76.39

* Maximum midspan moment at steel yielding point.

** Minimum midspan moment at steel yielding point.

The table above shows that steel reinforcement is yielded in all models studied, while Titanium did not reach the yielding stress. Maximum midspan moment at steel yielding point was 480.03 kN.m when applying two Titanium bars on each side with dimension of (25×25) mm for each bar. The steel yielded at 377.40 kN.m midspan moment (the least capacity) when Titanium bars were not applied on the beam.

Chapter 6: Conclusion

- Applying Titanium Alloy Bars (TiABs) on bottom grooves did not greatly enhance the strength of the beam.
- Applying TiABs on the two sides of the beam with straight line showed a significant strengthening specially when performing two grooves per each side.
- The best grooves' dimension was demonstrated to be (25 × 25) mm.
- Making inclined grooves on the area of the expansion of the beam and filling with Titanium showed that the beam will gain no additional strength.
- The propagation of the cracks is shaped according to the situation. Beam without Titanium strengthening makes cracks in the midspan and move horizontally and vertically. On the other hand, Titanium used for strengthening beams is making these cracks move horizontally more then moving vertically.

Chapter 7: References

ABAQUS_MANUAL. 2008. *ABAQUS Manual* [Online]. Available: http://130.149.89.49:2080/v6.8/index.html [Accessed].

ALMASSRI, B. & HALAHLA, A. M. Corroded RC beam repaired in flexure using NSM CFRP rod and an external steel plate. Structures, 2020. Elsevier, 343-351.

BALENDRAN, R., TANG, W., LEUNG, H. & NADEEM, A. Flexural behaviour of sand coated glass-fiber reinforced polymer (GFRP) bars in concrete. 29th Conference on "Our World in Concrete & Structures, 2004.

BAMONTE, P. & GAMBAROVA, P. G. 2007. High-bond bars in NSC and HPC: Study on size effect and on the local bond stress-slip law. *Journal of Structural Engineering,* 133**,** 225-234.

CHOI, E., CHUNG, Y.-S., CHOI, D.-H. & DESROCHES, R. 2012. Seismic protection of lap-spliced RC columns using SMA wire jackets. *Magazine of Concrete Research,* 64**,** 239-252.

CHOI, E. S., LEE, J. W., KIM, S. J. & KWARK, J. W. 2015. A study on the bond strength between high performance concrete and reinforcing bar. *Engineering,* 7**,** 373.

CIANCONE, G. G. 2007. *Behavior of Standard Hook Anchorage Made with Corrosion Resistant Reinforcement.* University of Florida.

CLADERA, A., MONTOYA-CORONADO, L. A., RUIZ-PINILLA, J. G. & RIBAS, C. 2020. Shear strengthening of slender reinforced concrete T-shaped beams using iron-based shape memory alloy strips. *Engineering Structures,* 221**,** 111018.

EFFENDY, E., LIAO, W., SONG, G., MO, Y. & LOH, C. 2006. Seismic behavior of low-rise shear walls with SMA bars. *Earth & Space 2006: Engineering, Construction, and Operations in Challenging Environment.*

EL-SOKKARY, H. Nonlinear behaviour of FRP-retrofitted RC coupled shear walls. Structures, 2023. Elsevier, 324-337.

ELKADY, A. 2023. Elkady, A. (2023) "ABAQUS_CDP_Generator: A tool for generating concrete damage parameters for ABAQUS" Zenodo, Version v23.04. DOI: 10.5281/zenodo.77559264.

ELKAFRAWY, M., KHALIL, A., ALHAMAYDEH, M., HAWILEH, R. & ABUZAID, W. 2023. Enhancing the Shear Capacity of RC Beams with Web Openings in Shear Zones Using Pre-Stressed Fe-SMA Bars: Numerical Study.

FAREED, S. 2014. Behaviour of reinforced concrete beams strengthened by CFRP wraps with and without end anchorages. *Procedia Engineering,* 77**,** 123-130.

FAWAZ, G. & MURCIA-DELSO, J. 2020. Bond behavior of iron-based shape memory alloy reinforcing bars embedded in concrete. *Materials and Structures,* 53**,** 114.

HADI, M. N. 2008. Bond of high strength concrete with high strength reinforcing steel.

HIGGINS, C., KNUDTSEN, J., AMNEUS, D. & BARKER, L. Shear and flexural strengthening of reinforced concrete beams with titanium alloy bars. Proceedings of the 2nd World Congress on Civil, Structural, and Environmental Engineering (CSEE'17), 2017. 1-8.

HILLERBORG, A., MODÉER, M. & PETERSSON, P.-E. 1976. Analysis of crack formation and crack growth in concrete by means of fracture mechanics and finite elements. *Cement and concrete research,* 6**,** 773-781.

HONG, K., LEE, S., HAN, S. & YEON, Y. 2018. Evaluation of Fe-based shape memory alloy (Fe-SMA) as strengthening material for reinforced concrete structures. *Applied sciences,* 8**,** 730.

JASON, L., PIJAUDIER-CABOT, G., HUERTA, A., CROUCH, R., GHAVAMIAN, S., LI, V., LEUNG, C., WILLIAM, K. & BILLINGTON, S. 2004. An elastic plastic damage formulation for the behavior of concrete. *stress (Etse et al, 1994),* 2**,** 1.

JIRSA, J. O. & MARQUES, J. L. 1972. *A study of hooked bar anchorages in beam-column joints,* Department of Civil Engineering, Structures Research Laboratory, University ….

JUNG, D., WILCOSKI, J. & ANDRAWES, B. 2018. Bidirectional shake table testing of RC columns retrofitted and repaired with shape memory alloy spirals. *Engineering structures,* 160**,** 171-185.

MAS, B., CLADERA, A. & RIBAS, C. 2016. Experimental study on concrete beams reinforced with pseudoelastic Ni-Ti continuous rectangular spiral reinforcement failing in shear. *Engineering Structures,* 127**,** 759-768.

MATTOCK, A. H. 1994. Effectiveness of loop anchorages for reinforcement in precast concrete

members. *PCI journal,* 39**,** 54-68.
MINOR, J. & JIRSA, J. O. Behavior of bent bar anchorages. Journal Proceedings, 1975. 141-149.
MOHAMMED, M., ELSHAFEY, A. A., EL-SHAMI, M. M. & KANDIL, K. S. 2013. Strengthening of concrete beams in shear. *Concrete Research Letters,* 4**,** 668-83.
MONTOYA-CORONADO, L. A., RUIZ-PINILLA, J. G., RIBAS, C. & CLADERA, A. 2019. Experimental study on shear strengthening of shear critical RC beams using iron-based shape memory alloy strips. *Engineering Structures,* 200**,** 109680.
MOTAVALLI, M., CZADERSKI, C., BERGAMINI, A. & JANKE, L. 2009. Shape memory alloys for civil engineering structures-on the way from vision to reality. *ACEE,* 2**,** 81-94.
REZAPOUR, M., GHASSEMIEH, M., MOTAVALLI, M. & SHAHVERDI, M. 2021. Numerical Modeling of Unreinforced Masonry Walls Strengthened with Fe-Based Shape Memory Alloy Strips. Materials 2021, 14, 2961. s Note: MDPI stays neutral with regard to jurisdictional claims in published ….
ROJOB, H. & EL-HACHA, R. 2017. Self-prestressing using iron-based shape memory alloy for flexural strengthening of reinforced concrete beams. *ACI Structural Journal,* 114**,** 523.
SAADAT, S., SALICHS, J., NOORI, M., HOU, Z., DAVOODI, H., BAR-ON, I., SUZUKI, Y. & MASUDA, A. 2002. An overview of vibration and seismic applications of NiTi shape memory alloy. *Smart materials and structures,* 11**,** 218.
SAADATMANESH, H., EHSANI, M. R. & LI, M.-W. 1994. Strength and ductility of concrete columns externally reinforced with fiber composite straps. *Structural Journal,* 91**,** 434-447.
SAIKIA, B., THOMAS, J., RAMASWAMY, A. & RAO, K. N. 2005. Performance of hybrid rebars as longitudinal reinforcement in normal strength concrete. *Materials and structures,* 38**,** 857-864.
SHIN, M. & ANDRAWES, B. 2011a. Emergency repair of severely damaged reinforced concrete columns using active confinement with shape memory alloys. *Smart Materials and Structures,* 20**,** 065018.
SHIN, M. & ANDRAWES, B. 2011b. Lateral cyclic behavior of reinforced concrete columns retrofitted with shape memory spirals and FRP wraps. *Journal of Structural Engineering,* 137**,** 1282-1290.
STRIEDER, E., AIGNER, C., PETAUTSCHNIG, G., HORN, S., MARCON, M., SCHWENN, M., ZEMAN, O., CASTILLO, P., WAN-WENDNER, R. & BERGMEISTER, K. 2019. Strengthening of reinforced concrete beams with externally mounted sequentially activated iron-based shape memory alloys. *Materials,* 12**,** 345.
SÜMER, Y. & AKTAŞ, M. 2015. Defining parameters for concrete damage plasticity model. *Challenge Journal of Structural Mechanics,* 1**,** 149-155.
TABRIZIKAHOU, A., KUCZMA, M., NOWOTARSKI, P., KWIATEK, M. & JAVANMARDI, A. 2021. Sustainability of civil structures through the application of smart materials: A review. *Materials,* 14**,** 4824.
THRÖ, H., SCHMIDT, G. & STÖCKL, S. Kupfer,"Anchorage of Reinforcement at an End Bearing with Uni-Axial Lateral Pressure,". *Ger. Comm. Reinf. Concr,* 389**,** 11-98.
UNTRAUER, R. E. & HENRY, R. L. Influence of normal pressure on bond strength. Journal Proceedings, 1965. 577-586.
XIAO, Y. & WU, H. 2000. Compressive behavior of concrete confined by carbon fiber composite jackets. *Journal of materials in civil engineering,* 12**,** 139-146.
YURDAKUL, Ö., TUNABOYU, O. & AVŞAR, Ö. 2018. Retrofit of non-seismically designed beam-column joints by post-tensioned superelastic shape memory alloy bars. *Bulletin of Earthquake Engineering,* 16**,** 5279-5307.